Design and Simulation of Novel Sabatier Reactors for the Thermocatalytic Conversion of CO_2 into Renewable Natural Gas

by

Robert Currie

A thesis
presented to the University of Waterloo
in fulfillment of the
thesis requirement for the degree of
Master of Applied Science
in
Chemical Engineering

Waterloo, Ontario, Canada, 2019

AUTHOR'S DECLARATION

This thesis consists of material all of which I authored or co-authored: see Statement of Contributions included in the thesis. This is a true copy of the thesis, including any required final revisions, as accepted by my examiners.

I understand that my thesis may be made electronically available to the public.

Statement of Contributions

The contents of section 3 and section 4 have been incorporated within a paper that has been submitted for publication. Robert Currie, Michael W. Fowler, David S. A. Simakov, “Catalytic Membrane Reactor for CO_2 Hydrogenation using Renewable Streams: Model-Based Feasibility Analysis”. Submitted to the Chemical Engineering Journal. Submission date Jan. 31, 2019.

The contents of section 3 and section 4 have been incorporated within a paper that has been submitted for publication. Robert Currie, Sogol Mottaghi-Tabar, Yichen Zhuang and David S. A. Simakov, “Design of an Actively Cooled Sabatier Reactor for Thermocatalytic Hydrogenation of CO_2: Model-Based Feasibility Analysis and Experimental Proof-of-Concept”. Submitted to the Journal of Industrial & Engineering Chemistry Research. Submission date Mar. 14, 2019.

Abstract

Producing synthetic chemicals and fuels using CO_2 as a feedstock through the thermocatalytic hydrogenation of CO_2 via the Sabatier reaction to produce synthetic CH_4 is both a CO_2 emissions reduction strategy and an intermittent energy storage solution. A simulation-based study of novel Sabatier reactor configurations was performed to study the effect a distributed H_2 supply would have on Ni-based catalyst deactivation and to optimize the production of CH_4 for the purposes of evaluating the economic feasibility of a renewable natural gas production facility. First, a heat-exchanger type, molten salt-cooled membrane reactor is analyzed using a transient mathematical model that accounts for dynamic catalyst deactivation. The simulation results showed significantly lower catalyst deactivation rates in the membrane reactor due to the distributed H_2 supply that results in more uniform temperature distribution. The model predicts that, with a proper selection of operating parameters, it is possible to achieve CO_2 conversions over 95% over extended periods of operation (10,000 h). Next, a heat-exchanger type, actively cooled Sabatier reactor is analyzed using a transient mathematical model to assess its techno-economic feasibility. Effect of cooling fluid, space velocity, and cooling rate on reactor performance was investigated. Simulation results show that with a proper selection of operating parameters, it is possible to achieve CO_2 conversions more than 90% with 100% CH_4 selectivity over extended periods of operation for a renewable natural gas production cost of $15/GJ with electricity at $0.05/kWh.

Acknowledgements

I would like to thank my supervisors, Professor David Simakov and Professor Michael Fowler for their insight, support and guidance throughout my Masters' program.

I would also like to thank my committee members: Professor Alexander Penlidis and Professor Luis Ricardez Sandoval for their constructive comments and suggestions on my research project.

Special thanks to my group members Yichen Zhuang and Sogol Mottaghi-Tabar. Without them this project wouldn't have been possible.

Lastly, thank you to my family and friends for their support and encouragement through my project.

I would also like to acknowledge the support of the Waterloo Institute of Sustainable Energy (WISE), the Ontario Centers of Excellence (OCE), the Canada Foundation for Innovation (CFI), the Natural Science and Engineering Research Council (NSERC) of Canada and Walker Industries.

Table of Contents

List of Figures

List of Tables

Nomenclature

a	activity factor
$a_{c,HE}$	cooling tube surface-to-volume ratio, m^{-1}
$a_{r,HE}$	cooling tube surface-to-packed volume ratio, m^{-1}
$a_{r,HL}$	reactor surface-to-volume ratio, m^{-1}
A_c	total cross-sectional area of cooling tubes, m^2
A_j	pre-exponential factor of the rate coefficient of reaction *j*, units of k_j
B_j	pre-exponential factor of the adsorption coefficient of species *i*, units of K_j
C_i	molar concentration of species i, mol/m^3
C_t	total molar concentration, mol/m^3
C_{pc}	coolant heat capacity, kJ/(kg K)
C_{pg}	gas heat capacity, kJ/(mol K)
d	wall thickness, m
d_p	catalytic pellet diameter, m
D	diameter, m
D_{ae}	effective axial diffusion coefficient, m^2/s
D_m	gas molecular diffusivity, m^2/s
E_j	activation energy of reaction *j*, kJ/mol
G	gravimetric (mass) flow rate, kg/s
h_{nc}	natural convection heat transfer coefficient, $kJ/(m^2\ s\ K)$
h_w	effective wall heat transfer coefficient, $kJ/(m^2\ s\ K)$
ΔH_i	adsorption enthalpy change of species *i*, kJ/mol
k_{ae}	effective axial thermal conductivity, kJ/(m s K)
k_j	rate constant of reaction *j*
K_i	adsorption constant of species *i*, bar^{-1}
$K_{j,eq}$	equilibrium constant of reaction *j*
L	reactor length, m
Nu	Nusselt number
p_i	partial pressure of gaseous species *i*, bar

P	reactor pressure, bar
Pr	Prandtl number
P_{tf}	total feed gas pressure, bar
Re	Reynolds number
R_j	rate of reaction *j*, mol/(kg s)
R_g	gas constant, kJ/(mol K)
SV	gas hourly space velocity, h^{-1}
t	time, s
T	reactor temperature, K
T_c	coolant temperature, K
T_e	environment temperature, K
U_w	overall effective wall heat transfer coefficient, kJ/(m^2 s K)
v	fluid velocity, m/s
V	compartment volume, m^3
z	reactor length coordinate, m

Greek letters

ε	catalyst bed porosity
ϕ	Thiele modulus
η_j	effectiveness factor of reaction *j*
λ	thermal conductivity, kW/(m K)
μ	viscosity, kg/(m s)
ρ_c	coolant density, kg/m^3
ρ_g	gas molar density, mol/m^3
ρ_s	solid density, kg/m^3
τ_b	catalyst bed tortuosity

Subscripts

c	coolant
eff	effective
eq	equilibrium
f	feed
g	gas
HE	heat exchange

HL	heat loss
int	initial
M	membrane
nc	natural convection
PB	packed bed
s	solid
r	reactor

1.0 Introduction

1.1 Problem statement and motivation

As renewable energy sources (RES) have increasingly become part of the global energy supply mix in recent years [1] , energy storage solutions have been implemented to stabilize the intermittent energy production [2]. Global CO_2 concentrations continue to rise [3] and various solutions for reducing emissions include improving energy efficiency, transitioning to lower carbon energy sources, and CO_2 capture for sequestration or conversion into synthetic fuels and chemicals. The benefits of utilizing CO_2 to produce fuels and chemicals has already been discussed in the literature [4-7]. There are several pathways to synthesize chemicals and fuels using CO_2 as a carbon source, including photo- and electro-chemical reduction, biological conversion, and thermocatalytic hydrogenation. Large-scale application of photo- and electro-chemical conversion is restricted by the low CO_2 solubility in water and transport limitations [8, 9]. The main drawback of biological conversion is the high cost of cultivation [10].

Thermocatalytic hydrogenation of CO_2 via the Sabatier reaction to produce synthetic methane (CH_4) offers the benefits of fast reaction rates and high conversion efficiencies allowing for compact, high throughput operation [10]. This synthetic methane will be renewable if the H_2 required for the reaction is produced via water electrolysis using renewable or low carbon footprint electricity (solar, wind, hydro or surplus nuclear). The highly exothermic Sabatier reaction, Eq. (3) can be represented as the combination of the mildly endothermic reverse water gas shift, Eq. (2), and the strongly exothermic CO methanation, Eq. (1):

$$CO + 3H_2 \rightleftarrows CH_4 + H_2O \qquad \Delta H^{\circ}_{298} = -206.1 \text{ kJ/mol} \tag{1}$$

$$CO_2 + H_2 \rightleftarrows CO + H_2O \qquad \Delta H^{\circ}_{298} = +41.2 \text{ kJ/mol} \tag{2}$$

$$CO_2 + 4H_2 \rightleftarrows CH_4 + 2H_2O \qquad \Delta H^{\circ}_{298} = -164.9 \text{ kJ/mol} \tag{3}$$

The overall process is highly exothermic, and reactor overheating is among the technological challenges yet to be resolved [11]. High temperatures are unfavorable to the exothermic and reversible methanation process and accelerate catalyst deactivation.

An actively cooled packed bed reactor design has shown promise in potentially providing a low-cost solution for a single-pass methanation process [11]. However, the issue of catalyst stability has not been yet properly addressed. The requirement to supply a pure H_2 stream for methanation is also a disadvantage, owning to the high capital and operating costs of water electrolysis. More than 35% of the power-to-gas (PtG) methanation system costs were predicted to be due to the electrolysis step, with 70% of that cost being the cost of electricity [12]. In this study, a solution for improving dynamic catalyst deactivation and the techno-economic feasibility of a methanation process are evaluated using a mathematical simulation of a Sabatier reactor.

1.2 Project Objectives

Recent modeling studies have either assumed simple first-order deactivation kinetics or omitted it completely from their catalytic system [13] . Such a situation is unlikely as it is known catalyst deactivation by coking can occur under the conditions relevant to CO_2 methanation [13, 14]. Other studies have also found differences between experimental and simulated methanation results, suggesting further study on the operation of larger CO_2 methanation reactors is required. Meanwhile, the economic feasibility of PtG systems has peaked significant interest in recent years and while the economic outlooks for PtG systems are improving, further work to increase its potential for widespread implementation are still required.

The project presented herein then has three parts. First, a distributed H_2 supply via a heat-exchanger type membrane Sabatier reactor is investigated via numerical simulation as a possible solution to improving catalyst deactivation by coking. Utilizing such a membrane will allow for H_2 extraction from H_2 containing off-gases from various industrial or renewable sources (e.g., biomass gasification). This approach can potentially eliminate the need for pure H_2, potentially improving process economics. A high-level, conceptual process flow diagram is presented in Figure 1.

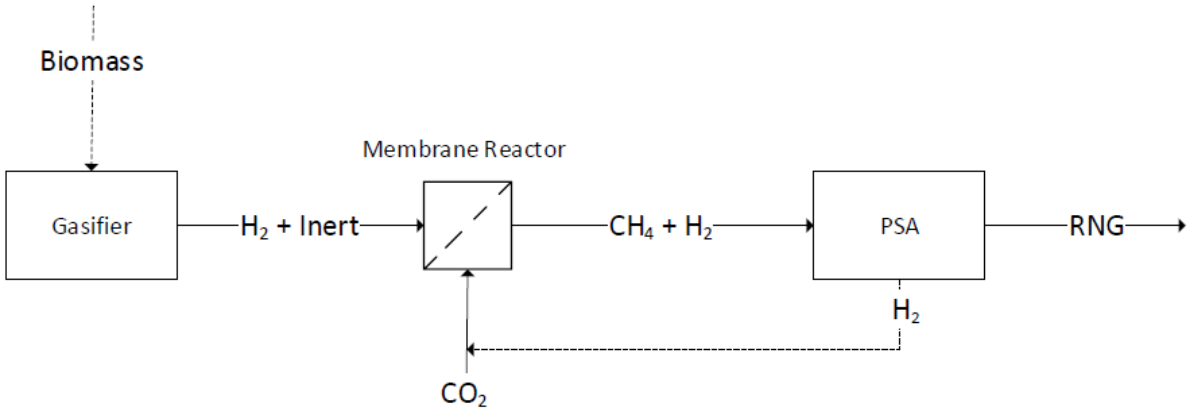

Figure 1. Schematic representation of the membrane Sabatier reactor system for generation of renewable natural gas (RNG) utilizing CO_2 and H_2-containing streams as feedstocks.

Reaction heat is actively removed from the reactor by the recirculation of molten salts. The performance of the suggested membrane reactor was compared to that of a non-membrane reactor. Second, an actively cooled packed bed Sabatier reactor was designed and investigated by numerical simulations to optimize CO_2 conversion and CH_4 production rate for its potential use in a PtG system. Finally, the techno-economic feasibility of using a single-pass actively cooled packed bed reactor for the thermocatalytic conversion of CO_2 to RNG in a power-to-gas (PtG) system was examined.

2.0 Literature Review

2.1 Power to gas system design

Power-to-gas is the process by which electrical power is converted and stored in a gas form for the purpose of deploying it later [15]. Many pathways for PtG exist including: power to hydrogen, power to RNG and power to renewable content in petroleum fuels. The PtG concept has been discussed as part of the solution to balancing intermittent renewable energy sources such as solar and wind for many years [16-19]. Power-to-gas is a two-step process; H_2 production by water electrolysis first and then H_2 conversion with an external CO or CO_2 source to CH_4 via methanation. Once the CH_4 is produced, it can be injected into the existing gas distribution grid and deployed when needed. An example PtG process chain can be seen in Figure 2.

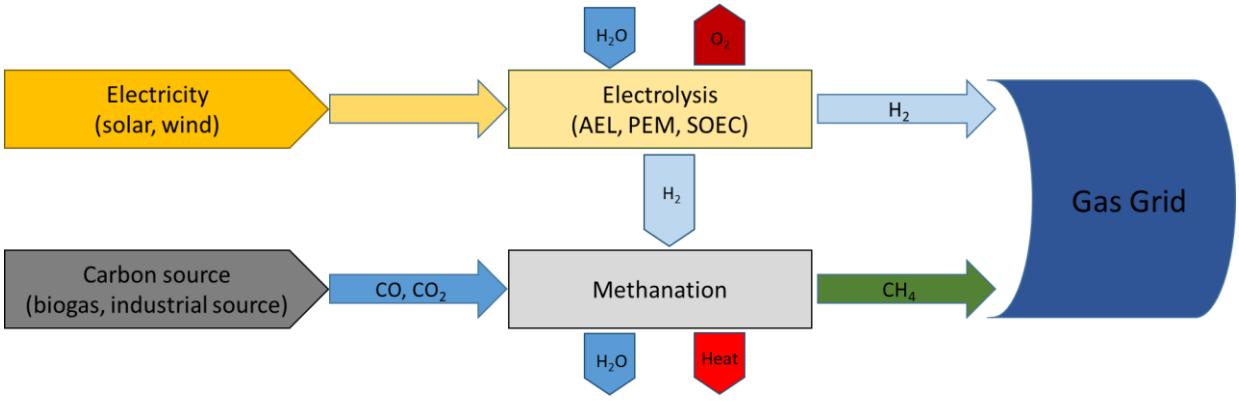

Figure 2. PtG process chain

The first step in the process, H_2 production via water electrolysis, is an electro-chemical reaction, Eq. (4) with the reduction reaction taking placed at the negatively charged cathode, Eq. (5) and the oxidation reaction occurs at the positively charged anode, Eq. (6) [15].

$$H_2O(l) \rightarrow H_2(g) + \frac{1}{2}O_2(g) \qquad \Delta H_r^\circ = +285.8 \text{ kJ/mol} \tag{4}$$

$$H_2O + 2e^- \rightarrow H_2 + O^{2-} \tag{5}$$

$$O^{2-} \rightarrow \frac{1}{2}O_2 + 2e^- \quad (6)$$

Water electrolysis is a well understood technology [15]. Currently, there are three different electrolysis technologies, alkaline electrolysis (AEL), polymer electrolyte membrane (PEM) electrolysis and solid oxide electrolysis (SOEC), which are of interest for PtG processes [15]. AEL is the most mature and understood technology [15] and has been commercially available for decades [20]. Currently, capital expenditures for AEL systems are predicted to be significantly lower than PEM and SOEC systems [15].

After electrolysis, the produced H_2 is combined with a carbon source such as CO or CO_2 where it is fed to the methanation process for conversion to CH_4. Several options for the carbon source to a PtG process exist. Industrial carbon sources (steel, iron cement production) are one of the largest stationary CO_2 sources in the world [21] but would require CO_2 capture and upgrading to prevent methanation catalyst poisoning from sulphourous or siloxane materials. Biogas as a CO_2 source in methanation applications has recently garnered interest [12]. Biogas' main components are CH_4 (50-70%) and CO_2 (30-50%) with H_2S and siloxanes as trace components [12]. Using biogas as a CO_2 source shows promise as the primary component in biogas is CH_4, which is the desired final product. As such, a smaller fraction of CO_2 in the feedstock requires less conversion, lowering capital investment and operational costs.

Early studies examining the economic feasibility of PtG systems focused on methanation of pure CO_2 streams into renewable natural gas (RNG) [22, 23]. One study evaluated the feasibility of a system with combined alkaline electrolysis and chemical methanation with a post combustion CO_2 feedstock [22]. Sources of revenue were identified as the product RNG and byproduct O_2 gas from the electrolysis. Results indicated the estimated cost of RNG to be 105 CAD/MWh, 3 times

higher than conventional natural gas prices in Ontario (33 CAD/MWh) [22]. A different study of pure CO_2 methanation evaluated the effects of production factors such as electricity price and loading period on overall feasibility [23]. Resulting data emphasized a significant correlation between low electricity prices and economic feasibility [23].

Recently, investigations of biogas as methanation feedstock instead of pure CO_2 have been conducted. With this, studies have evaluated feasibilities of systems with various system configurations, plant capacities and feed sources. One study focused on a 96 m^3/h system (1.34 MW power rating) for an onsite methanation facility to process biogas from dairy manure [24]. Capital investment for the process units required to upgrade the biogas was predicted to be approximately $5,194,000 CAD with an annual operating cost of $693,377 CAD [24]. By approximating the selling price of RNG at $40/GJ, it was found that the process would be feasible with a payout period of 4.54 years[24]. Another work focused on a 230 m^3/h system with feed from anaerobic digestion of sewage sludge[25]. This analysis compared existing upgrading and PtG technologies and found direct methanation pathways to be economically competitive[25]. It was also found that that direct methanation of biogas showed higher feasibility under continuous rather than intermittent operations. This was a result of a loss of production coming from increased downtime, decreasing revenue below minimal requirements for economic sufficiency[25]. Comparisons between systems with methanation of raw biogas with those separating CH_4 and CO_2 prior to methanation have also been made[24, 26]. It was found that there were negligible differences between the two in terms of reactor performance with the former option showing desirable economics[24, 26].

2.2 Methanation process and reactor design

Methanation reactors are typically operated between 200℃ and 550℃ and at pressures ranging from 1 to 100 bar [15]. The exothermic nature of the methanation reaction means reaction temperature control is a major concern in the design of methanation systems as high temperatures are unfavorable to the reversible methanation process and accelerate catalyst deactivation [11, 13]. Different reactor configurations have been suggested, including fixed bed, fluidized bed, microchannel, monolith, and three-phase slurry reactors. Their advantages and limitations have been outlined elsewhere [11].

2.3 Current uses of membrane reactors

Hydrogen on its own has already been discussed as an environmentally friendly fuel [27] and its production from natural gas is well known. Conventionally, hydrogen is produced in industrial-scale steam natural gas reformers [28], which is the reverse of Eq. (3). To overcome the disadvantages associated with traditional steam reforming technologies, which include equilibrium limitation and poor selectivity, fixed bed membrane reactors to in-situ remove H_2 have been suggested and studied [27, 29, 30]. Membrane reactors can be used to feed reactants or separate products [31] and are a good option for improving overall system efficiency by combining chemical reaction and hydrogen separation in hydrogen production facilities [31]. Dense Pd-based membranes, offer a complete hydrogen perm-selectivity with solution / diffusion being the transport mechanism through the membrane [32].

\

2.4 Catalyst deactivation

Various catalysts and supports for CO_2 methanation have been studied [33-37]. At this point, no consensus on the reaction's operating mechanism has been made due to the uncertainty involved with determining the intermediate compounds involved in the rate-determining step [38, 39].Currently, there are two popular suggested pathways, as seen in Figure 3. The first path considers the conversion of CO_2 to CO followed by the hydrogenation to CH_4. The second path considers the direct hydrogenation of CO_2 to CH_4 with no CO intermediate [40].

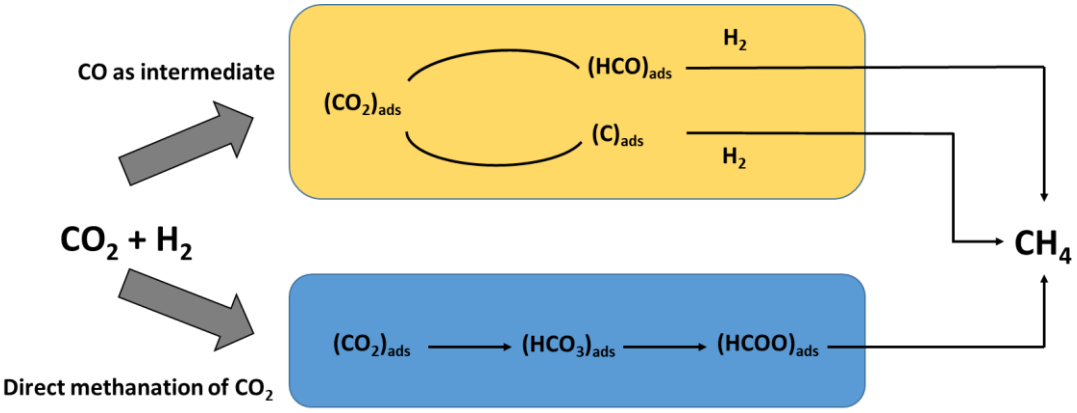

Figure 3. Suggested methanation pathways

Methanation of CO_2 over catalysts based on transition and platinum group metals (e.g., Co, Fe, Ru, Rh etc.) has been reported in literature[33-37, 41], with Ni based catalysts being the most popular choice for industrial applications due to their low cost and high activity[42]. Recently, the intrinsic kinetics of CO_2 methanation over an industrial based Ni catalyst was studied, with a formyl intermediate mechanism being selected then validated by the simulation of an isothermal plug-flow reactor [43]. Ni-based catalysts are known to undergo serious deactivation by poisoning [14], sintering [44] or coking at high temperatures [45] and the issue of catalyst stability has not been yet properly addressed.

The presence of sulphur compounds in the feed gas stream, e.g. H_2S in biogas, causes the poisoning of Ni-based catalysts by loss of catalytically active sites [46]. Deactivation by poisoning can be avoided through desulfurization treatments. Catalyst sintering by the formation of $Ni(CO)_4$ also plays an important role in the deactivation of Ni-based catalysts [44]. In the absence of catalytic poisons, Ni-based catalyst deactivation is mainly caused by carbon deposition. Catalyst deactivation by carbon deposition occurs by fouling the catalyst surface, blocking catalyst pores and disintegrating the catalyst support [47], as shown in Figure 4.

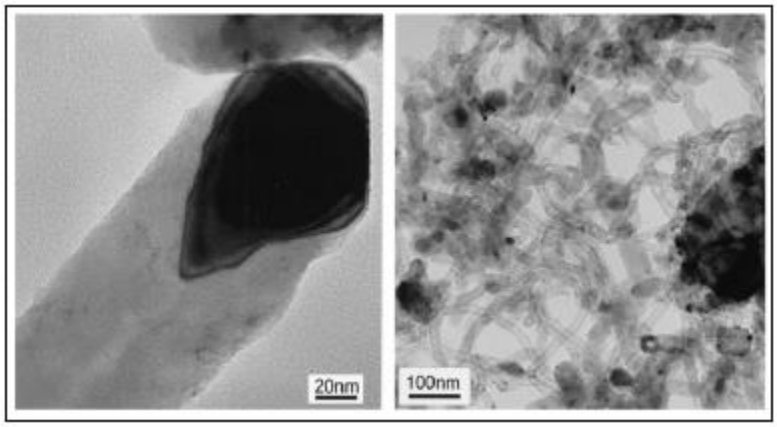

Figure 4. TEM images of carbon fibers deposited. Adapted from [47].

Whisker like carbon formation at temperatures greater than 450°C, encapsulating hydrocarbon films formed by polymerization at temperatures below 500°C and pyrolytic carbon formation by cracking of hydrocarbons above 600°C are the three major forms of carbon deposition on Ni-based catalysts [14]. Methane cracking, Eq. (7), the Boudouard reaction, Eq. (8) and CO reduction, Eq. (9) are the reactions leading to carbon deposition in the methanation process [48].

$$CH_4 \rightleftarrows C + 2H_2 \qquad \Delta H^{\circ}_{298} = -123.3 \text{ kJ/mol} \tag{7}$$

$$2CO \rightleftarrows C + CO_2 \qquad \Delta H^{\circ}_{298} = -125.2 \text{ kJ/mol} \tag{8}$$

$$CO+H_2 \rightleftarrows C+H_2O \qquad \Delta H^{\circ}_{298} = -84.0 \text{ kJ/mol} \tag{9}$$

Past study results have indicated that the major cause of carbon deposition on Ni-based catalysts in the CO_2 methanation process is methane cracking [49] and modelling studies have examined the importance of thermal management in a Sabatier reactor to prevent catalyst deactivation. However, these studies have assumed a first order deactivation reaction order [13]. Recently, kinetic models for the formation of nanofibrous carbon by methane cracking have been developed, which might help better explain the mechanism for carbon deposition over Ni-based catalysts [50].

While a great deal of work has gone into synthesizing and characterizing new methanation catalysts, more investigations into the use of these catalysts in larger scale reactors still needs to be done. One study examined a 2D heterogeneous fixed bed reactor model and compared the model results to both an annual fixed-bed reactor filled with approximately 400 g of nickel catalyst and a pseudo-homogenous model. At an operating temperature and pressure of 523K and 0.4MPa it was found that the pseudo-homogenous model predicted 95% CO_2 conversion while the experimental value and heterogeneous model prediction were found to be 86% and 89% respectively. The heterogeneous model also predicted large radial CH_4 production and temperature gradients within the reactor and strong diffusion limitations within the catalyst particle[51]. The difference in the model and experimental results work suggests further study on the operation of larger CO_2 methanation reactors is required, as it is already known that catalyst deactivation by coking can occur under CO_2 methanation reaction conditions.

3.0 Model Formulation

3.1.1 Membrane reactor configuration and dimensions

A schematic representation of the suggested membrane Sabatier reactor is shown in Figure 5. The reactor is a heat-exchanger type comprised of three compartments. The packed bed reaction compartment is internally cooled by molten salt flowing in multiple cooling tubes. The H_2 containing stream is fed to multiple membrane tubes (solely permeable to H_2). Molten salt was selected over conventional heat transfer fluids such as steam and mineral oils due to its higher operating temperatures, high density and heat capacity, and good thermal conductivity [11, 29]. The membrane dimensions (based on real, experimentally investigated membrane [52]) and corresponding reactor dimensions used in the simulation are listed in Tables 1, 2.

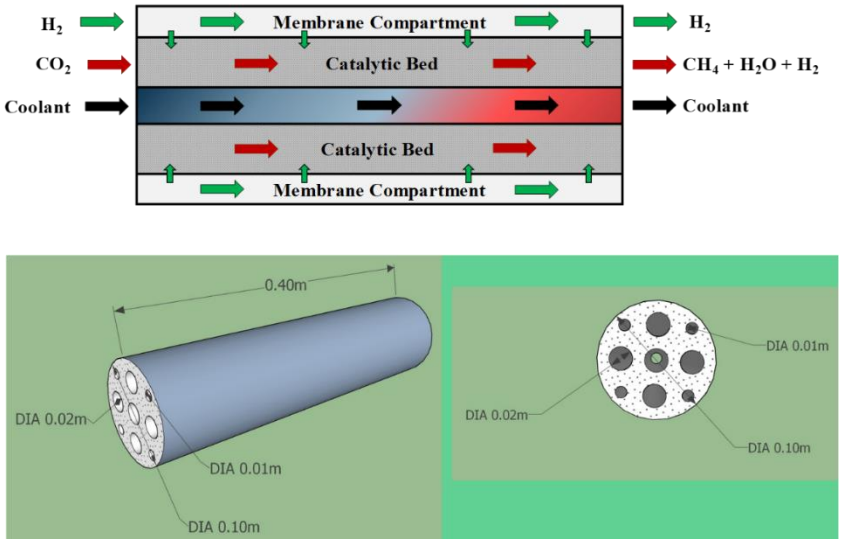

Figure 5. Molten salt cooled membrane Sabatier reactor, showing a conceptual schematic (upper figure) and multi-tube, heat exchanger-type configuration (bottom figure).

Table 1. Membrane dimensions and parameters

L (m)	D_m (m)	S_m (m^2)	E_{H_2} (kJ/mol)	A_{H_2} (mol / [m^2 s $bar^{0.5}$])
0.4	0.01	0.0126	11	5.6

D_m denotes the membrane diameter and L is the membrane length [20]. S_m is the membrane surface area. The membrane activation energy (E_{H_2}) and permeability (A_{H_2}) are from the literature [20].

Table 2. Membrane reactor dimensions

D_r (m)	D_c (m)	L (m)	d_w (m)	d_{iw} (m)	N_c	N_m	d_p (m)
0.1	0.02	0.4	0.002	0.05	5	4	0.003

D_r and D_c denote the diameter of the packed bed and coolant compartments, respectively. L is the reactor length. d_w is the wall thickness of the reactor and cooling tubes. d_{iw} is the insulation layer thickness. N_c and N_m is the number of cooling and membrane tubes, respectively. d_p is the spherical catalyst pellet diameter.

3.1.2 Actively cooled reactor configuration

A schematic representation of the suggested actively cooled Sabatier reactor is shown in Figure 6. The reactor is a heat-exchanger type comprised of two compartments. The packed bed reaction compartment is internally cooled by the coolant of choice flowing in multiple tubes. Reactor dimensions are listed in Table 3.

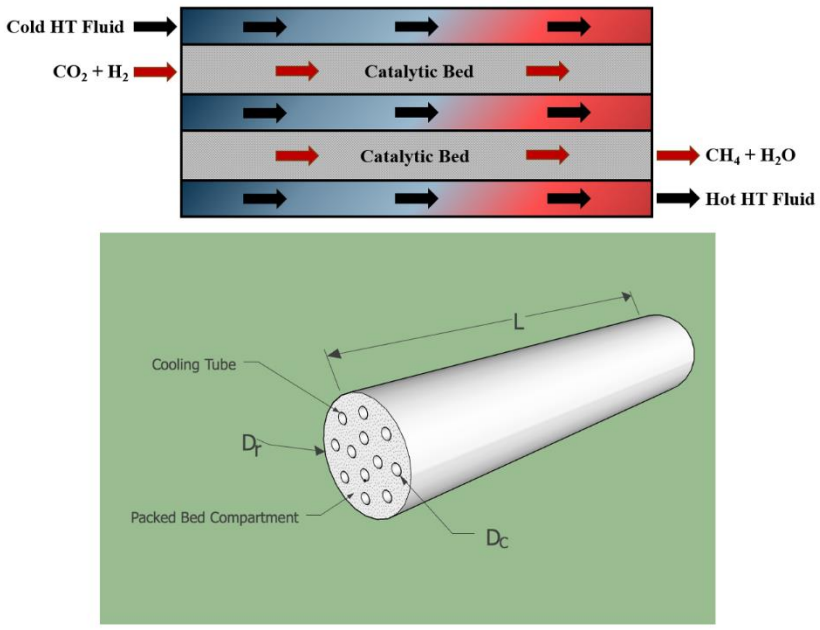

Figure 6. Actively cooled packed bed Sabatier reactor, showing a conceptual schematic (upper figure) and multi-tube, heat exchanger-type configuration (bottom figure).

Table 3. Actively cooled reactor dimensions

Parameter	Symbol	Value	Unit
Packed bed compartment diameter	D_r	0.1-0.3	m
Coolant compartment diameter	D_c	0.02-0.05	m
Reactor length	L	0.4-1.5	M
Number of cooling tubes	N_c	1-12	-
Reactor and cooling tube wall thickness	d_w	0.002	m
Insulation layer thickness	d_{iw}	0.05	m
Spherical catalyst pellet diameter	d_p	0.003-0.005	m

3.1.3 Model equations

A transient 1D pseudo-homogenous model [11, 13, 27, 30] was used to simulate the reactor. Although the model does not account for radial gradients, 1D models normally describe well relatively small packed beds, at least capturing qualitative trends [53]. Also, the reactor geometry was configured to minimize the radial distance between compartments [11, 13]. The model accounts for temperature variations in the heat transfer fluid, temperature dependence of thermo-physical properties, and includes axial mass and heat dispersion. The following assumptions were applied:

- Ideal Gas Law
- Radial gradients are negligible
- The membrane is exclusively permeable to H_2; and,
- The membrane interior is at the same temperature as the packed bed

Component mass balances for the packed bed ($k \equiv$ PB) and membrane ($k \equiv$ M) compartments are given by Eq. (10) ($i \equiv H_2$, CO_2, CO, CH_4, H_2O for $k \equiv$ PB and $i \equiv H_2$, I for $k \equiv$ M; I stands for gases not permeating the membrane). Note that $R_{ij} = 0$ for $k \equiv$ M and $A_i = 0$ for all i except for $i \equiv H_2$. Energy balances in the packed bed and molten salt compartments are described by Eqs (11) and (12), respectively. Dynamic evolution of the catalyst activity (a) reflecting the catalyst deactivation by carbon (c) deposition (coking) is described by Eqs (13, 14) [54]. Note that reaction terms in Eqs (10, 11) are multiplied by the catalyst activity. Kinetics and transport parameters are described in *Sections 3.1.4* and *3.1.5*. Notation is explained in *Nomenclature*. Initial and boundary conditions are listed in Eqs (15, 16).

$$\varepsilon^k \frac{\partial C_i^k}{\partial t} = D_{ae}^k \frac{\partial^2 C_i^k}{\partial z^2} - \varepsilon^k \frac{\partial \left(C_i^k v_g^k \right)}{\partial z} + a(1-\varepsilon^k)\rho_s^k \sum_j \eta_j R_{ij} -$$
$$-a_{v,M}^k A_i \exp\left(\frac{-E_a}{R_g T} \right) \Delta\left(\sqrt{p_i} \right)^k \tag{10}$$

$$(\rho C_p)_{eff} \frac{\partial T}{\partial t} = k_{ae} \frac{\partial^2 T}{\partial z^2} - \varepsilon \rho_g C_{pg} v_g \frac{\partial T}{\partial z} +$$
$$+a(1-\varepsilon)\rho_s \sum_j (-\Delta H_j)\eta_j R_j - U_{w,HE} a_{r,HE} (T - T_c) - U_{w,HL} a_{r,HL} (T - T_e) \tag{11}$$

$$\rho_c C_{pc} \frac{\partial T_c}{\partial t} = \lambda_c \frac{\partial^2 T_c}{\partial z^2} - \rho_c C_{pc} v_c \frac{\partial T_c}{\partial z} - U_{w,HE} a_{c,HE} (T_c - T) \tag{12}$$

$$\frac{da}{dt} = -k_a r_{\max}^2 ca \tag{13}$$

$$\frac{dc}{dt} = r_{\max} a \tag{14}$$

$$\begin{array}{lll} z = 0 & (\varepsilon v_{gf})^k (C_{i,f}^k - C_i^k) = -D_{ae}^k \frac{\partial C_i^k}{\partial z} & z = L \quad \frac{\partial C_i^k}{\partial z} = 0 \\ & \varepsilon \rho_g v_{gf} C_{pg} (T_f - T) = -k_{ae} \frac{\partial T}{\partial z} & \frac{\partial T}{\partial z} = 0 \\ & \rho_c v_c C_c (T_{c,f} - T_c) = -\lambda_c \frac{\partial T_c}{\partial z} & \frac{\partial T_c}{\partial z} = 0 \end{array} \tag{15}$$

$$\begin{array}{ll} t = 0 & C_i^k(0,z) = C_{i,\text{int}}^k \\ & T(0,z) = T_{\text{int}} \\ & T_c(0,z) = T_{c,\text{int}} \\ & a(0,z) = 1 \\ & c(0,z) = 0 \end{array} \tag{16}$$

The change in the gas velocity due to the change in number of moles in the reaction was calculated using Eq. (17). Pressure drop was accounted for using the Ergun equation, Eq. (18), with a fixed outlet pressure (in a practical situation will be set by a back pressure regulator). Note

that the total pressure (*P*) affects reaction kinetics through partial pressures, as shown in Eqs. (20-22) in *Section 3.1.4*. The effective heat capacity in Eq. (11) is defined by Eq. (19).

$$v_g = \frac{v_{gf}}{C_{tf}} \sum_i C_i \tag{17}$$

$$\frac{dP}{dz} = -150 \frac{(1-\varepsilon)^2 \mu_g}{d_p^2 \varepsilon^3} v_g - 1.75 \frac{(1-\varepsilon)\rho_g}{d_p \varepsilon^3} v_g^2 \tag{18}$$

$$(\rho C_p)_{eff} = \varepsilon \rho_g C_{pg} + (1-\varepsilon)\rho_s C_{ps} \tag{19}$$

3.1.4 Reaction and catalyst deactivation kinetics

A Ni/Al_2O_3 catalyst was selected for the reaction (packed bed) compartment. Reaction rate expressions from the literature were implemented, Eqs (20-22) [55]. These kinetic expressions, although originally developed for methane steam reforming, account for the reversibility of all reactions involved. Therefore, it is expected that Eqs (20-22) can describe the Sabatier-CO methanation-reverse water gas shift reaction system described by Eqs (1-3). This assumption was experimentally validated using a commercial Ni catalyst (12 wt% Ni/Al_2O_3, BASF, supplied by Research Catalysts, Inc. USA); kinetic parameters were estimated through the non-linear least squares regression (*Appendix A.2*).

$$R_1 = \frac{k_1}{p_{H_2}^{2.5}} \left(p_{CH_4} p_{H_2O} - \frac{p_{H_2}^3 p_{CO}}{K_{1,eq}} \right) \frac{1}{\text{den}^2} \tag{20}$$

$$R_2 = \frac{k_2}{p_{H_2}} \left(p_{CO} p_{H_2O} - \frac{p_{H_2} p_{CO_2}}{K_{2,eq}} \right) \frac{1}{\text{den}^2} \tag{21}$$

$$R_3 = \frac{k_3}{p_{H_2}^{3.5}} \left(p_{CH_4} p_{H_2O}^2 - \frac{p_{H_2} p_{CO_2}}{K_{3,eq}} \right) \frac{1}{\text{den}^2} \tag{22}$$

$$\text{den} = 1 + K_{CO} p_{CO} + K_{H_2} p_{H_2} + K_{CH_4} p_{CH_4} + \frac{K_{H_2O} p_{H_2O}}{p_{H_2}}$$

$$k_j = A_j \exp\left(\frac{-E_j}{R_g T}\right) \qquad K_i = B_i \exp\left(\frac{-\Delta H_i}{R_g T}\right) \qquad K_{j,eq} = B_j \exp\left(\frac{-\Delta H_j}{R_g T}\right)$$

The catalyst deactivation was assumed to be solely induced by CH_4 cracking [13], with the deactivation rate expression (k_a, r_{max} in Eqs (23, 24)) adopted from the literature [54]:

$$k_a = k_{a,ref} \exp\left(\frac{E_a}{R_g}\left[\frac{1}{T_{ref}} - \frac{1}{T}\right]\right) \tag{23}$$

$$r_{\max} = \frac{k_d\left(P_{CH_4} - \frac{P_{H_2}^2}{K_p}\right)}{\left(1 + K_H P_{H_2}^{0.5}\right)^2} \tag{24}$$

$$k_d = k_{d,ref} \exp\left(\frac{E_a}{R_g}\left[\frac{1}{T_{ref}} - \frac{1}{T}\right]\right) \qquad K_p = B_p \exp\left(-\frac{\Delta H}{R_g T}\right) \qquad K_H = k_{H,ref} \exp\left(\frac{E_a}{R_g}\left[\frac{1}{T_{ref}} - \frac{1}{T}\right]\right)$$

Parameters are given in *Appendix C* [54]. Note that Eq. (24) accounts for the reversibility of CH_4 cracking via carbon gasification by H_2.

3.1.5 Transport parameters

The analysis of standard criteria for transport limitations [56, 57] (*Appendix D*) under relevant conditions (600-800 K, 5-10 bar, gas velocity of 0.04-0.2 m/s), and using previously estimated kinetic parameters, has shown that interparticle and interphase transport limitations are negligible for methanation reactions. On the other hand, for the reverse water gas shift reaction the intraparticle mass transfer resistance was found to be significant. To account for that transport

limitation the internal effectiveness factor was calculated (for all reactions), using the standard expression for a spherical pellet [58]:

$$\eta_j = \frac{3}{\phi_j}\left(\frac{1}{\tanh\phi_j} - \frac{1}{\phi_j}\right) \qquad \phi_j = \sqrt{\frac{\hat{k}_j d_p^2}{4D_m}} \tag{24}$$

Axial mass and heat dispersion in a packed bed, Eqs (10,11), was accounted for through the following correlations:

$$D_{ae} = \varepsilon\left(\frac{D_m}{\tau_b} + 0.5 d_p v_g\right) \qquad \tau_b = \frac{1}{\varepsilon^{0.5}} \tag{25}$$

$$k_{ae} = \lambda_g\left(8 + 0.05\,\mathrm{Re}_p^{1.09}\right) \tag{26}$$

The effective axial mass dispersion coefficient, Eq. (25), was calculated using a typical correlation adopted from the literature [59]. The expression for the effective axial heat dispersion coefficient, Eq. (26), was derived from the heat conductivity correlations developed for catalytic fixed beds [60, 61], by plotting k_{ae} vs. $\mathrm{Re_p}$ in the relevant range and least squares fitting [11].

Wall heat transfer coefficients for heat exchange between the packed bed and cooling tube, Eq. (27), and heat loss to the environment, Eq. (28), were calculated by resistances in series. These parameters account for the contribution of the packed bed (h_{wr}), cooling tube or reactor wall (λ_w), molten salt (h_{wc}), insulation layer (λ_{iw}), and natural convection from the external reactor surface (h_{nc}).

$$U_{w,HE} = \left(\frac{1}{h_{wr}} + \frac{d_w}{\lambda_w} + \frac{1}{h_{wc}}\right)^{-1} \tag{27}$$

$$U_{w,HL} = \left(\frac{1}{h_{wr}} + \frac{d_w}{\lambda_w} + \frac{d_{iw}}{\lambda_{iw}} + \frac{1}{h_{nc}} \right)^{-1} \tag{28}$$

The effective wall heat transfer coefficient for the reaction compartment (h_{wr}) was estimated using the following correlation:

$$Nu_p = \frac{h_{wr} d_p}{\lambda_g} = 24 + 0.34\,\mathrm{Re}_p^{0.77} \tag{29}$$

This expression was obtained in a similar way as Eq. (26), using a complete set of the original correlations [60, 61] and least squares fitting [11]. The effective wall heat transfer coefficient for the coolant tube (h_{wc}) was estimated using the following correlations from the literature [62-64]:

$$\mathrm{Re}_c < 2030 \qquad Nu_c = 3.66 + \frac{0.065\,\mathrm{Re}_c\,\mathrm{Pr}_c (D_c / L)}{1 + 0.04[\mathrm{Re}_c\,\mathrm{Pr}_c (D_c / L)]^{2/3}} \tag{30a}$$

$$2030 < \mathrm{Re}_c < 4000 \qquad Nu_c = 0.012(\mathrm{Re}_c^{\,0.87} - 280)\,\mathrm{Pr}_c^{\,0.4} \left[1 + (D_c / L)^{2/3} \right] \tag{31b}$$

$$\mathrm{Re}_c > 4000 \qquad Nu_c = 0.027\,\mathrm{Re}_c^{\,0.8}\,\mathrm{Pr}_c^{\,1/3} \tag{32c}$$

$$Nu_c = \frac{h_{wc} D_c}{\lambda_c} \qquad \mathrm{Re}_c = \frac{v_c \rho_c D_c}{\mu_c} \qquad \mathrm{Pr}_c = \frac{C_{pc} \mu_c}{\lambda_c}$$

The values for the insulation layer (quartz wool) conductivity (λ_{iw}) and natural convection (h_{nc}) were adopted from the literature [65, 66]. These contributions were dominant in Eq. (28) and the wall heat loss coefficient was nearly constant in all simulations: $U_{w,HL} \approx 0.01$ W/(m^2 K).

3.1.6 Reactor performance

Space velocity is defined as follows ($k \equiv$ PB, M for the packed bed (PB) and membrane (M) compartments (note that v_{gf} enters boundary conditions, Eq. (17)):

$$SV_k = \frac{\varepsilon^k v_{gf}^k}{L} \tag{33}$$

The reference gravimetric flow rate of the coolant (molten salt) is calculated as follows:

$$G_{c,0} = \frac{y_{CO_2} \Delta H_{SR} F_{tf}}{C_{pc} \Delta T_{MS}} \qquad F_{tf} = \rho_{gf} V_{PB} SV_{PB} \tag{34}$$

In this equation, $G_{c,0}$ is calculated when the rate of heat generation (for complete CO_2 conversion and no CO formation) is equal to the rate of heat removal (assuming complete CO_2 conversion, no CO formation, and that ΔT_{MS} = 300 K.

In the Sabatier reactor simulations, the reactor performance is evaluated in terms of CO_2 conversion (Eq. (35)), selectivity to CH_4 formation (Eq. (36)), and CH_4 yield (Eq. (37)):

$$X_{CO_2} = \frac{y_{CO} + y_{CH_4} - \beta(y_{CO} + y_{CO_2} + y_{CH_4})}{(1-\beta)(y_{CO} + y_{CO_2} + y_{CH_4})} \tag{35}$$

$$S_{CH_4} = \frac{y_{CH_4} - \beta(y_{CO} + y_{CO_2} + y_{CH_4})}{y_{CO} + y_{CH_4} - \beta(y_{CO} + y_{CO_2} + y_{CH_4})} \tag{36}$$

$$Y_{CH_4} = X_{CO_2} S_{CH_4} \tag{37}$$

In Eqs. (35-37), y_{CO_2}, y_{CO}, and y_{CH_4} stand for mole fractions and β represents the fraction of CH_4 in the combined CH_4 and CO_2 feed (molar feed rate of CH4 divided by the sum of molar feed rates of CH_4 and CO_2). Note that $\beta = 0$ when there is no CH_4 in the feed. See *Appendix F* for derivations.

3.1.7 Numerical procedure

The model was solved using the MATLAB PDE solver with a second order accurate spatial discretization based on a fixed set of user-specified nodes and time integration done by the stiff

ODE solver (ode 15s). Dependences of thermophysical properties (density, viscosity, gas diffusivity, heat capacity and thermal conductivity) on temperature, pressure and composition were accounted for using polynomial regressions fitted to the data on thermophysical properties from the literature [64, 67-69]. Molten salt properties were adopted from the data on commercially available molten salts (Dynalene, Inc. [70], Dynalene MS-2). In all simulations, initial temperatures and concentrations, Eq. (16), were set to 550 K and 0 mol/m^3 respectively. Void fraction (ε) was set to 0.5.

4.0 Results and Discussion

4.1 Membrane Sabatier reactor model

4.1.1 Simulation Conditions

All simulation parameters are listed in Table 4. The reaction compartment is fed with a stoichiometric mixture of H_2 and CO_2 for the non-membrane reactor ($H_2/CO_2 = 4$) and a mixture of 10% H_2 and 90% CO_2 for the membrane reactor ($H_2/CO_2 = 0.11$). Membranes are assumed to be fed with a H_2-containing stream, assuming 60% H_2 content in a gasifier outlet [71]. Pressure drop was found to be negligible in all simulations. Membrane reactor code can be seen in *Appendix H.*

Table 4. Membrane reactor operating conditions.

Parameter	Symbol	Value	Unit
Reaction compartment feed composition	H_2/CO_2	4[a], 0.11[b]	-
Membrane feed H_2 mole fraction	$y_{H_2,M}$	0.6	
Packed bed space velocity	SV_{PB}	100-1000	h^{-1}
Space velocity ratio	SV_M / SV_{PB}	0-100	-
Normalized cooling rate	$G_c/G_{c,0}$	0.1-1	-
Reaction compartment feed pressure	$P_{t,f}$	5-10	bar
Membrane compartment pressure	$P_{t,M}$	20	bar
Reaction compartment feed temperature	T_f	650	K
Coolant feed temperature	$T_{c,f}$	550	K

a – non-membrane reactor

b – membrane reactor

4.1.2 Catalyst deactivation effect in a non-membrane reactor

First, the performance of a non-membrane packed bed Sabatier reactor is analyzed (by setting $SV_M = 0$). Typical spatial profiles of mole fractions and temperature in the packed bed and cooling compartments are shown in Figure 7, for low and intermediate space velocity. The simulation predicts that the reaction takes place predominately at the reactor entrance, where fast consumption of H_2 and CO_2 is accompanied by a rise in the reactor temperature. No CO formation was observed owning to efficient cooling, as is evident from almost overlapping packed bed and molten salt temperature profiles. Therefore, Eq. (34) can be used to estimate the gravimetric flow rate of the coolant. These results are expected and qualitatively consistent with previous studies [11, 13].

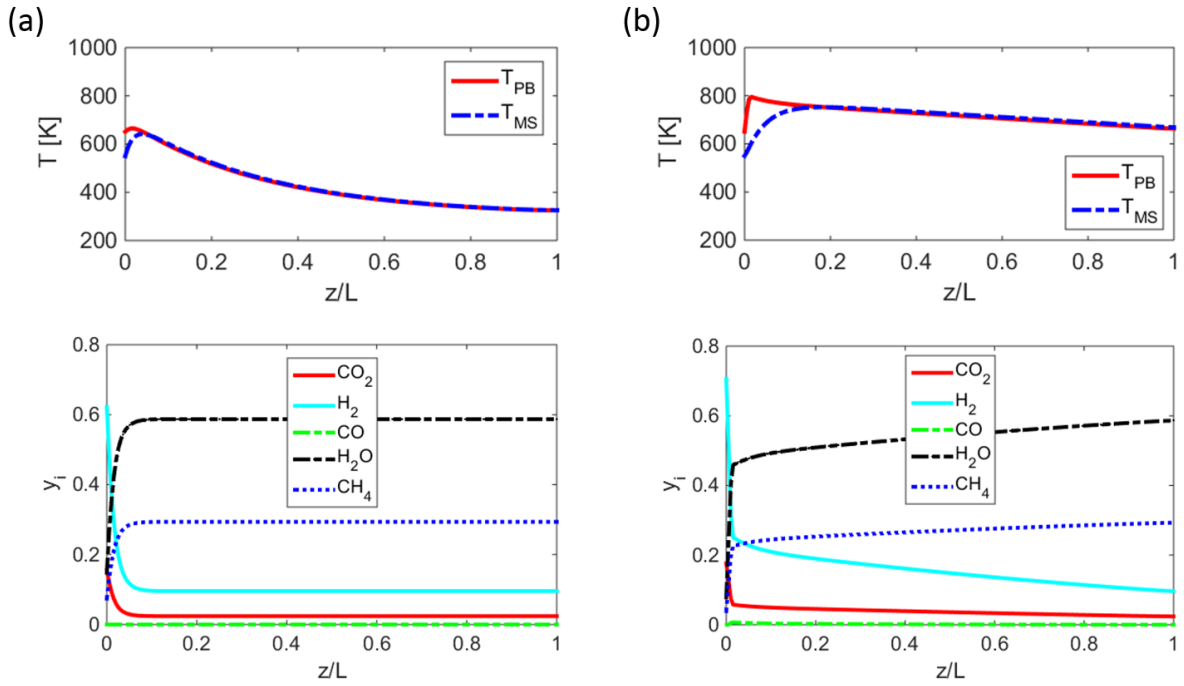

Figure 7. Spatial profiles of temperature (upper panels) and mole fractions (lower panels) in a non-membrane Sabatier reactor ($SV_M = 0$) for $SV_{PB} = 100\ h^{-1}$ (a) and $SV_{PB} = 1000\ h^{-1}$. T_{PB} and T_{MS} are the temperatures of the packed bed and coolant respectively. *Parameters:* $P_{t,f} = 5$ bar, $G_c = 0.1G_{c,0}$, $H_2/CO_2 = 4$, TOS = 10 h.

Spatial profiles of mole fractions and temperatures for a slightly higher feed pressure ($P_{t,f}$ = 10 bar) are shown in Figure 8. At TOS = 10 h the spatial profiles are similar to those obtained at identical space velocity at $P_{t,f}$ = 5, with the reactor outlet mainly containing CH_4 and H_2O, with some unreacted H_2 and CO_2. The temperature rise near the reactor's entrance is higher as compared to that shown in Figure 7, which can be attributed to the higher gas stream density. The difference between the temperature in the packed bed and molten salt compartments near the reactor entrance indicates that the rate of heat generation is significantly higher than the rate of heat removal. After 50 h of simulated time on stream, spatial profiles indicate that the reactor underwent extinction.

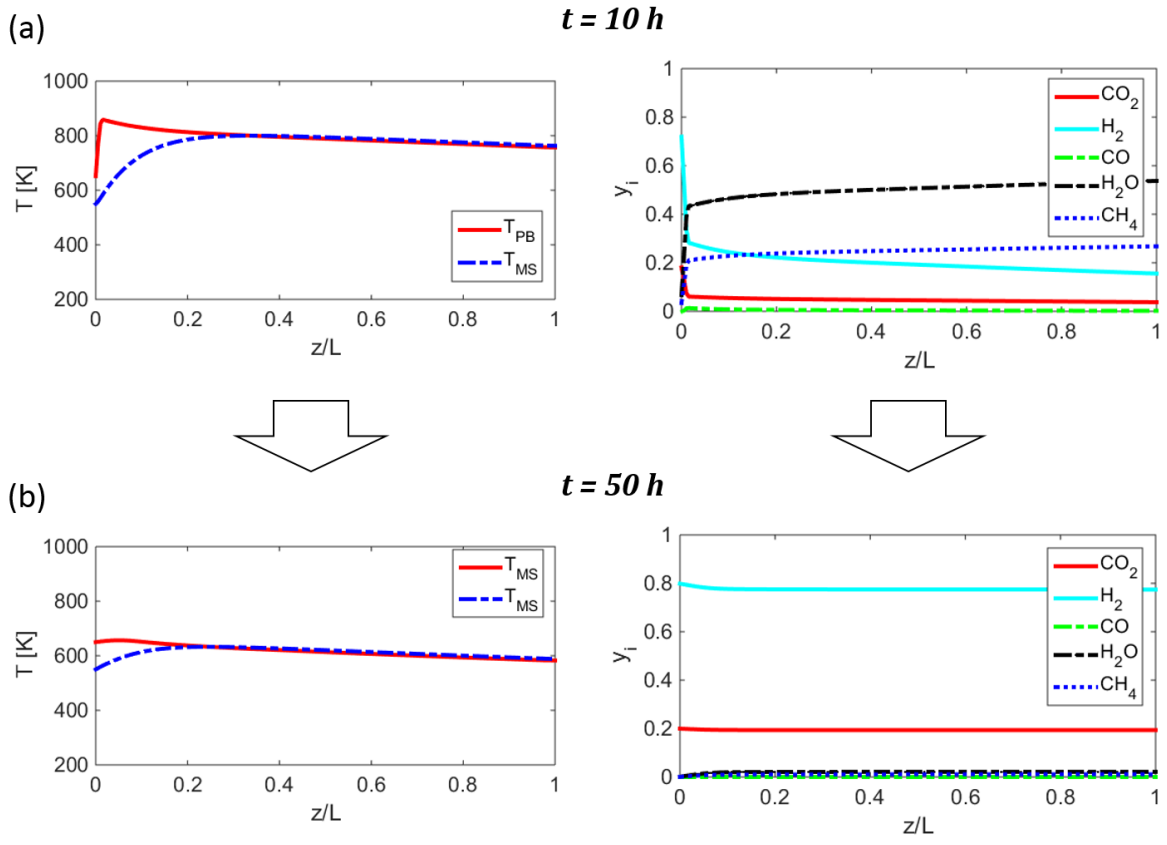

Figure 8. Spatial profiles of mole fractions and temperature in a non-membrane reactor for TOS = 10 h (a) and TOS = 50 h (b). *Parameters:* SV_M = 0, SV_{PB} = 1000 h^{-1}, $P_{t,f}$ = 10 bar, $G_c = 0.1G_{c,0}$, H_2/CO_2 = 4.

The reactor extinction is further demonstrated in Figure 9, showing the spatiotemporal evolution of the catalyst activity, temperature, mole fractions, conversion and selectivity. After approximately 20 h of simulated time, the activity starts to decrease at the reactor inlet forming a dynamic front that propagates towards the reactor outlet, Figure 9a. This drop in activity is due to the catalyst deactivation accelerated by the elevated temperature that also forms a dynamic front propagating downstream, Figure 9a.

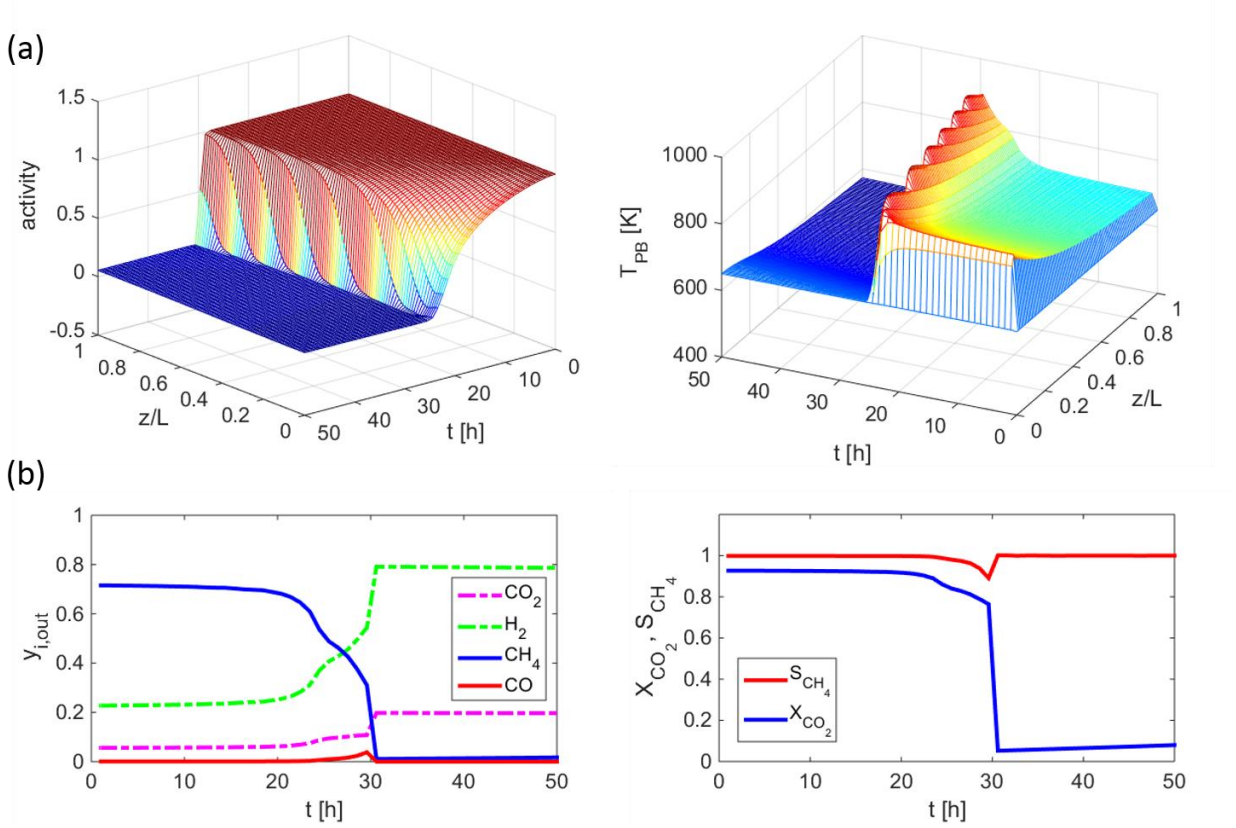

Figure 9. Dynamic behavior of the non-membrane reactor undergoing catalyst deactivation, showing spatiotemporal profiles of the catalyst activity and packed bed temperature (a) and the reactor outlet mole fractions (on dry basis), conversion and selectivity (b*). Parameters:* $SV_M = 0$, $SV_{PB} = 1000\ h^{-1}$, $P_{t,f} = 10$ bar, $G_c = 0.1G_{c,0}$, $H_2/CO_2 = 4$.

As the reactor undergoes extinction, the outlet CH_4 mole fraction and corresponding CO_2 conversion start to decrease gradually and eventually drop sharply, Figure 9b. The model clearly

demonstrates the catalyst deactivation and the dynamic phenomenon of reactor extinction. This observation is important and should be taken into consideration in the design of methanation reactors.

4.1.3 Membrane Sabatier reactor with distributed H_2 supply

One possible way to avoid the severe catalyst deactivation demonstrated in the previous section, Figure 9, is to supply H_2 in a distributed manner, through a H_2-selective membrane. Such reactor configuration could result in a more uniform temperature profile without a sharp temperature rise at the reactor entrance. Typical spatial profiles of mole fractions in the packed bed and membrane compartments for the membrane reactor are shown in Figure 10.

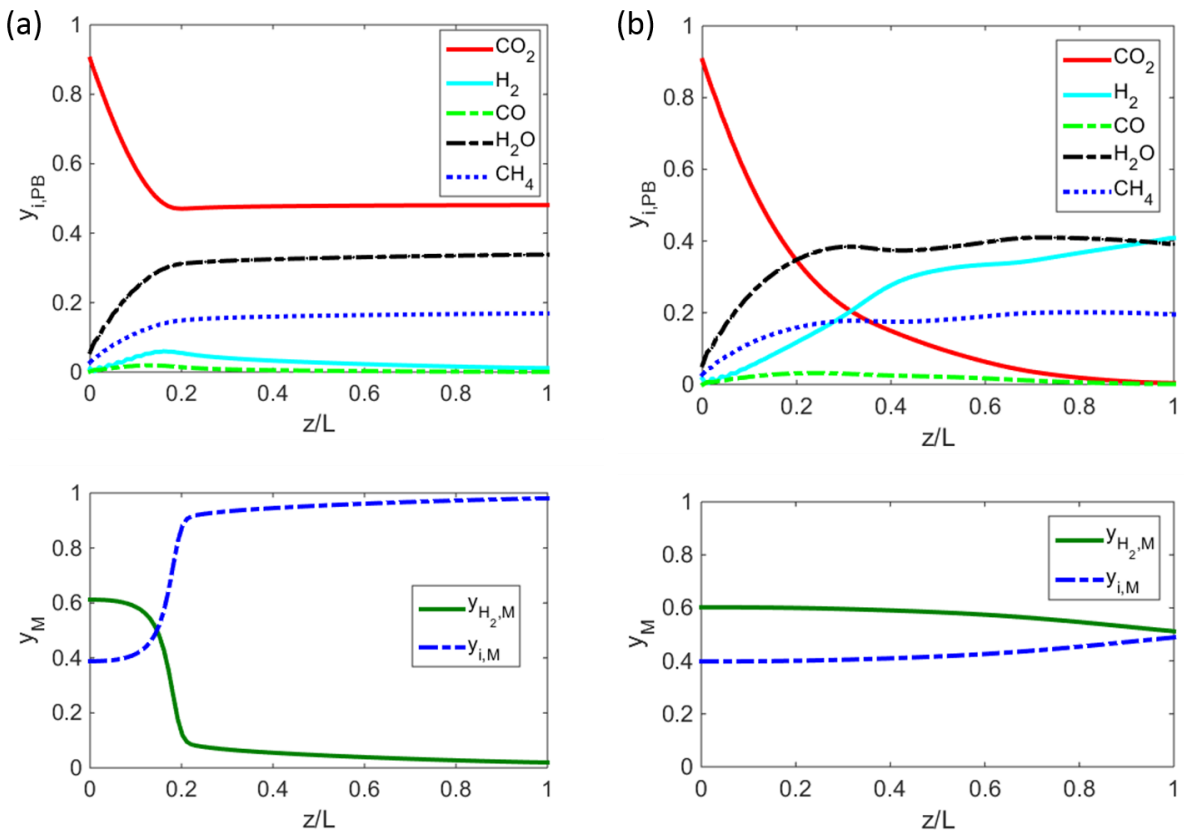

Figure 10. Spatial profiles of mole fractions in the membrane Sabatier reactor in the reaction (upper panels) and membrane (lower panels) compartments, for SV_M/SV_{PB} = 10 (a) and SV_M/SV_{PB} = 50 (b). *Parameters:* SV_{PB} = 222 h^{-1}, $P_{t,f}$ = 10 bar, $G_c = 0.1G_{c,0}$, H_2/CO_2 = 0.11, TOS = 100 h.

At a relatively low membrane space velocity, Figure 10a, H_2 is almost completely depleted in the membrane compartment at z/L = 0.2, leading to poor CO_2 conversion. Once the membrane space velocity is increased 5-fold, Figure 10b, nearly 100% of the CO_2 is converted in the reactor. In a practical application, the excess of H_2 in the outlet stream of the reaction compartment can be removed by standard separation techniques, such as pressure swing adsorption (PSA), and recycled back to the reactor inlet. Water can be easily removed by condensation, resulting in a product stream mainly containing CH_4 that is renewable natural gas (RNG).

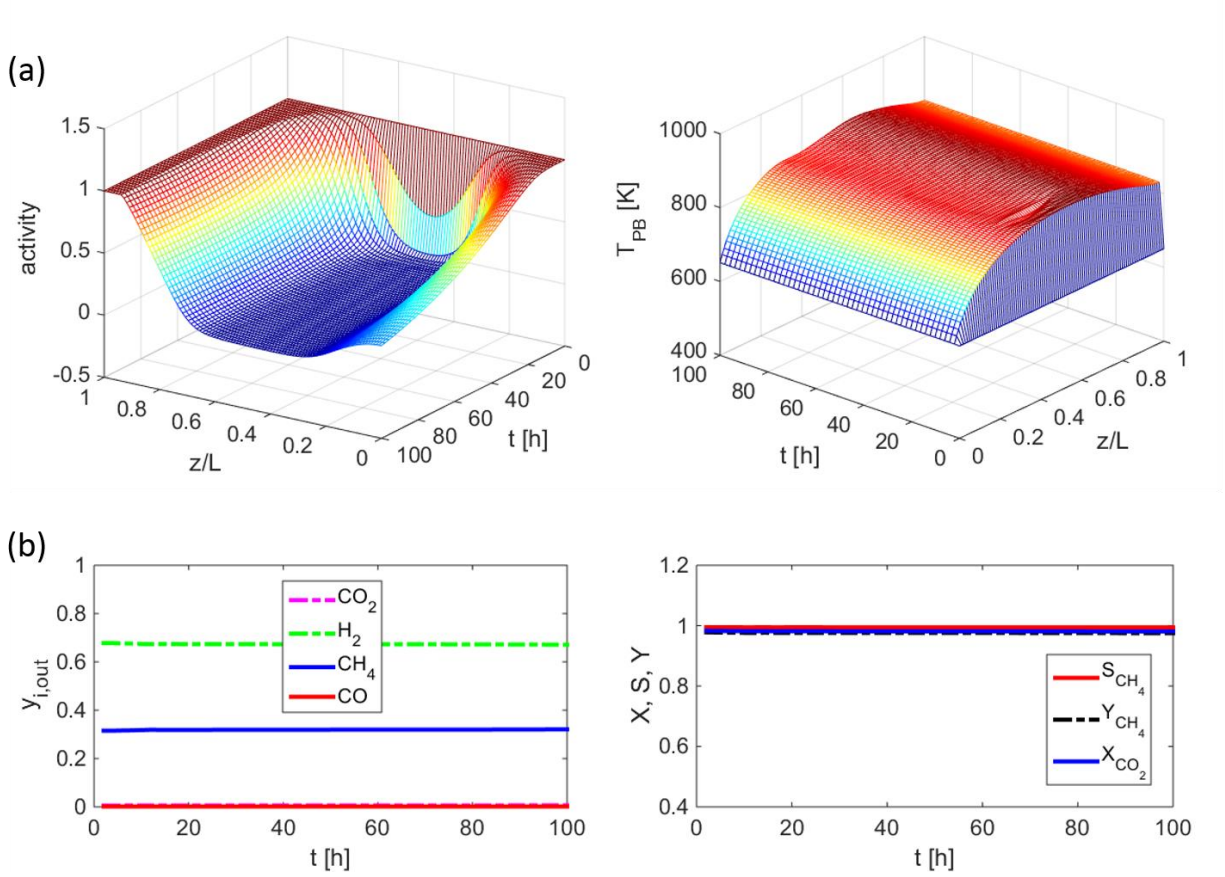

Figure 11. Spatiotemporal profiles of the packed bed temperature (a) and catalyst activity (b) for the membrane Sabatier reactor. *Parameters*: SVPB = 222 h-1, Pt,f = 10 bar, Gc = 0.1Gc,0. , SV,M/SV,PB = 50, H2/CO2 = 0.11.

Examination of the dynamic evolution of the membrane reactor has shown a very significant improvement of the reactor stability owing to a more uniform temperature profile in the reaction compartment, Figure 11a. Although catalyst deactivation still occurs in the central part of the reactor, where the temperature is relatively high, there is a sufficient catalyst activity near the reactor inlet and outlet. Over the simulated TOS of 100 h, there is no detectable deactivation, with CO_2 conversion, selectivity and yield achieving nearly 100%. Note that the CO_2 feed molar rate for SV_{PB} = 222 h^{-1} and H_2/CO_2 = 0.11 used to generate Figure 11 is equivalent to that obtained with SV_{PB} = 1000 h^{-1} and H_2/CO_2 = 4 for the non-membrane reactor, Figure 9. Therefore, for

identical CO_2 feed molar rate the membrane reactor shows better resistance to catalyst deactivation than the non-membrane reactor.

4.1.4 Effect of space velocity and cooling rate

Evolution of the reactor performance as a function of the normalized membrane space velocity is shown in Figure 12 (upper panel, other parameters are listed in the figure caption). As expected, increasing the membrane flow rate for a fixed packed be flow rate leads to higher conversions, simply because more H_2 is permeating through the membrane (see also Figure 11). For $SV_M/SV_{PB} > 50$, conversion, selectivity and yield attain their maximum values (100%).

Another important parameter is the cooling rate. For future RNG production system integration, minimizing the coolant flow rate will be desired to minimize operating costs. The reactor performance as a function of the normalized cooling rate is shown in the lower panel of Figure 12. For the $G_{MS}/G_0 = 0.01\text{-}1$ there is a maximum in the reactor performance, whereas for $G_{MS}/G_0 > 1$ there is a decline in CO_2 conversion, with no CO formation predicted. This observation is apparently contradictory because higher cooling rates are expected to improve CO_2 conversion in the highly exothermic Sabatier reaction. However, in the membrane Sabatier reactor, lowering the temperature also slows down the H_2 permeation through the membrane, which is temperature-activated, Eq. (10). Therefore, there is a trade-off between the positive effect of cooling that increases the CO_2 conversion (given that H_2 amount is sufficient) and also decreases the rate of catalyst deactivation, versus the negative effect of cooling on H_2 permeation. This is an interesting optimization problem for future work.

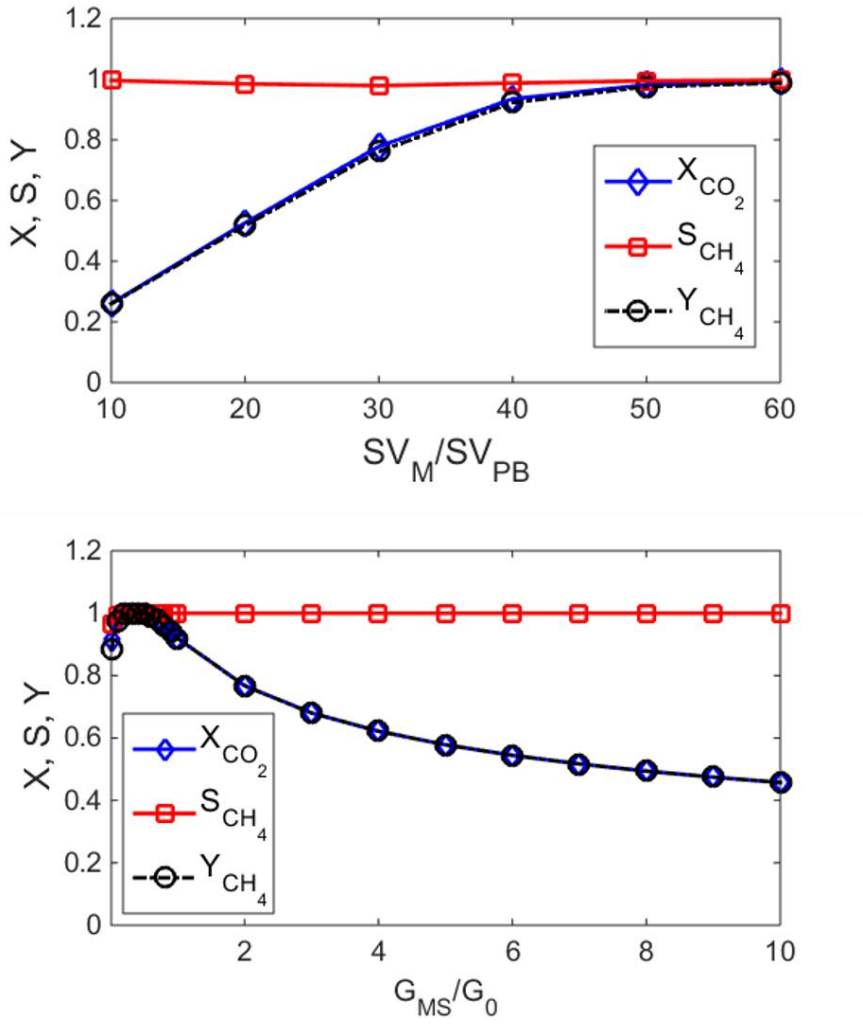

Figure 12. Reactor performance as a function of the normalized membrane space velocity (upper panel) and normalized cooling rate (lower panel, MS stands for molten salt). *Parameters:* SV_{PB} = 222 h^{-1}, $P_{t,f}$ = 10 bar, H_2/CO_2 = 0.11, TOS = 100 h, $G_c = 0.1G_{c,0}$ (upper panel), SV_M/SV_{PB} = 50 (lower panel).

An important requirement in improving the RNG generation system economics is maximizing the process throughput while maintaining high CH_4 yields. It is also important to reduce H2 concentration in the reactor outlet stream in order to lower the cost of downstream separation (see Figure 1 for a conceptual diagram of the process). In Figure 13, the CH_4 yield and reactor outlet

H_2 mole fraction are plotted as a function of the normalized cooling rate for different values of space velocities.

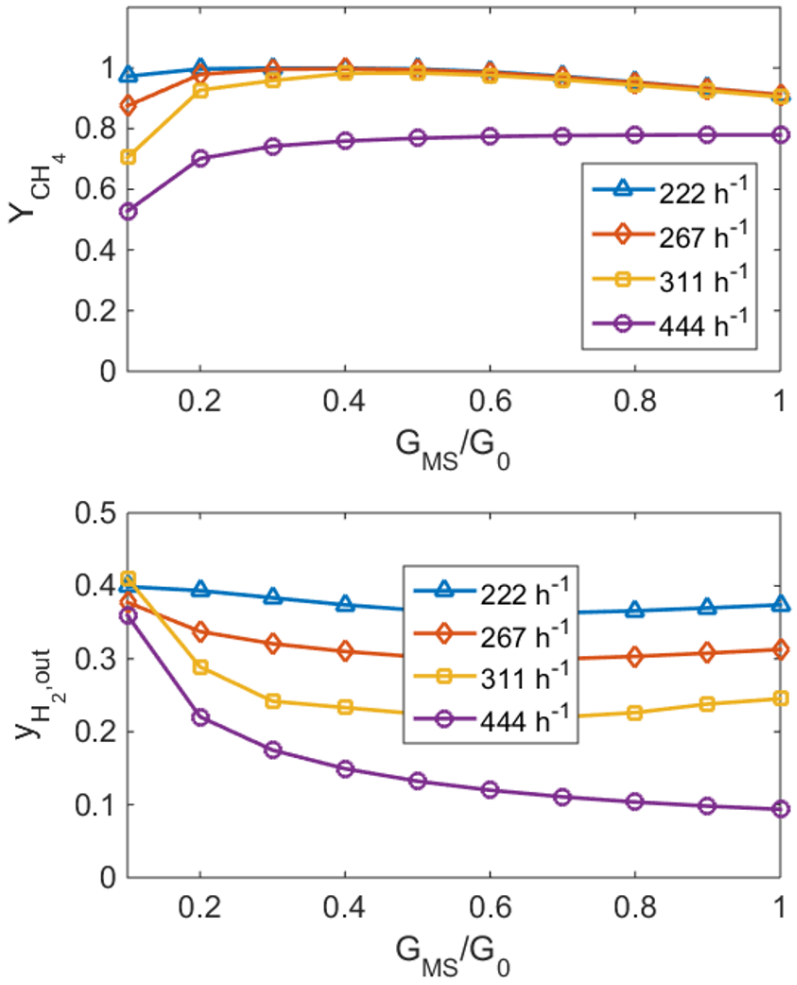

Figure 13. CH_4 yield (upper panel) and outlet H_2 mole fraction (lower panel) as a function of the normalized cooling rate for different values of space velocity (SV_{PB}). *Parameters*: $P_{t,f}$ = 10 bar, SV_M/SV_{PB} = 50, H_2/CO_2 = 0.11, TOS = 100 h.

For a particular cooling rate, increasing the packed bed space velocity (while keeping S_{VM}/SV_{PB} constant) leads to lower CH_4 yields. This behavior is expected and it was reported for the non-membrane, actively cooled Sabatier reactor [11, 13]. The drop in the CH_4 yield is due to lower residence time, but could be also a result of less efficient cooling [11]. However, there is

also a positive effect of the increasing space velocity as it leads to lower H_2 concentration in the reactor outlet stream (lower panel in Figure 13), as more H_2 is consumed. This observation represents another interesting optimization problem. This time a trade-off exists between the negative effect of the increasing space velocity on the CH_4 yield and its positive effect on lowering the H_2 content in the outlet steam. For $SV_{PB} = 311\ h^{-1}$ and $G_{MS}/G_0 = 0.4$, the H_2 outlet mole fraction dropped from 0.38 to 0.23, while keeping the CH_4 yield at nearly 100%. Such a significant difference in the H_2 content in the product stream would be beneficial for lowering the costs of H_2 separation.

4.1.5 Stability of the membrane Sabatier reactor

With a better understanding of how the membrane Sabatier reactor performs as a function of operating parameters, its long-term stability should now be evaluated. Temporal evolution of the packed bed temperature, catalyst activity and performance parameters (conversion, selectivity and yield) is shown in Figure 14 (operating parameters are listed in the figure caption). A stable temperature profile is formed, Figure 14a, with the reactor performance being stable during the 10,000 h of the simulated time, attaining the CO_2 conversion of 97% with no CO formation, therefore same CH_4 yield (97%), Figure 14b. Although there is a significant decline in the catalyst activity in the entire reactor, Figure 14b, the activity remains higher than 0.5, which is sufficient to attain a nearly complete CO_2 conversion. This result provides a theoretical (numerical) validation of the positive effect of distributed H_2 supply on the performance of a Sabatier reactor.

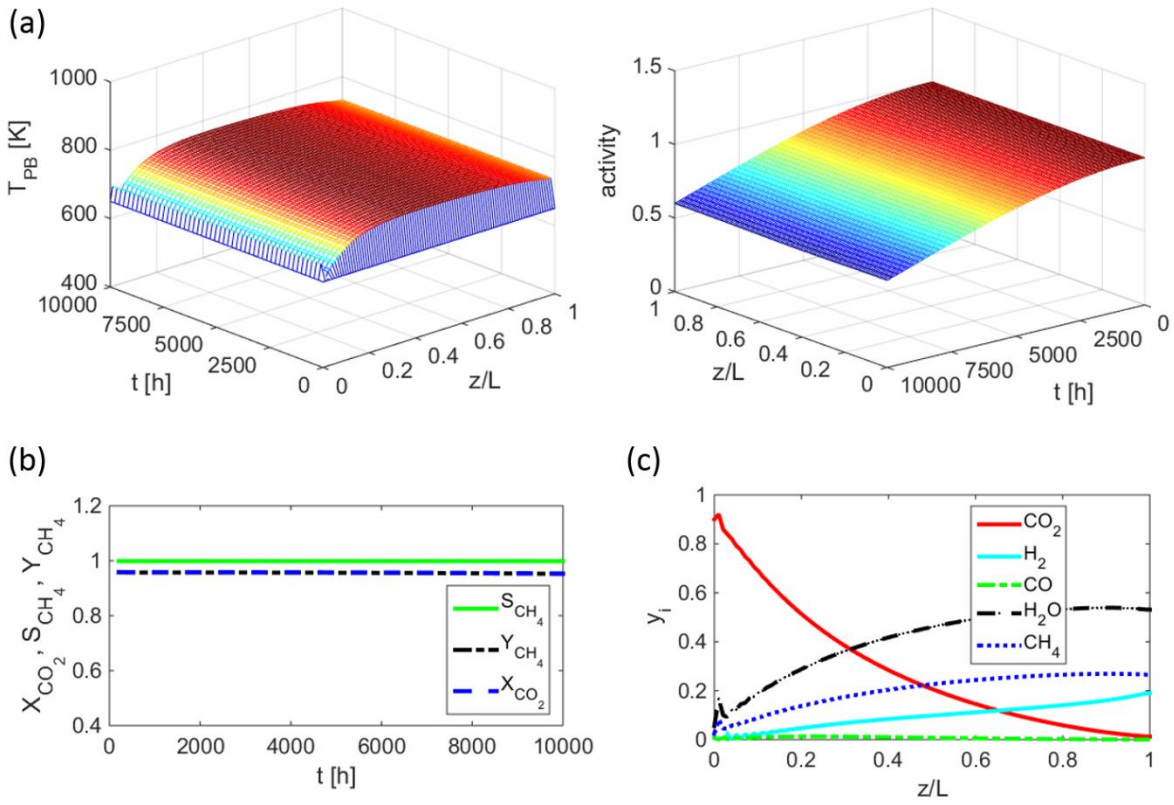

Figure 14. Dynamic evolution of the membrane reactor performance over 10,000 h, showing the spatiotemporal profiles of temperature and catalyst activity (a), temporal evolution of conversion, selectivity and yield (b), and spatial distribution of mole fractions at t = 10,000 h (c). *Parameters*: SV_{PB} = 333 h^{-1}, SV_M/SV_{PB} = 50, $G_c = 0.5G_{c,0}$, $P_{t,f}$ = 10 bar, H_2/CO_2 = 0.11

4.2 Actively cooled fixed bed Sabatier reactor model

The results of numerical simulations of the actively cooled packed bed Sabatier reactor are presented here. Compressed air is evaluated versus molten salt as a heat transfer fluid and effects of feed and cooling rates are investigated. The simulations results for pure CO_2 as a feedstock as well as for biogas feed are presented. Catalyst deactivation was not investigated in this study. Based on the results of the numerical investigation, a large-scale power-to-gas (PtG) system for

generating renewable natural gas (RNG) from landfill gas (LFG) is designed and simulated. The technoeconomic feasibility of the system is evaluated.

4.2.1 Simulation conditions

For a pure CO_2 feedstock, the reaction compartment is fed with a stoichiometric mixture of H_2 and CO_2 ($H_2/CO_2 = 4$). When biogas is used as feedstock, the feed mixture contains CH_4, CO_2 ($CH_4/CO_2 = 1.44$), and N_2, while keeping identical H_2/CO_2 ratio ($H_2/CO_2 = 4$). It is assumed that the biogas only contains CH_4, CO_2, and N_2, with all impurities being removed upstream (more details provided in *section 4.3*). Pressure drop was found to be negligible in all simulations and catalyst activity assumed to be unity. All simulation parameters are listed in Table 5. All symbols and abbreviations listed in *Nomenclature*. Actively cooled Sabatier reactor code can be seen in *Appendix I.*

Table 5. Actively cooled reactor operating conditions.

Parameter	**Symbol**	**Value**	**Unit**
Reaction compartment feed composition	H_2/CO_2	4	-
Reaction compartment biogas composition	CH_4/CO_2	0-1.44	-
Packed bed space velocity	SV	750-7000	h^{-1}
Normalized cooling rate	$G_c/G_{c,0}$	0.1-10	-
Reaction compartment feed pressure	$P_{t,f}$	10	bar
Reaction compartment feed temperature	T_f	550-650	K
Coolant feed temperature	$T_{c,f}$	550-650	K

4.2.2 Reactor simulations with pure CO_2 as a feedstock

For an actively cooled reactor, one of the crucial aspects is selection of an appropriate heat transfer fluid. Recent modeling studies have shown that molten salts could be a suitable cooling medium for Sabatier reactors.[11, 13] However, practical utilization of a molten salt-based cooling system could be challenging from a technical point of view, especially for large-scale systems. Molten salts solidify below certain temperature and decompose at high temperatures, with quite narrow operating ranges.[11, 13] It would be highly beneficial to use a heat transfer fluid as simple as compressed air. However, heat conductivity and capacity of compressed air are significantly lower than those for molten salts. Herein, we examine the possibility of using compressed air as a coolant for the packed bed Sabatier reactor. Steady-state spatial profiles of temperatures, mole fractions and reactor performance parameters for molten salt- and compressed air-cooled reactors obtained after 1 h simulated time-on-stream (TOS) are compared in Figure 15.

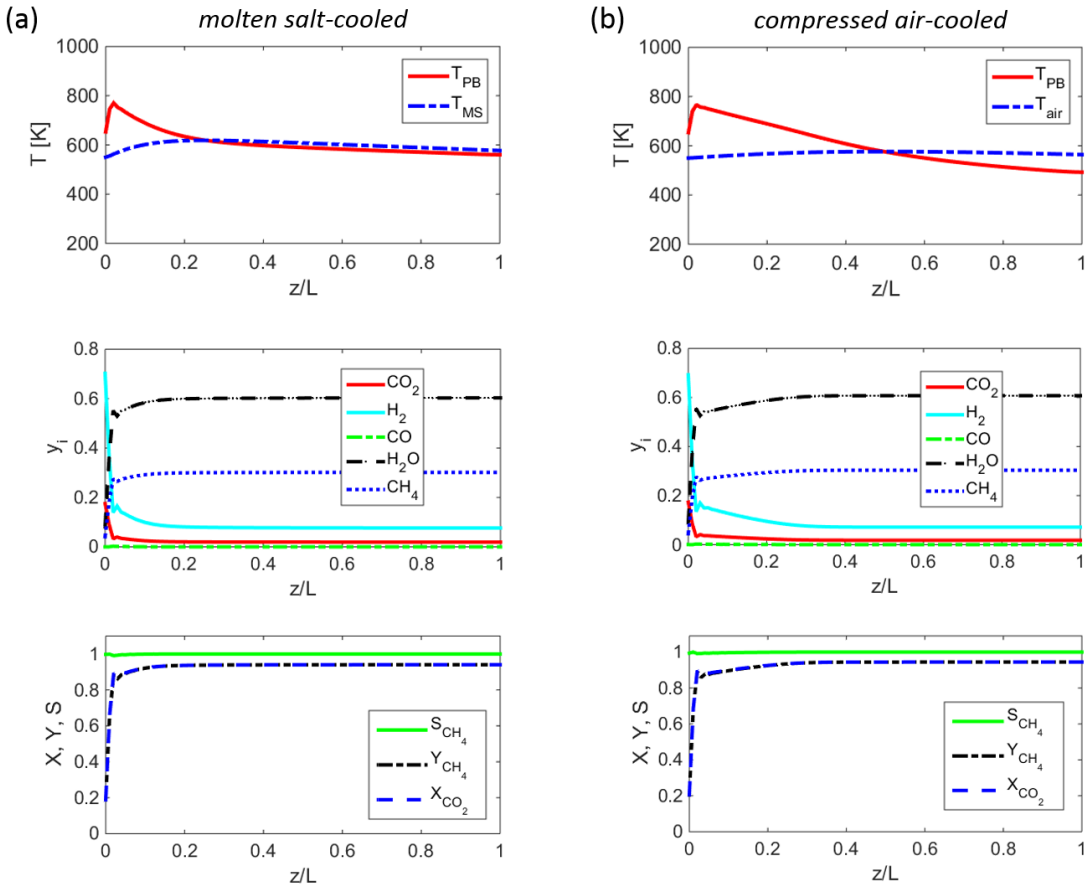

Figure 15. Spatial profiles of temperatures (T), mole fractions (y_i) and reactor performance (lower panel) for molten salt-cooled reactor (a) and compressed air-cooled reactor (b). TOS = 1 h; T_{PB}, T_{MS} and T_{air} are the temperatures of the packed bed, molten salt and air. Parameters: $T_f = T_{c,f} = 550$ K, SV = 250 h^{-1}, $G_c = G_{c,0}$, $CH_4/CO_2 = 0$, $D_r = 0.1$ m, $D_c = 0.02$ m, L = 0.4 m, $d_p = 0.003$ m, $N_c = 5$; other parameters are listed in Table 5.

Note that in both cases the gravimetric flow rate of cooling is identical, as $G_c = G_{c,0}$ (Eq (34)). In both cases (molten salt vs. compressed air), the reaction takes place at the reactor entrance, evidenced by the fast consumption of H_2 and CO_2 accompanied by a rise in the reactor temperature. The simulation predicts that both coolants can provide sufficient heat removal such that 95% CO_2 conversion is obtained with no CO formation observed (100% selectivity to CH_4 formation). An

important observation is that Eq. (34) provides a good estimate for a sufficient cooling rate, regardless of the type of coolant (liquid vs. gas).

Although the coolant temperature profiles are very similar in both cases, the packed bed temperature (T_{PB}) profiles are quite different. These differences can be attributed to the difference in heat transfer properties between the two cooling fluids. Compared to compressed air, molten salt has a high thermal conductivity and is much denser, allowing for the efficient removal of heat from the packed bed compartment. This is evident from the almost overlapping packed bed and molten salt temperature profiles in the molten-salt cooled reactor. Compressed air, with its heat transfer properties, is less efficient than MS in terms of heat removal evidenced by the difference in the compartment temperatures exiting the reactor. The gas exiting the packed bed compartment in the air-cooled reactor is cooler than the compressed air due to the poor heat transfer between the packed bed and coolant compartments and heat losses between the reaction compartment and the environment.

Despite the differences in heat transfer properties, the difference in the reactor performance between the two cases is negligible, meaning that it is possible to use compressed air as a heat transfer fluid for methanation (at least for low and intermediate space velocities). Using compressed air instead of molten salt is highly desirable from the point of view of system design due to its relatively low cost (compression power) and simplicity of operation. The performance of the air-cooled Sabatier reactor is further examined in Figure 16, showing spatiotemporal profiles and reactor performance (outlet temperatures, conversion and selectivity) as a function of space velocity. The number of cooling tubes was increased to 12 to increase the heat transfer efficiency.

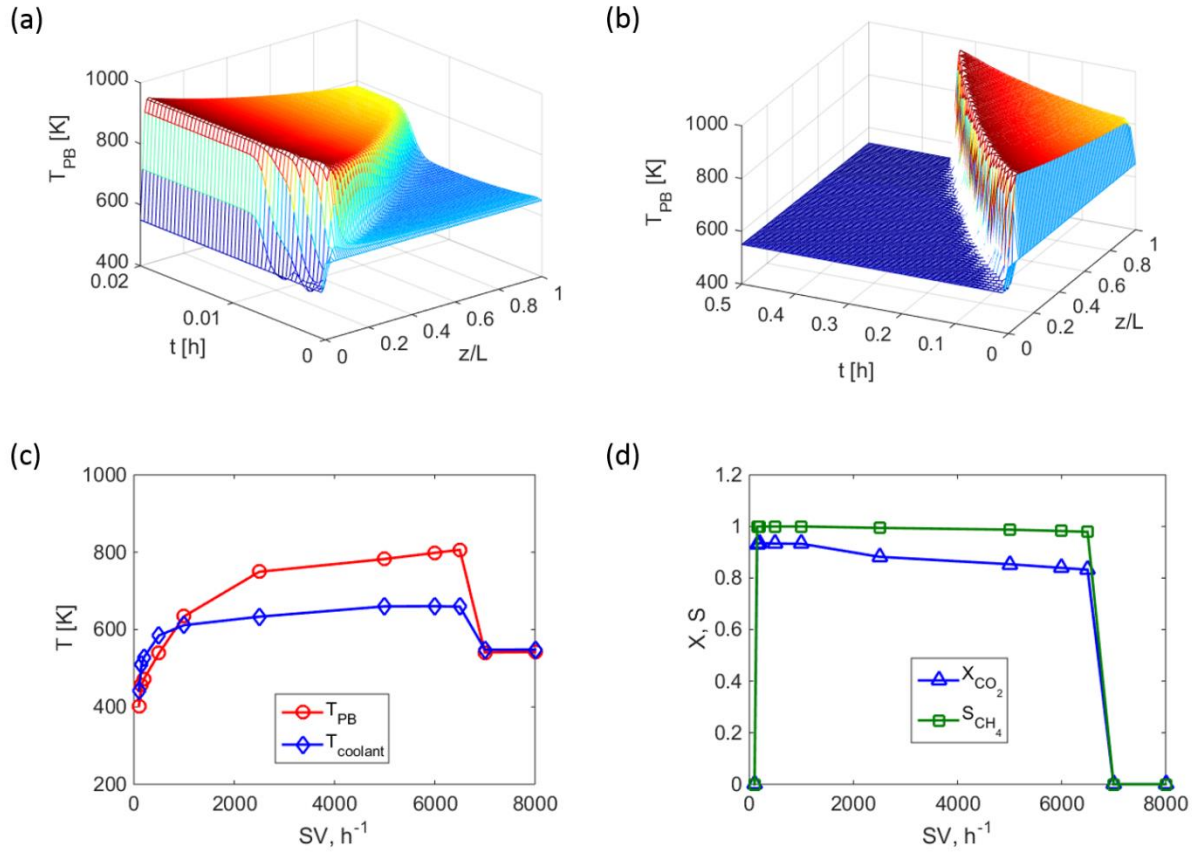

Figure 16. Air-cooled Sabatier reactor: spatiotemporal profiles of the packed bed temperature for SV = 5000 h^{-1} (a) and SV = 7000 h^{-1} (b), and the steady state reactor performance (TOS = 10 h) in terms of the outlet temperatures (c) and conversion, selectivity (d) as a function of space velocity. Parameters: $G_c = G_{c,0}$, $T_f = T_{c,f}$ = 550 K, CH_4/CO_2 = 0, D_r = 0.1 m, D_c = 0.02 m, L = 0.4 m, d_p = 0.003 m, N_c = 12; other parameters are listed in Table 5.

Figure 16a shows the ignition and stabilization of the reactor temperature profile at an elevated space velocity (SV = 5000 h^{-1}). The simulation predicts that ignition happens on a time scale of minutes establishing a stable temperature profile with a hot spot at the reactor entrance and a graduate decline in temperature along the axial dimension due to cooling. At a higher space velocity (SV = 7000 h^{-1}) the reactor, although initially ignited, undergoes gradual extinction driven by a downstream propagating thermal front (Figure 16b). This transient phenomenon is known to occur in exothermic packed beds under certain conditions.[11, 13, 27, 30] From a steady state

perspective, the case shown in Figure 16b represents a situation when the heat balance is such that there is not enough heat generated to sustain the reactor hot.

This is a very important phenomenon, which should be carefully considered, as even a slight increase in the reactor throughput can lead to its extinction. This extinction does not occur immediately but as a graduatal process, therefore could be difficult to recognize in a practical situation. Figures 16c and 16d clearly demonstrate the maximum limit of the reactor operation with respect to feed space velocity, which is equivalent to reactor throughput. As can be seen in Figure 16c, as space velocity is gradually increased, the outlet temperature of both the packed bed and coolant increases, which is attributed to more heat generation. For SV > 1000 h^{-1}, the difference between the packed bed and coolant outlet temperatures becomes significant and CO_2 conversion drops due to overheating (methanation reactions are exothermic and reversible, Eqs (1-3)). As CO_2 conversion decreases (Figure 16d), the reactor reaches the point where the heat generation is not sufficient to compensate for the cooling effect of increasing feed rate and the reactor becomes extinguished. Note that as space velocity is increased, the rate of cooling is increased accordingly since the $G_c/G_{c,0}$ ration is kept constant (Eq. (34)).

4.2.3 Reactor simulations with biogas feed

As previously mentioned (see *section 2.1*), investigations into methanation of biogas as a feedstock alternative to pure CO_2 have garnered interest due to the lowered capital and operating costs. Biogas already contains a significant fraction of CH_4 and has smaller amount of CO_2 that must be converted, as compared to a pure CO_2 stream. Direct use of biogas also eliminates the need in costly CO_2 separation, storage and transportation. First, the technical feasibility of the Sabatier reactor with a biogas feed needs to be investigated. The simulation results below are

obtained with the biogas feed composition that is typical for large landfill sites. These data were cordially provided by our industrial partner (Walker Industries Inc., Ontario, Canada). In the reactor simulations presented below, it was assumed that, after removing O_2 and N_2 from the raw gas, the landfill gas (LFG) contains 43 vol% CH_4, 30 vol% CO_2 and 27 vol% N_2.

Figure 17 shows the spatiotemporal profiles of temperature, time evolution of exit mole fractions and spatial profile of mole fractions for the air-cooled Sabatier reactor with a biogas feed. Reactor ignition occurs slightly after the reactor entrance for SV = 2500 h^{-1} (Figure 17a) and the ignition dynamics is slower than that shown in Figure 16a, which can be attributes to the lower feed rate of CO_2. Once the reactor is ignited, the temperature profile stabilizes similarly to the air-cooled reactor with pure CO_2 feed. Increasing space velocity to SV = 3000 h^{-1} leads to the downstream propagating thermal front followed by reactor extinction, similarly to the air-cooled reactor with pure CO_2 feed (Figure 16b).

Examining the exit mole fractions calculated on dry basis (after removal of water from the product stream) shows that, for the ignited reactor, the outlet stream contains 55% CH_4, 20% of unreacted H_2, 20% N_2, and 5% of unreacted CO_2. Such stream will clearly require post-processing to remove H_2 and N_2, and probably CO_2 (depending on the pipeline injection requirements). The steady state profile of mole fractions shows that a very significant amount of water (Figure 17a) will have to be removed from the outlet stream (ca. 30 vol%). This aspect will be addressed in *section 4.3*

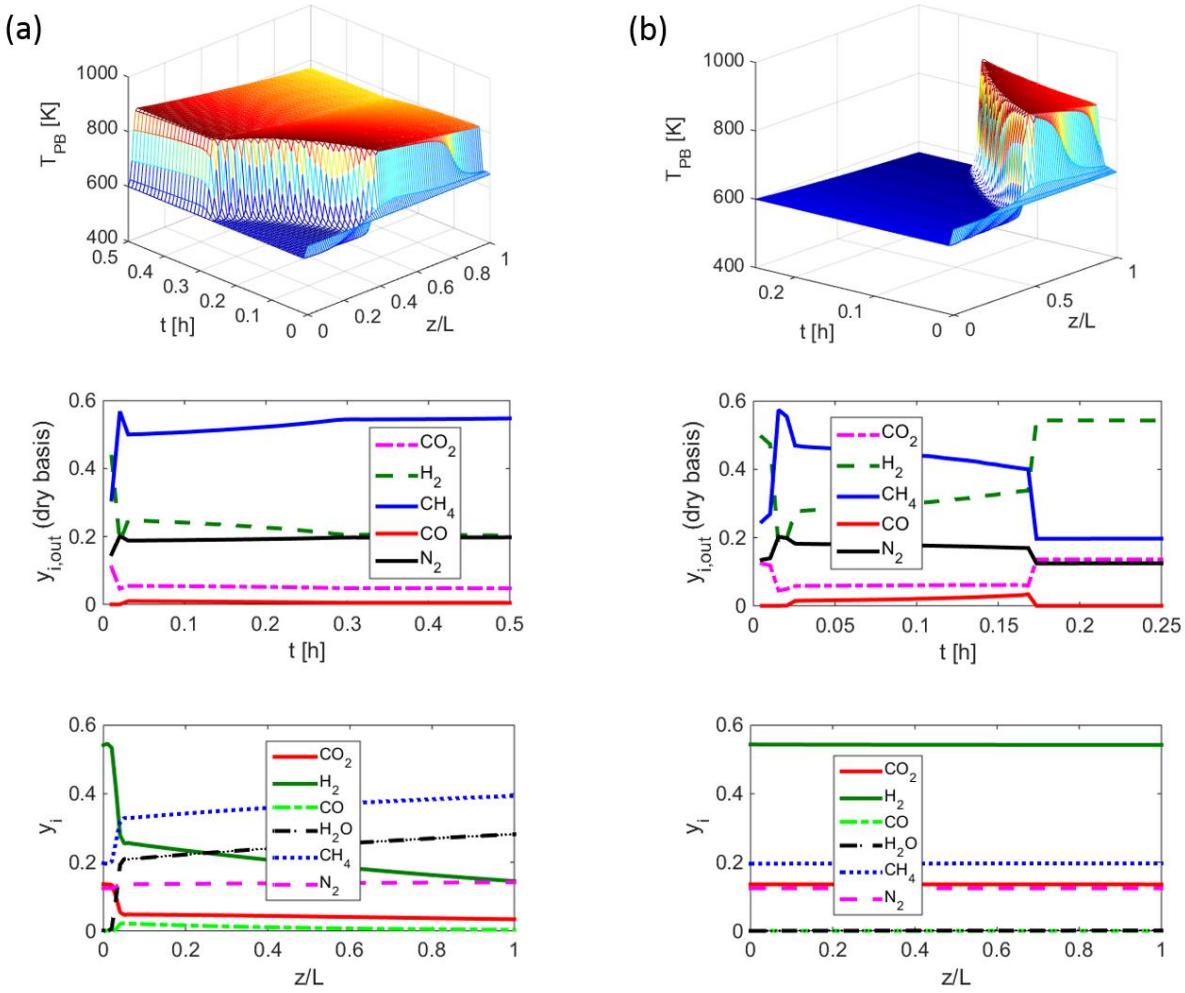

Figure 17. Air-cooled, biogas-fed Sabatier reactor simulated at SV = 2500 h^{-1} (a) and SV = 3000 h^{-1} (b), showing spatiotemporal temperature profiles (upper panels), temporal evolution of the outlet mole fractions (middle panel), and stationary spatial profiles of mole fractions (lower panel, TOS = 1 h). Parameters: $G_c = G_{c,0}$, $T_f = T_{c,f}$ = 600 K, CH_4/CO_2 = 1.44, D_r = 0.1 m, D_c = 0.02 m, L = 0.4 m, d_p = 0.003 m, N_c = 12; other parameters are listed in Table 5.

The combined effect of space velocity and cooling rate on the air-cooled, biogas-feed Sabatier reactor is examined in Figure 18. The obtained profiles resemble those obtained for the reactor with pure CO_2 feed, Figure 16. However, reactor extinction occurs at lower space velocity, which is attributed to a lower CO_2 content in biogas (30 vol%). Decreasing the cooling rate (G/G_0 = 0.1)

results in higher reactor bed temperatures (as expected) and leads to lower CO_2 conversions. Increasing the cooling rate to $G/G_0 = 10$ results in the overcooled reactor with no ignition. This finding points out at the importance of selecting a proper cooling rate. In addition, a simple estimation provided by Eq. (34) provides a good starting point for the reactor thermal management. The important outcome is that the model predicts CH_4 yields of up to 90%, Figure 18b.

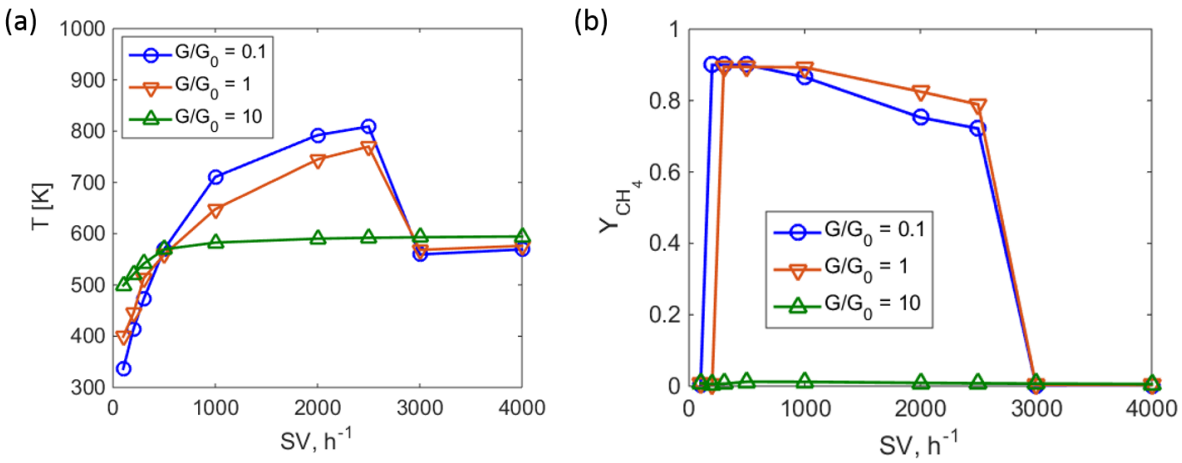

Figure 18. Air-cooled, biogas-fed Sabatier reactor: Steady state packed bed outlet temperature (a) and CH_4 yield (b) as a function of space velocity at varying cooling rates. Parameters: $T_f = T_{c,f} =$ 600 K, $CH_4/CO_2 = 1.44$, $D_r = 0.1$ m, $D_c = 0.02$ m, $L = 0.4$ m, $d_p = 0.003$ m, $N_c = 12$.

The simulations results have predicted that it is possible to achieve high CH_4 yields in a small-scale reactor ($L = 0.4$ m). It is now important to examine the performance of a scaled-up Sabatier reactor that could be integrated into a large-scale LFG upgrading facility. Figure 19 shows the performance of a large-scale (67 L) reactor, which could be run in parallel with other reactors in an array. Figure 19a and 19b show that the spatiotemporal temperature profile and spatial temperature and mole fraction profiles of the larger reactor are similar to those for a smaller reactor (Figure 17). The heat transfer between the packed bed and coolant tubes is quite efficient, although there is a significant difference between the bed and coolant temperatures (Figure 19b).

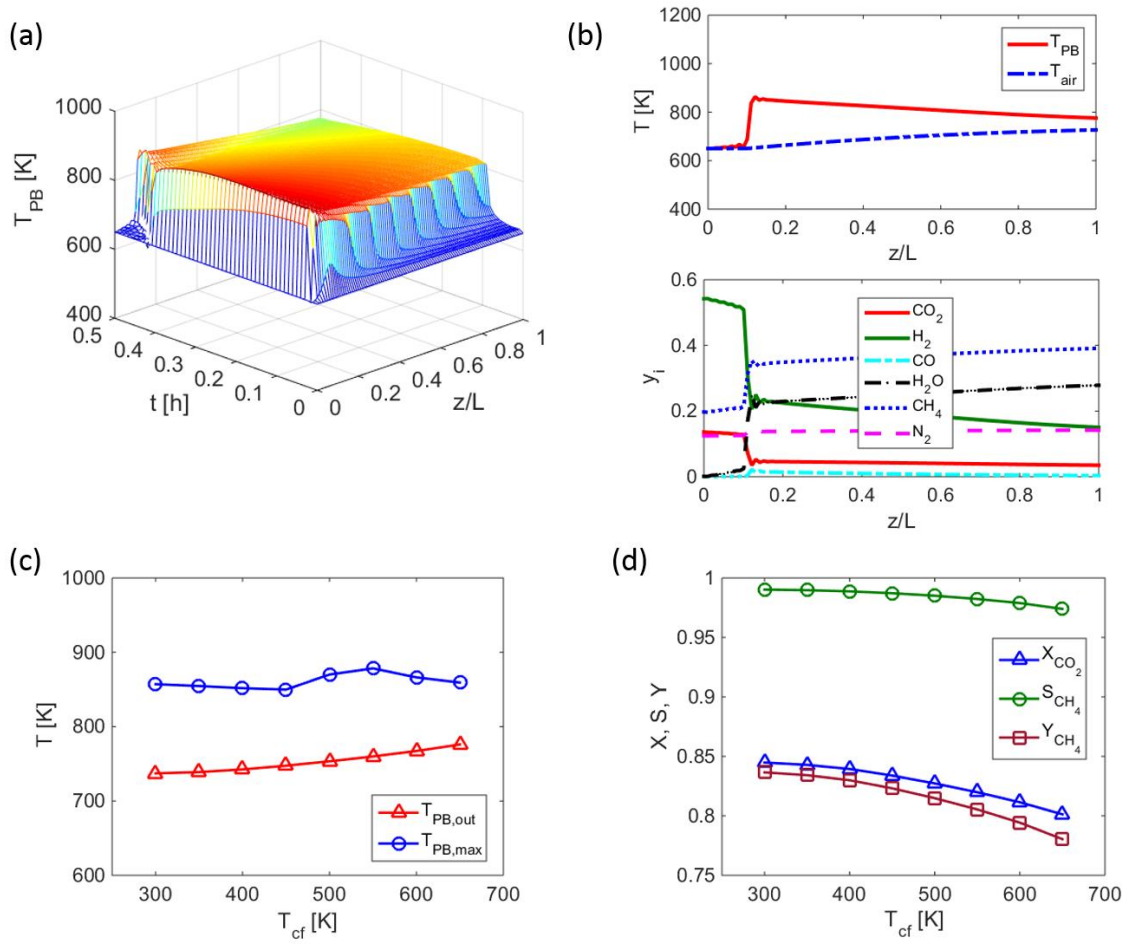

Figure 19. Air-cooled, biogas-fed Sabatier reactor: Spatiotemporal profile of the packed bed temperature (a) and stationary (TOS = 1 h) spatial profiles of temperatures and mole fractions (b). Packed bed temperature as a function of the inlet coolant temperature is shown in (c), with the corresponding reactor performance shown in (d). Parameters: SV = 750 h^{-1}, $G_c = 0.5G_{c,0}$, T_f = 650 K, $T_{c,f}$ = 650 K (a, b), CH_4/CO_2 = 1.44, **D_r = 0.3 m, D_c = 0.05 m, L = 1.5 m**, d_p = 0.005 m, N_c =12.

Next, the reactor performance is evaluated as a function of the coolant feed temperature (Figure 19c and 19d). Lowering the inlet coolant temperature decreases the reactor outlet temperature significantly, while the maximum bed temperature remains similar (Figure 19a). An important

observation is that decreasing the packed bed outlet temperature due to more efficient cooling results in a significant conversion improvement (Figure 19d).

4.3 Techno-economic assessment

After proving the technical feasibility of the air-cooled Sabatier reactor via numerical simulations, techno-economic evaluation is curried out in this section, assessing the techno-economic feasibility of a large-scale PtG system for converting LFG into RNG. Raw LFG is mainly composed of CH_4, CO_2, N_2, and O_2, with trace amounts of H_2S, siloxanes (Si), volatile organic compounds (VOC) and water vapor. Typical LFG specifications for a large landfill site (cordially provided by our industrial partner, Walker Industries Inc., Ontario, Canada) are listed in Table 6.

Table 6. Typical landfill gas feed specifications.

Parameter	**Value**
y(CH_4)	42% vol.
y(CO_2)	29% vol.
y(N_2)	23% vol.
y(O_2)	4% vol.
y(H_2O)	2% vol
y(Si)	60 ppm
y(H_2O)	600 ppm
y(VOC)	3000 ppm
Temperature	35 °C
Pressure	2.7 bar
Flow rate	5000 scfm

First, to verify that the reactor model simulated in MATLAB can be reproduced in the process simulation software, a packed bed, air-cooled reactor model was defined and simulated in Aspen HYSYS.

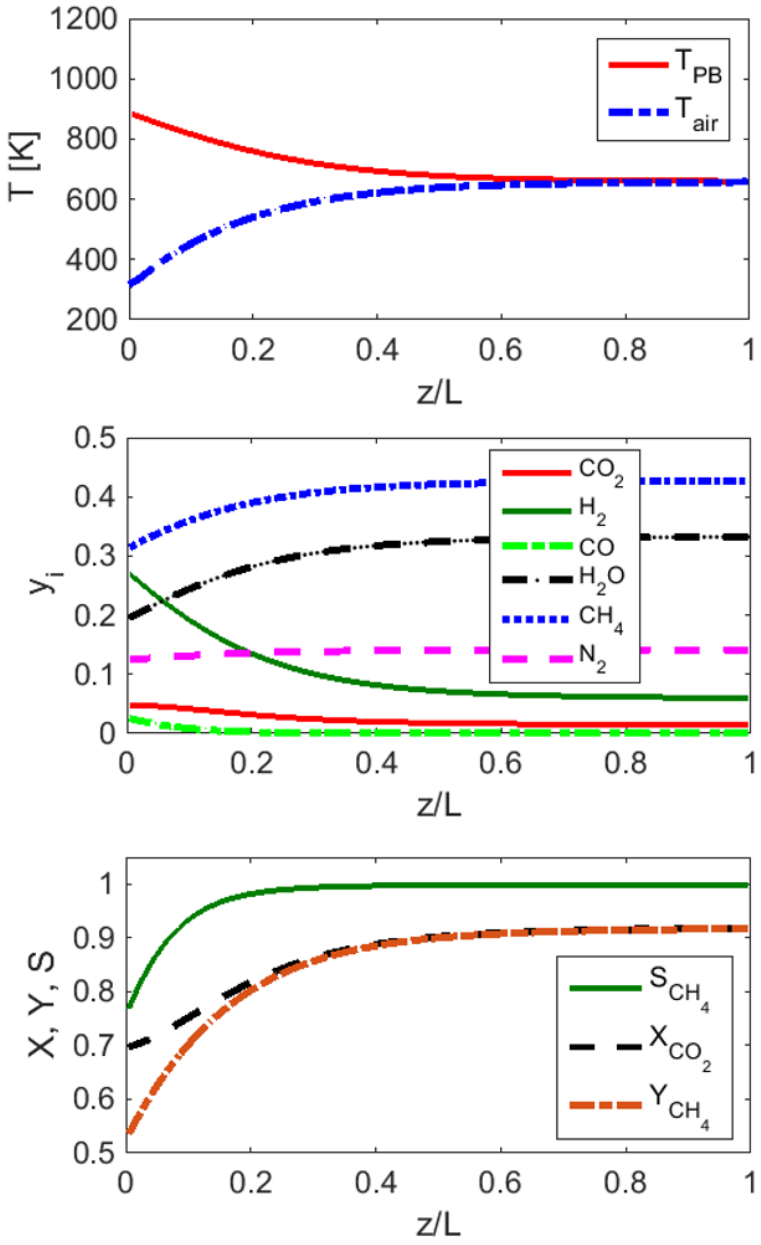

Figure 20. Spatial profiles of temperature (upper panels), mole fractions (middle panels) and reactor performance (lower panel) in the HYSYS simulated actively cooled packed bed Sabatier reactor. T_{PB} and T_{air} are the temperatures of the packed bed and air coolant respectively. *Parameters*: $P_{t,f}$ = 10 bar, $G_c = 0.90G_{c,0}$, SV = 750 h^{-1}, H_2/CO_2 = 4, CH_4/CO_2 = 1.44, D_r = 0.3m, L = 1.5m, d_p = 0.005m, T_f = 575K, $T_{c,f}$ = 300K.

The HYSYS reactor model dimensions were chosen to match the dimensions of the previously examined air-cooled, biogas-fed reactor (Figure 19). The same reaction rate expressions and kinetic parameters used in the MATLAB model were used in the HYSYS model. Pressure drop in the HYSYS model was calculated using the Ergun equation and found to be negligible. Catalyst properties and heat transfer parameters were also taken from the MATLAB model. Figure 20 shows simulated spatial profiles of the reactor temperature, mole fractions and reactor performance (conversion, selectivity and yield). Examination of these results showed that the HYSYS simulated reactor produced results resembling those simulated in MATLAB. The HYSYS reactor model predicts that the hot spot is located at the reactor entrance and that the outlet streams exit at identical temperatures.

In order to inject the produced RNG into a natural gas pipeline it has to contain approximately 96% CH_4 with small fractions of inert gases (specifications may vary depending on distributors). To successfully market and distribute product RNG using pre-existing natural gas infrastructure, the process must address these requirements. This is the main constraint in the system design described below. The system design must address the removal of inert gases and other unwanted components contained in LFG to produce RNG in line with natural gas pipeline specifications. A process flow diagram of the designed system is shown in Figure 21. Feed LFG enters the system at conditions specified in Table 6. Water is required for electrolysis and is fed to the system simultaneously at a molar ratio chosen to provide a 4:1 ratio of H_2 to CO_2. Electricity is purchased from the grid to meet the power demand of the system. Feed biogas is passed through a cooler, followed by a water knockout drum to produce a dehydrated stream. Subsequently, the process stream is desulfurized as it passes through a bed of activated carbon where the H_2S adsorbs. In the following step, the stream goes through a temperature swing adsorption (TSA) unit where the

siloxanes and VOCs are separated from the main stream. Siloxanes, H_2S, VOCs and water vapor are removed upstream of the methanation process as their presence downstream can lead to equipment wear and operational failure. Water is fed to the electrolysis system that utilizes electrical power to generate H_2 and O_2. Since O_2 is not used in this system, it is vented to atmosphere. Both the H_2 stream and LFG stream are now individually compressed and heated before entering the methanation reactor.

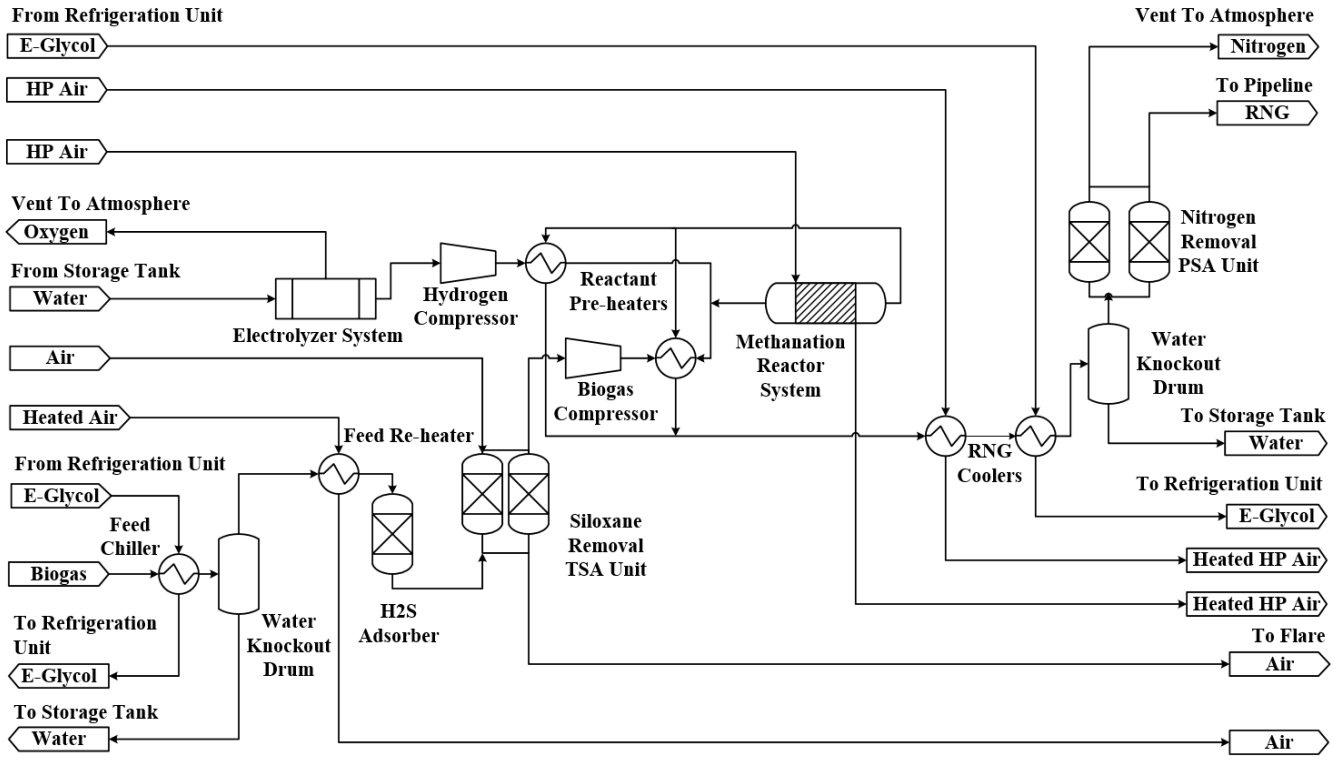

Figure 21. Process flow diagram of the renewable natural gas production facility.

During the methanation reaction, the majority of the CO_2 is converted to CH_4. It is expected that any O_2 present in the biogas stream will react with H_2 producing water. To ensure adequate thermal management, the reactor is actively cooled with compressed air. In order to recycle energy in the system, the hot reactor outlet is used as a heat exchange fluid for H_2 and LFG preheating.

The outlet is further cooled down and sent through a knockout drum to dehydrate the gas. As a final step, the gas is sent though a pressure swing adsorption (PSA) unit, where remaining fractions of N_2 and H_2 are removed.

The entire RNG production process described and shown in Figure 21 except for the dynamic adsorption columns (H_2S adsorption, PSA), was synthesized and modelled in the process simulation software Aspen HYSYS. Design of each unit operation with detailed heat and material balances allowed for equipment sizes and operating costs for the system to be generated. Column sizing and operating costs were provided by industrial partners. The constructed HYSYS flowsheet can be seen in *Appdenix G.*

Table 7. Summary of process streams, power ratings and associated costs.

Unit	No. of Units	Process Stream (Sm^3/h)	Total Power/Duty (kW)	Total Size (m^3)	OPEX (1000s/yr)	BMC (1000s)
Compressors & Pumps						
LFG Compressor	1	8,815	563	19	$293	$1,170
Air Compressor	2	47,290	4340	164	$1,983	$3,551
Glycol Pump	1	59	0.5	0.02	$3	$49
Heat Exchangers						
H_2 Pre-Heater	1	10,690	521	0.52	$7	$135
LFG Pre-Heater	1	8,815	501	0.5	$7	$136
RNG Cooler 1	1	14,750	800	0.95	$12	$250
RNG Cooler 2	2	14,750	3317	2.86	$15	$307
Feed Re-heater	1	8,815	176	0.26	$5	$109
Feed Chiller	1	8,966	190	1.61	$10	$196
Glycol Refrigerator	1	59	5870	9.4	$2,449	$140
Methanation System	50	19,505/14,750	-	5.3	$49	$791
Electrolysis System	21	9.1/10,690	44620	4,725 m^2	$20,019	$31,787
Separators						
Feed KO Drum	1	8,966/8,815	-	2.9	$5	$94

Product KO Drum	1	14,750/9,859	-	2.9	$5	$106
TSA	1	8,966	97	100	$120	$867
PSA	1	9,859/6,749	408	100	$250	$6,538
AC Column	2	8,966	-	86	$1,177	$308
Flare	1	variable	-	-	$1	$136
Electrical/ Civil/Piping	-	-	-	-	-	$2,000
Total			**55,899**		**$26,411**	**$47,669**

The output from Aspen HYSYS Economics paired with the information provided by industrial partners resulted in a base modular cost of $48 million for the system. All individual contributions are listed in Table 7, providing also power ratings and sizing. Individual contributions of each sub-system are also outlined in Figure 22a.

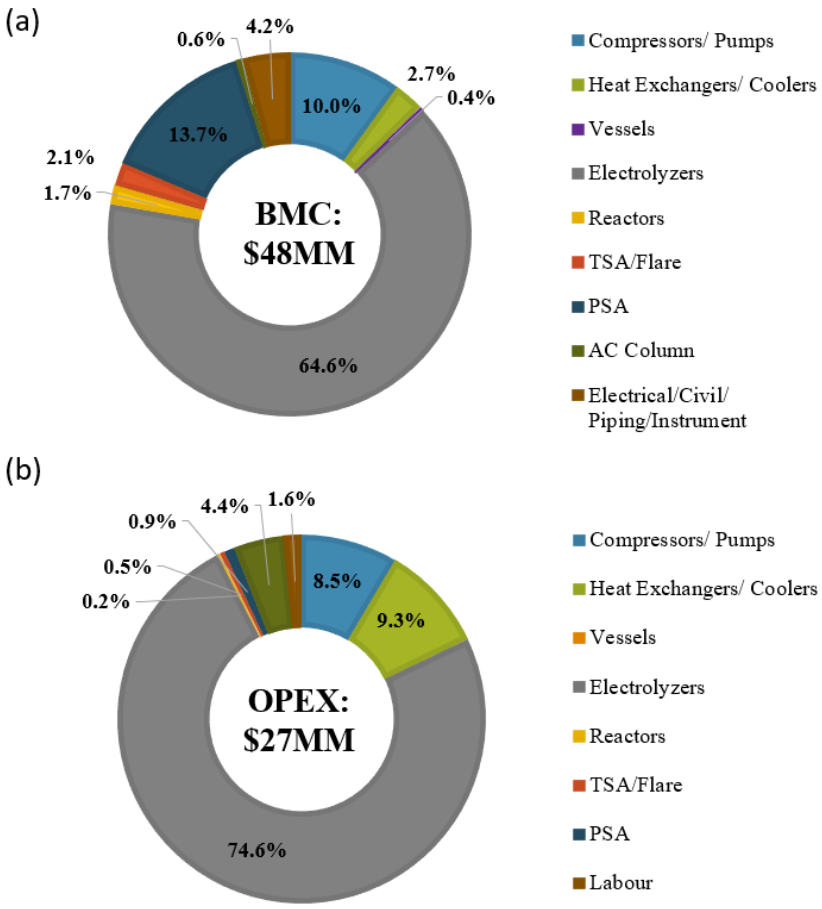

Figure 22. Base modular cost of process equipment (a) and annual operational cost of renewable natural production (b) categorized by process equipment type.

Assuming no land must be purchased for this venture, the direct fixed capital investment (FCI) equates to the base modular cost of equipment. The indirect fixed capital investment consists of engineering supervision, construction, contractor fees and contingency. These amounts are estimated as a percentage of the base modular cost. The total capital investment (TCI) for the project is calculated using Eq. (45) and comes to $87 million.

$$TCI = FCI\ Direct\ +\ FCI\ Indirect \tag{45}$$

The heat and material balances for the system provide utility requirements in terms of water, electricity, heat exchange fluids and catalyst amounts. These data is used to calculate operational

expenses of the plant. Commodity prices are chosen to reflect current market prices and provide an accurate operational cost value. An exception to this was the price of electricity, which was set to \$0.05/kWh for all subsequent evaluations. An early sensitivity study revealed that the process would not be profitable if the price of electricity was higher than \$0.07/kWh. Maintenance costs are calculated individually for each equipment type taking into consideration the lifetime of media for the PSA, TSA and H_2S removal column, catalyst for the reactor and cell stacks for the electrolyzers. For equipment where detailed maintenance breakdowns are not available, the annual maintenance cost is estimated as 5% of the base modular cost of the specific piece of equipment. The total annual operational and maintenance cost for the abovementioned process came to be \$27 million, which is broken down by unit type in Figure 22b. The most significant contribution to the operational cost is the total 56 MW of electricity required by the system with approximately 80% of this value demanded by the electrolyzer. The RNG production cost was estimated at \$15/GJ for \$0.05/kWh electricity price.

The feasibility study was conducted by setting the selling price of RNG to \$20/GJ, the tax rate to 25% and the plant life to 20 years. The net present worth of the project after 20 years was calculated using Eq. (46) and found to be \$16 million. The payback period was found through Eq. (47) to be 5.5 years. This value is reasonable equating to approximately 25% of the plant life. Additionally, the internal rate of return (IRR) for the system is 13%.

$$\text{Net Present Worth} = \sum_{0}^{20} \frac{\text{Profit After Tax - TCI + Salvage Value}}{\left[1+i\right]^{n}} \tag{46}$$

$$\text{Payout period} = \frac{\text{Direct FCI}}{\text{Profit before tax}} \tag{47}$$

This process shows to be feasible only in circumstances where low cost electricity is available. The electrolysis system is unanimously the most expensive from both a capital investment and operational cost standpoint. Further technological advancement in the field of water electrolysis are required to reduce associated costs and increase the feasibility of this system. A potential revenue stream may arise from selling the large volumes of high purity oxygen gas produced during electrolysis. Though this pathway is not considered in this study, its inclusion in the economics can lead to higher feasibility. Additionally, the high temperature compressed air stream leaving the cooling compartments of the reactor can be utilized to provide heat to nearby buildings or put though generators to provide some onsite electricity. This can also alleviate some operational expenses and increase feasibility.

5.0 Concluding Remarks

5.1 Conclusions

A mathematical model was developed and analyzed using numerical simulations to study novel Sabatier reactor configurations. First, the effect a distributed H_2 supply would have on Ni-based catalyst deactivation was investigated in a membrane Sabatier reactor. The reactor utilized a heat-exchanger design for cooling and a H_2 permeable membrane compartment, supplying H_2 for the packed bed reaction compartment. The model considered inter-compartment heat exchange and catalyst deactivation by coking on a commercial Ni/Al_2O_3 catalyst. Reactor performance was evaluated in terms of CO_2 conversion and CH_4 yield as a function of membrane space velocity and reactor cooling rate.

Low membrane spaces velocities resulted in an exhaustion of H_2 in the membrane compartment, undersupplying and limiting the methanation reaction in the packed bed compartment. Higher membrane space velocities led to a sufficient supply of H_2 being fed such that 100% of the CO_2 in the packed be compartment was converted. Oversupply of H_2 to the packed bed compartment was observed at higher membrane space velocities, meaning separation from the RNG downstream via the use of a PSA would be required. Reactor cooling rate was shown to be a crucial operating parameter, with higher cooling rates lowering reactor performance contrary to expectations due to mass transfer limitations with the H_2 permeable membrane. This created an interesting optimization problem between how much cooling can be supplied to facilitate CH_4 formation and suppress catalyst deactivation without limiting the flow of a reactant into the reaction compartment.

Catalyst stability comparisons were made against a standard packed bed reactor setup for equivalent operating parameters. The simulations showed that the addition of the distributed H_2

supply improved the reactor production and catalyst stability, achieving nearly 100% CO_2 conversion for 100 h time on stream. This was a result of the distributed H_2 supply eliminating the hot spot commonly observed near the entrance of the standard packed bed reactor due to the sudden high consumption of reactants and subsequent heat release, which promotes catalyst deactivation.

Next, the techno-economic feasibility of a heat-exchanger type, actively cooled Sabatier reactor was assessed. Reactor performance was evaluated in terms of CO_2 conversion and CH_4 yield as a function of cooling fluid, space velocity and reactor cooling rate. A 56 MW system for converting LFG collected from a large-scale landfill site was designed and simulated to assess its profitability.

Numerical investigations confirmed that compressed air could be used to sufficiently cool down the Sabatier reactor, acting as a more practical reactor heat transfer fluid compared to molten salt, with no drop-in reactor performance parameters. The feasibility of using biogas as feedstock to the actively cooled reactor was confirmed, with CH_4 yields as high as 90% being achevied using a Ni-based catalyst and space velocities of ca. 500-3000 h^{-1}.

The techno-economic assessment predicted the RNG production cost of $15/GJ for the electricity price of $0.05/kWh. The total capital investment and annual operating expenditures are $87 million and $27 million respectively. At the selling price of RNG of $20/GJ, the payback period is 5.5 years and the net present worth is $16 million. The system is predicted to be economically viable only under circumstances where low cost electricity is available. The electrolysis system is responsible for 65% of the base modular cost and 75% of operational expenditures with the contributions of the methanation system being negligible.

5.2 Future Work

Further work is required on both reactor design and system optimization. Development of 2D and 3D mathematical models of the proposed reactor designs to evaluate the presence and severity of radial gradients within each reactor should be completed. Thermal management has already been shown to be a key component in methanation applicatons and so radial thermal gradients have the potential to significantly affect reactor performance and the techno-economic feasibility of operating the proposed reactors. With this, experimental proof-of-concept validation of the model results should also be done to validate the use of these models in techno-economic evaluations. In terms of system design, better system integration is required in order to minimize power consumption, which can be done through more efficient utilization of the reaction heat. Altogether, these future investigations should allow for the further determination of the feasibility of utilizing the proposed reactor setups.

References

[1] REN21, Renewables 2018 Global Status Report, REN21 Secretariat, Paris, 2018.
[2] A.B. Gallo, J.R. Simoes-Moreira, H.K.M. Costa, M.M. Santos, E.M. dos Santos, Energy storage in the energy transition context: A technology review, Renewable Sustainable Energy Rev. 65 (2016) 800-822.
[3] NOAA, Global Monthly Mean CO_2, 2018.
[4] G. Centi, S. Perathoner, Opportunities and prospects in the chemical recycling of carbon dioxide to fuels, Catal Today 148 (2009) 191-205.
[5] S. Perathoner, G. Centi, CO2 recycling: a key strategy to introduce green energy in the chemical production chain, ChemSusChem 7 (2014) 1274-1282.
[6] D.S.A. Simakov, Renewable synthetic fuels and chemicals from carbon dioxide, Springer International Publishing New York, NY, 2017.
[7] W. Wang, S.P. Wang, X.B. Ma, J.L. Gong, Recent advances in catalytic hydrogenation of carbon dioxide, Chem Soc Rev 40 (2011) 3703-3727.
[8] Y.K. Chen, N.S. Lewis, C.X. Xiang, Operational constraints and strategies for systems to effect the sustainable, solar-driven reduction of atmospheric CO2, Energ Environ Sci 8 (2015) 3663-3674.
[9] B. Kumar, M. Llorente, J. Froehlich, T. Dang, A. Sathrum, C.P. Kubiak, Photochemical and Photoelectrochemical Reduction of CO2, Annu Rev Phys Chem 63 (2012) 541-+.
[10] D.S.A. Simakov, Renewable Synthetic Fuels and Chemicals from Carbon Dioxide: Fundamentals, Catalysis, Design Considerations and Technological Challenges, Springer International Publishing2017.
[11] D. Sun, D.S.A. Simakov, Thermal management of a Sabatier reactor for CO2 conversion into CH4: Simulation-based analysis, J Co2 Util 21 (2017) 368-382.
[12] P. Collet, E. Flottes, A. Favre, L. Raynal, H. Pierre, S. Capela, C. Peregrina, Techno-economic and Life Cycle Assessment of methane production via biogas upgrading and power to gas technology, Appl Energ 192 (2017) 282-295.
[13] D. Sun, F.M. Khan, D.S.A. Simakov, Heat removal and catalyst deactivation in a Sabatier reactor for chemical fixation of CO2: Simulation-based analysis, Chem Eng J 329 (2017) 165-177.
[14] C.H. Bartholomew, Catalyst Deactivation and Regeneration, Kirk-Othmer Encyclopedia of Chemical Technology2003.
[15] M. Gotz, J. Lefebvre, F. Mors, A.M. Koch, F. Graf, S. Bajohr, R. Reimert, T. Kolb, Renewable Power-to-Gas: A technological and economic review, Renew Energ 85 (2016) 1371-1390.
[16] G. Plessmann, M. Erdmann, M. Hlusiak, C. Breyer, Global energy storage demand for a 100% renewable electricity supply, Enrgy Proced 46 (2014) 22-31.
[17] M. Jentsch, T. Trost, M. Sterner, Optimal Use of Power-to-Gas Energy Storage Systems in an 85% Renewable Energy Scenario, Enrgy Proced 46 (2014) 254-261.
[18] K. Hashimoto, M. Yamasaki, K. Fujimura, T. Matsui, K. Izumiya, M. Komori, A.A. El-Moneim, E. Akiyama, H. Habazaki, N. Kumagai, A. Kawashima, K. Asami, Global CO2 recycling - novel materials and prospect for prevention of global warming and abundant energy supply, Mat Sci Eng a-Struct 267 (1999) 200-206.
[19] H.S. de Boer, L. Grond, H. Moll, R. Benders, The application of power-to-gas, pumped hydro storage and compressed air energy storage in an electricity system at different wind power penetration levels, Energy 72 (2014) 360-370.

[20] W. Kreuter, H. Hofmann, Electrolysis: The important energy transformer in a world of sustainable energy, International Journal of Hydrogen Energy 23 (1998) 661-666.
[21] T.A. Napp, A. Gambhir, T.P. Hills, N. Florin, P.S. Fennell, A review of the technologies, economics and policy instruments for decarbonising energy-intensive manufacturing industries, Renew Sust Energ Rev 30 (2014) 616-640.
[22] J. Guilera, J.R. Morante, T. Andreu, Economic viability of SNG production from power and CO_2, Energ Convers Manage 162 (2018) 218-224.
[23] F. Re, C. Toro, E. Sciubba, Sabatier Based Cycle for CO_2 Methanation: Exergy and Thermo-Economic Analysis, Proceedings of the Asme International Mechanical Engineering Congress and Exposition, 2017 Vol 6 (2018).
[24] S.B. Walker, D. Sun, D. Kidon, A. Siddiqui, A. Kuner, M. Fowler, D.S.A. Simakov, Upgrading biogas produced at dairy farms into renewable natural gas by methanation, Int J Energ Res 42 (2018) 1714-1728.
[25] P. Collet, E. Flottes, A. Favre, L. Raynal, H. Pierre, S. Capela, C. Peregrina, Techno-economic and Life Cycle Assessment of methane production via biogas upgrading and power to gas technology, Appl Energ 192 (2017) 282-295.
[26] T.T.Q. Vo, D.M. Wall, D. Ring, K. Rajendran, J.D. Murphy, Techno-economic analysis of biogas upgrading via amine scrubber, carbon capture and ex-situ methanation, Appl Energ 212 (2018) 1191-1202.
[27] D.S.A. Simakov, M. Sheintuch, Model-Based Optimization of Hydrogen Generation by Methane Steam Reforming in Autothermal Packed-Bed Membrane Reformer, Aiche J 57 (2011) 525-541.
[28] A.P. Simpson, A.E. Lutz, Exergy analysis of hydrogen production via steam methane reforming, International Journal of Hydrogen Energy 32 (2007) 4811-4820.
[29] S.A.M. Said, D.S.A. Simakov, M. Waseeuddin, Y. Roman-Leshkov, Solar molten salt heated membrane reformer for natural gas upgrading and hydrogen generation: A CFD model, Sol Energy 124 (2016) 163-176.
[30] D.S.A. Simakov, M. Sheintuch, Design of a thermally balanced membrane reformer for hydrogen production, Aiche J 54 (2008) 2735-2750.
[31] A. Basile, F. Gallucci, Membranes for membrane reactors : preparation, optimization, and selection, Wiley, Chichester, 2011.
[32] T.L. Ward, T. Dao, Model of hydrogen permeation behavior in palladium membranes, J Membrane Sci 153 (1999) 211-231.
[33] P.J. Lunde, F.L. Kester, Carbon-Dioxide Methanation on a Ruthenium Catalyst, Ind Eng Chem Proc Dd 13 (1974) 27-33.
[34] F. Solymosi, A. Erdohelyi, T. Bansagi, Methanation of Co2 on Supported Rhodium Catalyst, J Catal 68 (1981) 371-382.
[35] K.R. Thampi, J. Kiwi, M. Gratzel, Methanation and Photo-Methanation of Carbon-Dioxide at Room-Temperature and Atmospheric-Pressure, Nature 327 (1987) 506-508.
[36] G.D. Weatherbee, C.H. Bartholomew, Hydrogenation of Co2 on Group-Viii Metals .4. Specific Activities and Selectivities of Silica-Supported Co, Fe, and Ru, J Catal 87 (1984) 352-362.
[37] Y.Q. Zhang, G. Jacobs, D.E. Sparks, M.E. Dry, B.H. Davis, CO and CO2 hydrogenation study on supported cobalt Fischer-Tropsch synthesis catalysts, Catal Today 71 (2002) 411-418.

[38] S. Ronsch, J. Schneider, S. Matthischke, M. Schluter, M. Gotz, J. Lefebvre, P. Prabhakaran, S. Bajohr, Review on methanation - From fundamentals to current projects, Fuel 166 (2016) 276-296.
[39] X. Su, J.H. Xu, B.L. Liang, H.M. Duan, B.L. Hou, Y.Q. Huang, Catalytic carbon dioxide hydrogenation to methane: A review of recent studies, J Energy Chem 25 (2016) 553-565.
[40] P. Frontera, A. Macario, M. Ferraro, P. Antonucci, Supported Catalysts for CO2 Methanation: A Review, Catalysts 7 (2017).
[41] G.A. Mills, F.W. Steffgen, Catalytic Methanation, Cat. Rev. Sci. Eng. 8 (1973) 159-210.
[42] K. Stangeland, D. Kalai, H. Li, Z. Yu, CO_2 Methanation: The Effect of Catalysts and Reaction Conditions, Energy Procedia 105 (2017) 2022-2027.
[43] V. Miguel, A. Mendes, L.M. Madeira, Intrinsic kinetics of CO_2 methanation over an industrial nickel-based catalyst, J Co2 Util 25 (2018) 128-136.
[44] M. Agnelli, M. Kolb, C. Mirodatos, Co Hydrogenation on a Nickel-Catalyst .1. Kinetics and Modeling of a Low-Temperature Sintering Process, Journal of Catalysis 148 (1994) 9-21.
[45] H.H. Gierlich, M. Fremery, A. Skov, J.R. Rostrup-Nielsen, Deactivation Phenomena of a Ni-based Catalyst for High Temperature Methanation, in: B. Delmon, G.F. Froment (Eds.) Studies in Surface Science and Catalysis, Elsevier1980, pp. 459-469.
[46] R.P.W.J. Struis, T.J. Schildhauer, I. Czekaj, M. Janousch, S.M.A. Biollaz, C. Ludwig, Sulphur poisoning of Ni catalysts in the SNG production from biomass: A TPO/XPS/XAS study, Applied Catalysis a-General 362 (2009) 121-128.
[47] F. Frusteri, L. Spadaro, F. Arena, A. Chuvilin, TEM evidence for factors affecting the genesis of carbon species on bare and K-promoted Ni/MgO catalysts during the dry reforming of methane, Carbon 40 (2002) 1063-1070.
[48] M.N. Pedernera, J. Pina, D.O. Borio, Kinetic evaluation of carbon formation in a membrane reactor for methane reforming, Chemical Engineering Journal 134 (2007) 138-144.
[49] J.B. Claridge, M.L.H. Green, S.C. Tsang, A.P.E. York, A.T. Ashcroft, P.D. Battle, A Study of Carbon Deposition on Catalysts during the Partial Oxidation of Methane to Synthesis Gas, Catal Lett 22 (1993) 299-305.
[50] S.G. Zavarukhin, G.G. Kuvshinov, The kinetic model of formation of nanofibrous carbon from CH4-H-2 mixture over a high-loaded nickel catalyst with consideration for the catalyst deactivation, Appl Catal a-Gen 272 (2004) 219-227.
[51] J. Ducamp, A. Bengaouer, P. Baurens, Modelling and Experimental Validation of a CO_2 Methanation Annular Cooled Fixed-Bed Reactor Exchanger, Can. J. Chem. Eng. 95 (2017) 241-252.
[52] M. Patrascu, M. Sheintuch, On-site pure hydrogen production by methane steam reforming in high flux membrane reactor: Experimental validation, model predictions and membrane inhibition, Chem Eng J 262 (2015) 862-874.
[53] D. Schlereth, O. Hinrichsen, A fixed-bed reactor modeling study on the methanation of CO2, Chem Eng Res Des 92 (2014) 702-712.
[54] S.G. Zavarukhin, G.G. Kuvshinov, The kinetic model of formation of nanofibrous carbon from CH_4-H_2 mixture over a high-loaded nickel catalyst with consideration for the catalyst deactivation, Appl. Catal. A: Gen. 272 (2004) 219-227.
[55] J.G. Xu, G.F. Froment, Methane steam reforming, methanation and water-gas shift : I. Intrinsic kinetics, AIChE J. 35 (1989) 88-96.
[56] D.E. Mears, Tests for Transport Limitations in Experimental Catalytic Reactors, Ind Eng Chem Proc Dd 10 (1971) 541-&.

[57] D.S.A. Simakov, H.Y. Luo, Y. Román-Leshkov, Ultra-low loading Ru/g-Al_2O_3: A highly active and stable catalyst for low temperature solar thermal reforming of methane, Appl. Catal. B: Environ. 168-169 (2015) 540-549.
[58] G.F. Froment, K.B. Bischoff, Chemical Reactor Analysis and Design, Wiley1979.
[59] R.J. Berger, J. Perez-Ramirez, F. Kapteijn, J.A. Moulijn, Catalyst performance testing - Radial and axial dispersion related to dilution in fixed-bed laboratory reactors, Appl Catal a-Gen 227 (2002) 321-333.
[60] O.R. Derkx, A.G. Dixon, Effect of the wall Nusselt number on the simulation of catalytic fixed bed reactors, Catal Today 35 (1997) 435-442.
[61] A.G. Dixon, D.L. Cresswell, Theoretical Prediction of Effective Heat-Transfer Parameters in Packed-Beds, Aiche J 25 (1979) 663-676.
[62] V. Gnielinski, New Equations for Heat and Mass-Transfer in Turbulent Pipe and Channel Flow, Int Chem Eng 16 (1976) 359-368.
[63] J.P. Holman, Heat transfer, 9 ed., McGraw-Hill, New York, 2002.
[64] A.F. Mills, Heat Transfer, Irwin 1992.
[65] O.A. Sergeev, A.G. Shashkov, A.S. Umanskii, Thermophysical properties of quartz glass, J. Eng. Phys. Thermophys. 43 (1982) 1375-1383.
[66] S.W. Churchill, H.H.S. Chu, Correlating Equations for Laminar and Turbulent Free Convection from a Horizontal Cylinder, Int J Heat Mass Tran 18 (1975) 1049-1053.
[67] G.J. Janz, Molten Salts Handbook, Elsevier, New York, 1967.
[68] R. Morrell, Handbook of properties of technical & engineering ceramics, Her Majesty's Stationery Office, London, 1985.
[69] Y.S. Touloukian, R.K. Kirby, E.R. Taylor, T.Y.R. Lee, Thermophysical properties of matter, Purdue University1977.
[70] High Temperature Molten Salt Heat Transfer Fluid (270°F to 1050°F), Dynalene Molten Salts.
[71] S. Rapagna, N. Jand, P.U. Foscolo, Catalytic gasification of biomass to produce hydrogen rich gas, Int J Hydrogen Energ 23 (1998) 551-557.
[72] S.H. Wu, K.B. McAuley, T.J. Harris, Selection of Simplified Models: Ii. Development of a Model Selection Criterion Based on Mean Squared Error, Can. J. Chem. Eng. 89 (2011) 325-336.
[73] S.S.E.H. Elnashaie, A.M. Adris, A.S. Alubaid, M.A. Soliman, On the Non-Monotonic Behavior of Methane Steam Reforming Kinetics, Chem Eng Sci 45 (1990) 491-501.
[74] J.G. Xu, G.F. Froment, Methane Steam Reforming, Methanation and Water-Gas Shift .1. Intrinsic Kinetics, Aiche J 35 (1989) 88-96.
[75] N. Frössling, Uber die Verdunstung fallender Tropfen, Gerlands Beitr. Geophys. 52 (1938) 170-216.
[76] W.E. Ranz, W.R. Marshall, Evaporation from Droplets: part I and II, Chem. Eng. Prog. 48 (1952) 141-173.
[77] E.E. Shpilrain, AIR (PROPERTIES OF), Thermopedia, Begell House Inc, 2011.

Appendix

A. Dimensionless model

$$\frac{\partial u_{CO_2}}{\partial \tau}=\left(\frac{1}{Pe_m}\right)\frac{\partial^2 u_{CO_2}}{\partial \xi^2}-u_t\frac{\partial u_{CO_2}}{\partial \xi}-u_{CO_2}\frac{\partial u_t}{\partial \xi}+Da(\hat{k}_2\ f_2\eta_2+\hat{k}_3\ f_3\eta_3)$$

$$\frac{\partial u_{H_2}}{\partial \tau}=\left(\frac{1}{Pe_m}\right)\frac{\partial^2 u_{H_2}}{\partial \xi^2}-u_t\frac{\partial u_{H_2}}{\partial \xi}-u_{H_2}\frac{\partial u_t}{\partial \xi}+Da(3\hat{k}_1\ f_1\eta_1+\hat{k}_2\ f_2\eta_2+4\hat{k}_3\ f_3\eta_3)+Pe_{c,M}\Delta\sqrt{Py_{H_2}}$$

$$\frac{\partial u_{CO}}{\partial \tau}=\left(\frac{1}{Pe_m}\right)\frac{\partial^2 u_{CO}}{\partial \xi^2}-u_t\frac{\partial u_{CO}}{\partial \xi}-u_{CO}\frac{\partial u_t}{\partial \xi}+Da(\hat{k}_1\ f_1\eta_1-\hat{k}_2\ f_2\eta_2)$$

$$\frac{\partial u_{H_2O}}{\partial \tau}=\left(\frac{1}{Pe_m}\right)\frac{\partial^2 u_{H_2O}}{\partial \xi^2}-u_t\frac{\partial u_{H_2O}}{\partial \xi}-u_{H_2O}\frac{\partial u_t}{\partial \xi}+Da(-\hat{k}_1\ f_1\eta_1-\hat{k}_2\ f_2\eta_2-2\hat{k}_3\ f_3\eta_3)$$

$$\frac{\partial u_{CH_4}}{\partial \tau}=\left(\frac{1}{Pe_m}\right)\frac{\partial^2 u_{CH_4}}{\partial \xi^2}-u_t\frac{\partial u_{CH_4}}{\partial \xi}-u_{CH_4}\frac{\partial u_t}{\partial \xi}+Da(-\hat{k}_1\ f_1\eta_1-\hat{k}_3\ f_3\eta_3)$$

$$\sigma\frac{\partial \theta}{\partial \tau}=\frac{1}{Pe_r}\frac{\partial^2 \theta}{\partial \xi^2}-\frac{\partial \theta}{\partial \xi}+\beta Da[k_1 f_1\left(\Delta H_1\right)\eta_1+k_2 f_2\left(\Delta H_2\right)\eta_2+k_3 f_3\left(\Delta H_3\right)\eta_3]-nSt_{r1}\left(\theta-\theta_c\right)-St_{r2}\left(\theta-\theta_e\right)$$

$$\frac{\partial \theta_c}{\partial \tau}=\frac{1}{Pe_c}\frac{\partial^2 \theta_c}{\partial \xi^2}-\frac{\partial \theta_c}{\partial \xi}-nSt_c\left(\theta_c-\theta\right)$$

$$P=1-J\left(150S\hat{v}_g+1.75\,\mathrm{Re}\,\hat{v}_g^2\right)\xi$$

Dimensionless parameters:

$$\tau=\frac{t}{L/v_{gf}}\quad \xi=\frac{z}{L}\quad \theta=\frac{T}{T_f}\quad \theta_c=\frac{T_c}{T_f}\quad \theta_e=\frac{T_e}{T_f}\quad \theta_{cf}=\frac{T_{cf}}{T_f}\quad u_t=\frac{C_t}{C_{tf}}\quad P=\frac{P_t}{P_{tf}}\quad y_i=\frac{u_i}{u_t}=\frac{P_i}{P_t}\quad u_i=\frac{C_i}{C_{tf}}$$

$$u_f=\frac{C_f}{C_{tf}}\quad \hat{v}_g=\frac{v_g}{v_{gf}}\quad \left(\Delta H_j\right)=\frac{-\Delta H_j}{-\Delta H_1}$$

$$f_1 = \left(\frac{y_{CH_4} y_{H_2O}}{y_{H_2}^{2.5}} - \frac{y_{H_2}^{0.5} y_{CO}}{\hat{K}_{eq1}} \right) / \left(\hat{DEN} \right)^2 \quad f_2 = \left(\frac{y_{CO} y_{H_2O}}{y_{H_2}} - \frac{y_{CO_2}}{K_{eq2}} \right) / \left(\hat{DEN} \right)^2$$

$$f_3 = \left(\frac{y_{CH_4} y_{H_2O}^2}{y_{H_2}^{3.5}} - \frac{y_{H_2}^{0.5} y_{CO2}}{\hat{K}_{eq3}} \right) / \left(\hat{DEN} \right)^2 \quad \hat{DEN} = 1 + \hat{K}_{CO}\, y_{CO} + \hat{K}_{H_2}\, y_{H_2} + \hat{K}_{CH_4}\, y_{CH_4} + \frac{K_{H_2O} P_{H_2O}}{P_{H_2}}$$

$$k_{1ad} = A_1 \exp(\gamma_{1ad}) \quad \gamma_{1ad} = \frac{Ea_1}{RT_{ad}} \quad k_1 = \frac{k_1}{k_{1ad}} \quad k_2 = \frac{P^{1.5} k_2}{k_{1ad}} \quad k_3 = \frac{k_3}{k_{1ad}}$$

$$K_{eq1} = \frac{K_{eq1}}{P_t^2} \quad K_{eq3} = \frac{K_{eq3}}{P_t^2}$$

$$\sigma = \frac{\varepsilon \rho_g C_{pg} + (1-\varepsilon) \rho_s C_{ps}}{\varepsilon \rho_g C_{pg}} \quad \beta = \frac{(-\Delta H_1) C_{tf}}{\rho_g C_{pg} T_f} \quad Pe_m = \frac{\varepsilon v_{gf} L}{D_{ae}} \quad Pe_r = \frac{L v_{gf} \varepsilon \rho_g C_{pg}}{k_{ae}} \quad Pe_c = \frac{L v_{gf} \rho_c C_{pc}}{\lambda_c}$$

$$Pe_{c,M} = \frac{S_a L k_p}{V C_{tf} v_{gf}} \quad Da = \frac{\rho_s (1-\varepsilon) k_{1f}}{P_t^{0.5} (v_{gf} / L) \varepsilon C_{tf}} = \frac{W_c k_{1f}}{F_{tf} P_t^{0.5}} \quad J = \frac{v_{gf} \mu_g (1-\varepsilon)}{P_{tf} \varepsilon^3 d_p} \quad S = \frac{(1-\varepsilon) L}{d_p}$$

$$St_{r1} = \frac{U_{cw} a_{v,he}}{\varepsilon \rho_g C_{pg} v_{gf} / L} \quad St_{r2} = \frac{U_{rw} a_{v,hl}}{\varepsilon \rho_g C_{pg} v_{gf} / L} \quad St_c = \frac{U_{cw} a_{c,he}}{\rho_c C_{pc} v_{gf} / L}$$

Dimensionless initial and boundary conditions:

$$\xi = 0: \; -\frac{1}{Pe_m} \frac{\partial u_i}{\partial \xi} = (u_{fi} - u_i) \qquad \xi = 1: \; \frac{\partial u_i}{\partial \xi} = 0 \qquad \tau = 0: \; u_i(0, \xi) = u_{i,\text{int}}$$

$$-\frac{1}{Pe_r} \frac{\partial \theta}{\partial \xi} = (1 - \theta) \qquad \frac{\partial \theta}{\partial \xi} = 0 \qquad \theta(0, \xi) = \theta_{\text{int}}$$

$$-\frac{1}{Pe_c} \frac{\partial \theta_c}{\partial \xi} = (\theta_{cf} - \theta_c) \qquad \frac{\partial \theta_c}{\partial \xi} = 0 \qquad \theta_c(0, \xi) = \theta_{c,\text{int}}$$

B. Kinetic parameter estimation

To estimate E_{aj}, A_j, B_i and ΔH_i (total 14 parameters) a set of lab experiments to monitor change in species concentrations as a function of temperature and space velocity were carried out. CO_2 and H_2 were fed by mass flow controllers to a lab scale flow reactor containing ~0.5g of catalyst with the outlet concentrations continuously monitored using an infrared analyzer. Parameter estimation

was done by minimizing the sum of the squared residuals of the CO2, CO and CH_4 concentrations by means of the Trust-Region Reflective Algorithm [72]. Simulated mole fractions were obtained by integrating a set of ordinary differential equations described by Eq. B1 (MATLAB ode15s) representing the time evolution of all species participating in the reaction system. Initial guesses for the reaction and adsorption constants were adopted from Xu and Froment [73, 74].

$$\varepsilon \frac{dC_i}{dt} = -\varepsilon v_g \frac{\left(C_i - C_{i,f}\right)}{L} + \rho_c (1-\varepsilon) \sum_j \alpha_i R_{ij} \tag{B1}$$

The parameter estimation results are shown in *Appendix C* based on the data shown in Figure B1. The adopted rate expressions with the estimated parameters listed in Table C.1 accurately predicts the experimentally measured mole fractions of CO_2, CO and CH_4 over a variety of operating conditions as shown in Figure B1. Parameter estimation code is shown in *Appendix J.*

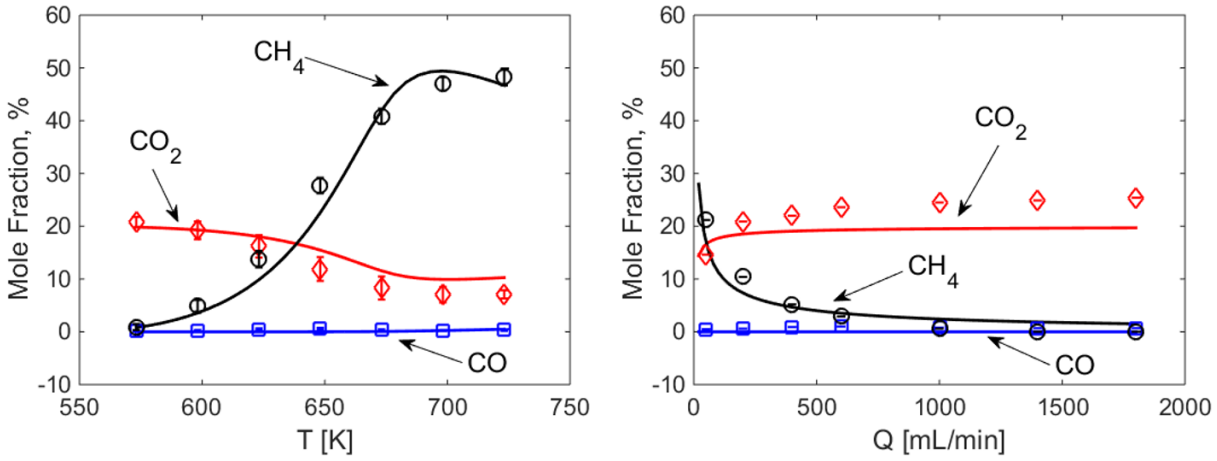

Figure B1. Simulation results (lines) vs. experimental data (symbols) in terms of species concentrations as a function of temperature (a) and feed flow rate (b). Experimental conditions H2/CO2 = 4 in the feed, P = 3 bar, 256 mg of undiluted Ni/α-Al2O3 catalyst, 125 mL/min total flow (a) and T = 623 K (b)

C. Kinetic data

Table C.1. Reaction kinetic parameters

A_1	A_2	A_3	B_{CO}	B_{H2}	B_{CH4}	B_{H2O}
8.90e8	3.42e6	9.22e-5	1.50e-9	1.86e-12	5.48e-7	6.43e3
Ea_1	Ea_2	Ea_3	ΔH_{CO}	ΔH_{H2}	ΔH_{CH4}	ΔH_{H2O}
122.4	93.1	104.8	-97.3	-103.4	-57.7	104.4

Table C.2. Deactivation parameters

Constant	T_{ref} (K)	k_{ref} and B	Ea and ΔH (kJ/mol)
k	612	1	104.2
k_H	875	1	163.2
k_a	508	1	135.6
K_p	-	5.088e5	91.2

D. Transport limitations criteria

Intraparticle and interphase mass and heat transfer limitations were assessed using the following criteria [56, 57]:

$$\phi_j^2 = \frac{\hat{k}_j d_p^2}{4D_m} << 1 \tag{D1}$$

$$\frac{\varepsilon \rho_g \left|\Delta H_{RWGS}\right| \hat{k}_j d_p^2}{4k_s T} << \frac{0.75TR_g}{E_a} \tag{D2}$$

$$\frac{\hat{k}_j d_p}{2y_{CO_2,f} k_c} << 0.15 \tag{D3}$$

$$\frac{\varepsilon\rho_g \left|\Delta H_{RWGS}\right| \hat{k}_j d_p}{2h_{gs}T} << \frac{0.75TR_g}{E_a} \tag{D4}$$

$$\hat{k}_1 = \frac{k_1\rho_s(1-\varepsilon)}{\sqrt{P_{tf}}\,\rho_g\varepsilon} \qquad \hat{k}_2 = \frac{k_2\rho_s(1-\varepsilon)P_{tf}}{\rho_g\varepsilon} \qquad \hat{k}_3 = \frac{k_3\rho_s(1-\varepsilon)}{\sqrt{P_{tf}}\,\rho_g\varepsilon}$$

In the equations above, k_s is the thermal conductivity of the pellet which was assumed to be the same as for alumina and calculated using an empirical correlation [68]. The gas mass transfer coefficient (k_c) was calculated from the Sherwood number, estimated by the Frossling correlation [75], Eq. (D5). The effective gas heat transfer coefficient (h_{gs}) was calculated from the Nusselt number, estimated by the analogous correlation for heat transfer [76], Eq. (D6).

$$Sh = \frac{k_c d_p}{D_m} = 2 + 0.6\,\mathrm{Re}^{0.5}\,\mathrm{Sc}^{\frac{1}{3}} \qquad \mathrm{Re}_p = \frac{v_g\rho_g d_p}{\mu_g} \qquad Sc = \frac{\upsilon}{D_m} \tag{D5}$$

$$Nu_p = \frac{h_{gs} d_p}{k_t} = 2 + 0.6\,\mathrm{Re}^{0.5}\,\mathrm{Pr}^{\frac{1}{3}} \qquad \mathrm{Pr} = \frac{\upsilon}{\alpha_t} \tag{D6}$$

E. Regression equations of thermophysical properties

Gas components [69] :

Heat Capacity (kJ/molK):

$$C_{p,CO_2} = -2\times10^{-8}T^2 - 5\times10^{-5}T + 0.0256$$

$$C_{p,H_2} = 3\times10^{-9}T^2 - 2\times10^{-6}T + 0.0297$$

$$C_{p,CO} = 10^{-8}T^2 - 7\times10^{-6}T + 0.0301$$

$$C_{p,H_2O} = 10^{-8}T^2 - 5\times10^{-6}T + 0.0356$$

$$C_{p,CH_4} = 0.03\ln\left(T\right) - 0.1394$$

Viscosity (Pa s):

$$\mu_{CO_2} = 4\times10^{-8}T + 6\times10^{-6}$$

$$\mu_{H_2O} = 4\times10^{-8}T - 3\times10^{-6}$$

$$\mu_{H_2} = 2\times10^{-8}T + 5\times10^{-6}$$

$$\mu_{CH_4} = 3\times10^{-8}T + 4\times10^{-6}$$

$$\mu_{CO} = 4\times10^{-8}T + 7\times10^{-6}$$

Alumina support [68] :

Heat capacity (kJ/kg-K): $C_{ps} = 1.0446 + 1.742\times10^{-4}T - 2.796\times10^{4}T^2$

Thermal conductivity (kW/m-K): $\lambda_s = 5.5\times10^{-3} + 34.5\times10^{-3}\exp\left[-0.0033\times\left(T-273\right)\right]$

Density (kg/m^3): $\rho_s = 3.85\times10^{3}$

Molten salt [70]:

Heat capacity (kJ/kg-K): $C_{pMS} = 2\times10^{-4}T + 1.2738$

Thermal conductivity (kW/m-K): $\lambda_{MS} = 2\times10^{-7}T - 4\times10^{-4}$

Density (kg/m^3): $\rho_{MS} = -0.5572T + 2219.1$

Compressed air [77]:

Heat capacity (kJ/kg-K): $C_{pair} = 1.1142 - 0.005 \times T + 9 \times 10^{-7} T^2 - 4 \times 10^{-10} T^3$

Viscosity (Pa s):

$\mu_{air} = 1 \times 10^{-5} + 3 \times 10^{-8} T$

Thermal conductivity (kW/m-K): $\lambda_{MS} = 7.4 \times 10^{-6} + 6 \times 10^{-8} T$

Density (kg/m^3): $\rho_{air} = \dfrac{P}{RT}$

F. Conversion, selectivity derivation

CO_2 conversion (X_{CO_2}) and CH_4 selectivity (S_{CH_4}) were obtained from the following equations:

$$X_{CO_2} = \frac{y_{CO} + y_{CH_4} - \beta(y_{CO} + y_{CO_2} + y_{CH_4})}{(1-\beta)(y_{CO} + y_{CO_2} + y_{CH_4})} \quad \text{(F1)}$$

$$S_{CH_4} = \frac{y_{CH_4} - \beta(y_{CO} + y_{CO_2} + y_{CH_4})}{y_{CO} + y_{CH_4} - \beta(y_{CO} + y_{CO_2} + y_{CH_4})} \quad \text{(F2)}$$

To obtain Eqs (F1, F2), CO_2 conversions to CO, Eq. (F3), and to CH_4, Eq. (F4) are first defined:

$$f_1 = \frac{y_{CO}}{(1-\beta)(y_{CO} + y_{CO_2} + y_{CH_4})} \equiv \frac{F_{CO,out}}{F_{CO_2,f}} \quad \text{(F3)}$$

$$f_2 = \frac{y_{CH_4} - \beta(y_{CO} + y_{CO_2} + y_{CH_4})}{(1-\beta)(y_{CO} + y_{CO_2} + y_{CH_4})} \equiv \frac{F_{CH_4,gen}}{F_{CO_2,f}} \quad \text{(F4)}$$

β is the CH_4 content in the carbon-based feed, as defined in Eq. (F5):

$$\beta = \frac{F_{CH_4,f}}{F_{CH_4,f} + F_{CO_2,f}} = \frac{F_{CH_4,f}}{F_{C,f}} \quad \text{(F5)}$$

The total CO_2 conversion and CH_4 selectivity are then obtained as follows:

$$X_{CO_2} = f_1 + f_2 \tag{F1a}$$

$$S_{CH_4} = \frac{f_2}{f_1 + f_2} \tag{F2a}$$

G. HYSYS model PFD

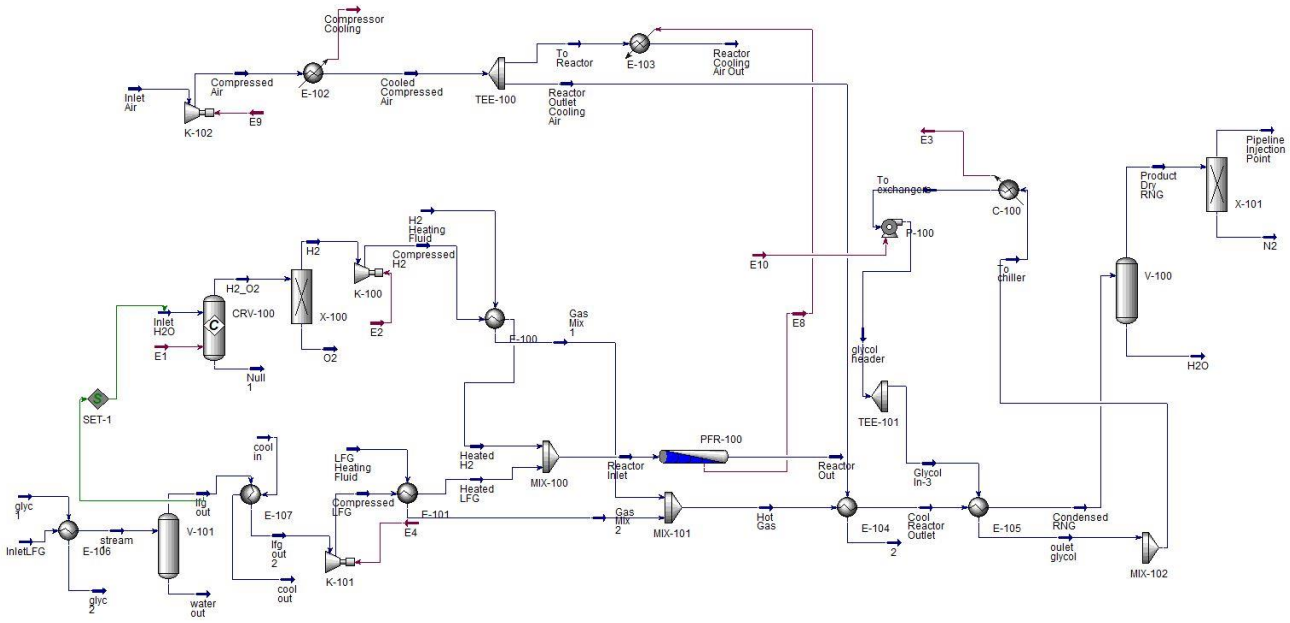

Figure G1. Aspen HYSYS RNG Facility Simulation Flowsheet

H. Membrane reactor simulation code

```
function SR
close all

% --------- REACTOR GEOMETRY ------------------------------------------------
L=0.4; dp=0.003; dr=0.1; dc=0.02; dw=0.002; dm = 0.01; %m
epsi=0.5; n=5; %dimensionless
%------------------------------------ $$$ NUMBER OF MEMBRANES $$$ --------
                                                nm =4; %dimensionless
%-------------------------------------------------------------------------
ro_s=1.274e+3; %kg/m3
ache=4/dc; avhe=4*(dc+dw)/(dr^2-n*(dc+dw)^2-nm*dm^2); %1/m
avhl=4*dr/(dr^2-n*(dc+dw)^2-nm*dm^2); %1/m
A=n*pi*(dc/2)^2; A_pb=pi*(dr^2-n*(dc+dw)^2-nm*dm^2)/4; %m^2
A_total=pi*((dr+dw)^2-n*dc^2-nm*dm^2)/4; %m^2
```

```
Sm = pi*dm*L; %m^2 membrane surface area
VT=L*pi*(dr/2)^2-n*L*pi*((dc+dw)/2)^2-nm*L*pi*(dm/2)^2; %m^3
VTM = L*pi*(dm/2)^2; %single membrane volume
alpha=A_pb/A_total; %dimensionless
%------------- Membrane Permeability ---------------------------------------
Ap = 5.6; % Hydrogen permeability pre-exponential factor mol/m2 s bar0.5
Ap = Ap*sqrt(0.01); %mol/m2 s kPa0.5
D0 = 0.294*10^-6; %hydrogen diffusion pre-exponential factor m2/s
% ------ Heat Losses to Environment ----------------------------------------
                                                    Urw=10e-3; %kW/(m2 K)

%------------------- KINETICS (Xu & Froment; NEW PARAMETERS) --------------
R=8.314e-3;    %kJ/(mol K)
% ---- Parameters for Equilibrium Constants ----------
deltaHeq1=26830; deltaHeq2=-4400; deltaHeq3=22430; %K
B1=1.198e17; %kPa^2         (MSR)
B2=1.767e-2; %dimensionless (WGS)
B3=2.117e15; %kPa^2      (MSR + WGS)
% ---- Parameters for Reaction Rate Constants---------
Ea1=122.4; Ea2=93.1; Ea3=104.8; %kJ/mol
EaP = 11; %hydrogem permeability activation energy kJ/mol
EaH = 22; %Hydrogen diffusion activation energy kJ/mol
kref1=6.55e-3;       %(kmol bar^0.5)/(kg h)
kref2=91.2e-3;    %kmol/(kPa kg h)
kref3=23.38e-15;        %(kmol bar^0.5)/(kg h)
kref1 = kref1/(sqrt(0.01));  %(kmol kPa^0.5)/(kg h)
kref3 = kref3/(sqrt(0.01));  %(kmol kPa^0.5)/(kg h)
kref1 = kref1*1000/3600;     %(mol kPa^0.5)/(kg s)
kref2 = kref2*1000/3600;     %mol/(kPa kg s)
kref3 = kref3*1000/3600;     %(mol kPa^0.5)/(kg s)
% conversion to pre-exponent factors according to A*exp(-Ea/RT)
A1 = kref1*exp(Ea1/(R*598.15)) %(mol kPa^0.5)/(kg s)
A2 = kref2*exp(Ea2/(R*598.15)) %mol/(kPa kg s)
A3 = kref3*exp(Ea3/(R*598.15)) %(mol kPa^0.5)/(kg s)
% ---- Parameters for Adsorption Constants -----------
deltaHCO=-97.3;  %kJ/mol
deltaHCH4=-57.7; %kJ/mol
deltaHH2O=104.4;  %kJ/mol
deltaHH2=-103.4;   %kJ/mol
KCOref=104.79e-3; %1/kPa
KH2Oref=1.52e-3; %dimensionless
KH2ref=401.9e-6; %1/kPa
KCH4ref=2.52e-3; %1/kPa
ACO = KCOref*exp(deltaHCO/(R*648))
ACH4 = KCH4ref*exp(deltaHCH4/(R*823))
AH2 = KH2ref*exp(deltaHH2/(R*648))
AH2O = KH2Oref*exp(deltaHH2O/(R*823))

%------------------------------ DEACTIVATION KINETICS --------------------
deltaH1=206; %kJ/mol
deltaH2=-41; %kJ/mol
deltaH3=165; %kJ/mol
deltaHcap1=(-deltaH1)/(-deltaH1); %dimensionless
deltaHcap2=(-deltaH2)/(-deltaH1); %dimensionless
deltaHcap3=(-deltaH3)/(-deltaH1); %dimensionless
```

```
%------------------ MOLECULAR WEIGHTS (CO@, H2, CO, H2O, CH4) -------------
M_CO2=44e-3; M_H2=2e-3; M_CO=28e-3; M_H2O=18e-3; M_CH4=16e-3; %kg/mol

% ************************** REACTOR OPERATING CONDITIONS ***************

%---- Packed bed feed (CO2,H2,CO,H2O,CH4), dimensionless -----
%---- Deactivation feed parameters---(carbon deposition, catalyst activity)
                                        uf6 = 0; uf7 = 1;

%                   uf1=0.2;uf2=0.8;uf3=0;uf4=0;uf5=0; % ***NON-MEMBRANE***
                    uf1=0.9;uf2=0.1;uf3=0;uf4=0;uf5=0; % $$$ MEMBRANE $$$

%---- Membrane feed -----------------------------------------------------
           uf8=0.6; uf9=0; uf10=0; uf11=1-uf8;    %pure H2
%          uf8=0.56; uf9=0.247; uf10=0.133; uf11=0.06; %gasified biomass
% ----------- OUTLET Pressure, Space Velocity, & Temperatures -------------

                                                    Ptf=1000; %kPa
%                                 SVf=(1000)/3600; %1/s ***NON-MEMBRANE***
                            SVf=(0.2/0.9)*1000/3600; %1/s $$$ MEMBRANE $$$

   % !!!!!!!!-----molten salt range: 523-838K (Dynalene MS-1) ------- !!!!!
Te=298;                                             Tf=650+100*0; Tcf=550; %K
% ---------- Membrane Pressure, Space Velocity ------
                                                       PtfM = 2000; %kPa
                                                    SVfM =50*SVf ; %1/s

% ---------------- LOOP FOR SCANS OVER PARAMETER RANGES -------------------
count = 1;
for k=1:count

% ----------- Reference Molten Salt Mass Flow Rate ----
dT=300; %K
Cpcf=1.425; %kJ/(kg K)
G0=uf1*deltaH3*VT*(Ptf/(R*Tf))*SVf/(dT*Cpcf); %kg/s
                                                              G=0.1*G0; %kg/s
ro_mean=1850;      %kg/m3
Ctf=Ptf/(R*Tf);    %mol/m3
vgf=L*SVf/epsi;    %m/s
vc=G/(ro_mean*A); %m/s
ratio=vc/vgf;      %dimensionless

vgfM = L*SVfM; %m/s
CtfM = PtfM/(R*Tf); %mol/m3

% ----- Adiabatic Temperature ----------------------
Cpgf=uf1*(-2e-8*Tf^2+5e-5*Tf+0.0256)+uf2*(3e-9*Tf^2-2e-6*Tf+0.0297)+uf3*(4e-
6*Tf+0.0276)+uf4*(1e-8*Tf^2-5e-6*Tf+0.0356)+uf5*(0.03*log(Tf)-0.1394);
%kJ/(mol K)
Tad=Tf+deltaH1*0.2/Cpgf; %K
% ---- Dimensionless Feed and Environment Temperatures ---------
thetaf=Tf/Tad; thetae=Te/Tad; thetacf=Tcf/Tad; %dimensionless

% ---------------- SIMULATIONS PARAMETERS --------------------------------
m=0;      % cartezian geometry
```

```
tcnt=50;  % number of time output point
N=100; x=linspace(0,1,N);   %number of space points
%N1=80; N2=50; x=[linspace(0,0.2,N1) linspace(0.21,1,N2)]; N=N1+N2;

% ------------ Maximum Time of Simulation --------------------------------
                                                          tmax_h=100; %h
t_max=tmax_h*(vgf/L)*3600    %dimensionless
tao=linspace(0,t_max,tcnt);   %dimensionless time
t=tao*L/(3600*vgf);           %dimensional time, h

%-------------------- PDE SOLVER ----------------------------------------
options=odeset('RelTol',1e-3,'AbsTol',1e-6,'Normcontrol','on');
sol=pdepe(m,@eqns,@eqn_ic,@eqn_bc,x,tao,options,N,Tad,deltaHcap1,deltaHcap2,d
eltaHcap3,Tf,Ptf,PtfM,R,L,n,dp,epsi,dw,dc,ache,avhe,avhl,vc,uf1,uf2,uf3,uf4,u
f5,uf6,uf7,uf8,uf9,uf10,uf11,Tcf,Te,Ea1,Ea2,Ea3,EaP,EaH,deltaHeq1,deltaHeq2,d
eltaHeq3,thetaf,thetae,thetacf,vgf,vgfM,Ctf,CtfM,M_CH4,M_H2,M_H2O,M_CO2,M_CO,
A1,A2,A3,Ap,D0,B1,B2,B3,ACO,ACH4,AH2O,AH2,deltaHCO,deltaHCH4,deltaHH2O,deltaH
H2,deltaH1,ro_s,G,t_max,Urw,alpha,VT,A,A_pb,SVf,Sm,nm,VTM);

%---------------------- SOLVER OUTPUT ------------------------------------
%----- dimensionless concentrations & temperatures -----
Y1=real(sol(:,:,1));%CO2
Y2=real(sol(:,:,2));%H2
Y3=real(sol(:,:,3));%CO
Y4=real(sol(:,:,4));%H2O
Y5=real(sol(:,:,5));%CH4
Y6=real(Tad*sol(:,:,6));%reactor temp
Y7=real(Tad*sol(:,:,7));%coolant temp
Y8=real(sol(:,:,8));% carbon
Y9=real(sol(:,:,9));% activity
Y10 = real(sol(:,:,10));% H2 membrane
Y11 = real(sol(:,:,11));% H2 membrane

%---- steady state moole fractions & temperatures -----
Y1_s=real(sol(tcnt,:,1));
Y2_s=real(sol(tcnt,:,2));
Y3_s=real(sol(tcnt,:,3));
Y4_s=real(sol(tcnt,:,4));
Y5_s=real(sol(tcnt,:,5));
T_rs=real(Tad*sol(tcnt,:,6));
T_cs=real(Tad*sol(tcnt,:,7));
Y8_s=real(sol(tcnt,:,8));% carbon
Y9_s=real(sol(tcnt,:,9));% activity
Y10_s=real(sol(tcnt,:,10)); % H2 Membrane
Y11_s=real(sol(tcnt,:,10)); % Inert Membrane
%---- deactivation temperature plot ------
T_rd=real(Tad*sol(:,end,6));
T_cd=real(Tad*sol(:,end,7));
Trdmax=max(Y6,[],2);
Tcdmax=max(Y7,[],2);
%---- maximum temperature -----
Trmax(1,k)=max(T_rs);
Tcmax(1,k)=max(T_cs);
for i=1:N
    for j=1:tcnt
```

```
if Y8(j,i)<0
    Y8(j,i)=0;
end
if Y9(j,i)>1
    Y9(j,i)=1;
end
if Y9(j,i)<0
    Y9(j,i)=0;
end

% ---------- Gas velocities & Mole fractions -----------------------------
%-----ut-------
ut(j,i)=Y1(j,i)+Y2(j,i)+Y3(j,i)+Y4(j,i)+Y5(j,i);
utm(j,i) = Y10(j,i)+Y11(j,i);
% -----y=Pi/Pt=ui/ut------
yCO2(j,i)=Y1(j,i)/ut(j,i);yH2(j,i)=Y2(j,i)/ut(j,i);
yCO(j,i)=Y3(j,i)/ut(j,i);yH2O(j,i)=Y4(j,i)/ut(j,i);
yCH4(j,i)=Y5(j,i)/ut(j,i);

% yH2M (j,i) = Y10(j,i);
yH2M (j,i) = Y10(j,i) /utm(j,i);
yIM(j,i) = Y11(j,i) /utm(j,i);

%----velocity of gas-----------
vg(j,i)=vgf*ut(j,i); vgcap(j,i)=vg(j,i)/vgf; vgm(j,i) = vgfM*utm(j,i);

%---------thermophysical properties of gas, solid, and coolant---------
%----gas: mol/m^3, kJ/mol K, kW/mk, pa*s; solid : kg/m^3, kJ/kg K, kW/mk;
% coolant: kg/m^3, kJ/kg K, kW/mk, pa*s(kg/m s)
M_gf=uf2*M_H2+uf4*M_H2O+uf5*M_CH4+uf1*M_CO2+uf3*M_CO;
M_g(j,i)=yH2(j,i)*M_H2+yH2O(j,i)*M_H2O+yCH4(j,i)*M_CH4+yCO2(j,i)*M_CO2+yCO(j,
i)*M_CO;
ro_gmf=M_gf*Ctf;
Cp_H2(j,i)=3e-9*Y6(j,i)^2-2e-6*Y6(j,i)+0.0297; lamda_H2(j,i)=5e-7*Y6(j,i)+4e-
5; miu_H2(j,i)=2e-8*Y6(j,i)+5e-6;
Cp_H2O(j,i)=1e-8*Y6(j,i)^2-5e-6*Y6(j,i)+0.0356; lamda_H2O(j,i)=1e-7*Y6(j,i)-
2e-5; miu_H2O(j,i)=4e-8*Y6(j,i)-3e-6;
Cp_CH4(j,i)=0.03*log(Y6(j,i))-0.1394; lamda_CH4(j,i)=2e-7*Y6(j,i)-3e-5;
miu_CH4(j,i)=3e-8*Y6(j,i)+4e-6;
Cp_CO2(j,i)=-2e-8*Y6(j,i)^2+5e-5*Y6(j,i)+0.0256; lamda_CO2(j,i)=8e-8*Y6(j,i)-
4e-6; miu_CO2(j,i)=4e-8*Y6(j,i)+6e-6;
Cp_CO(j,i)=4e-6*Y6(j,i)+0.0276; lamda_CO(j,i)=6e-8*Y6(j,i)+8e-6;
miu_CO(j,i)=4e-8*Y6(j,i)+7e-6;
Cp_g(j,i)=yH2(j,i)*Cp_H2(j,i)+yH2O(j,i)*Cp_H2O(j,i)+yCH4(j,i)*Cp_CH4(j,i)+yCO
2(j,i)*Cp_CO2(j,i)+yCO(j,i)*Cp_CO(j,i);
lamda_g(j,i)=yH2(j,i)*lamda_H2(j,i)+yH2O(j,i)*lamda_H2O(j,i)+yCH4(j,i)*lamda_
CH4(j,i)+yCO2(j,i)*lamda_CO2(j,i)+yCO(j,i)*lamda_CO(j,i);
miu_g(j,i)=yH2(j,i)*miu_H2(j,i)+yH2O(j,i)*miu_H2O(j,i)+yCH4(j,i)*miu_CH4(j,i)
+yCO2(j,i)*miu_CO2(j,i)+yCO(j,i)*miu_CO(j,i);%gas
lamda_s(j,i)=5.5e-3+(34.5e-3)*exp(-0.0033*(Y6(j,i)-273));Cp_s=1.0446+(1.742e-
4)*Y6(j,i)-(2.796e+4)*Y6(j,i)^-2; %solid
%ro_c=350.95/Tc; Cp_c=10^3*(2e-10*Tc^2-1e-8*Tc+0.001); lamda_c=6e-8*Tc+9e-6;
miu_c=4e-11*Tc+8e-9;%air
%ro_c=244.05/Tc; Cp_c=10^3*(6e-12*Tc^3+1e-8*Tc^2-8e-6*Tc+0.0037); lamda_c=8e-
8*Tc-7e-6; miu_c=4e-11*Tc-1e-9;%steam
```

```
%ro_c(j,i)=-0.5572*Y7(j,i)+2219.1; Cp_c(j,i)=2e-
4*Y7(j,i)+1.2738;lamda_c(j,i)=2e-7*Y7(j,i)+4e-4; miu_c(j,i)=0.0744*exp(-
0.005*Y7(j,i));%molten salt MS-1
ro_c(j,i)=-0.6882*Y7(j,i)+2287.8;Cp_c(j,i)=6e-
5*Y7(j,i)+1.5557;lamda_c(j,i)=2e-7*Y7(j,i)+5e-4;miu_c(j,i)=0.4134*exp(-
0.008*Y7(j,i)); %MS-2 (403-773)

%--------- pressure drop -------------
vgsuper(j,i)=vg(j,i)*epsi;MASS(j,i)=ro_gmf*vgsuper(j,i);
J(j,i)=vgsuper(j,i)*miu_g(j,i)*(1-epsi)/(1e3*Ptf*epsi^3*dp);
S=150*(1-epsi)*L/dp;Re(j,i)=L*MASS(j,i)/miu_g(j,i);
Ptcap(j,i)=1+J(j,i)*(S+1.75*Re(j,i))*(1-x(i));
Pt(j,i)=Ptcap(j,i)*Ptf;
ro_g(j,i)=Pt(j,i)/(R*Y6(j,i));
% ro_g(j,i)=ut(j,i)*Ctf;
ro_gm(j,i)=M_g(j,i)*ro_g(j,i);

%--------- kinetic parameters ---------
yita1ad=Ea1/(R*Tad);
yita1(j,i)=Ea1/(R*Y6(j,i)); yita2(j,i)=Ea2/(R*Y6(j,i));
yita3(j,i)=Ea3/(R*Y6(j,i));
yitaeq1(j,i)=deltaHeq1/Y6(j,i);yitaeq2(j,i)=deltaHeq2/Y6(j,i);yitaeq3(j,i)=de
ltaHeq3/Y6(j,i);
k1ad=A1*exp(-yita1ad);
k1(j,i)=A1*exp(-yita1(j,i));k2(j,i)=A2*exp(-yita2(j,i));k3(j,i)=A3*exp(-
yita3(j,i));
k1cap(j,i)=k1(j,i)/k1ad;k2cap(j,i)=k2(j,i)*Pt(j,i)^1.5/k1ad;k3cap(j,i)=k3(j,i
)/k1ad;
Keq1(j,i)=B1*exp(-yitaeq1(j,i));Keq2(j,i)=B2*exp(-
yitaeq2(j,i));Keq3(j,i)=B3*exp(-yitaeq3(j,i));
Keq1cap(j,i)=Keq1(j,i)/(Pt(j,i)^2);Keq3cap(j,i)=Keq3(j,i)/(Pt(j,i)^2);
%---- gas adsorption equilibrium constants -----
KCO(j,i)=ACO*exp(-deltaHCO/(R*Y6(j,i)));KCH4(j,i)=ACH4*exp(-
deltaHCH4/(R*Y6(j,i)));KH2O(j,i)=AH2O*exp(-
deltaHH2O/(R*Y6(j,i)));KH2(j,i)=AH2*exp(-deltaHH2/(R*Y6(j,i)));
KCOcap(j,i)=KCO(j,i)*Pt(j,i);KCH4cap(j,i)=KCH4(j,i)*Pt(j,i);KH2cap(j,i)=KH2(j
,i)*Pt(j,i);
% %------ reaction rate ------
DEN(j,i)=1+KCOcap(j,i)*yCO(j,i)+KH2cap(j,i)*yH2(j,i)+KCH4cap(j,i)*yCH4(j,i)+K
H2O(j,i)*yH2O(j,i)/yH2(j,i);
f1(j,i)=(yCH4(j,i)*yH2O(j,i)/(yH2(j,i)^2.5)-
yH2(j,i)^0.5*yCO(j,i)/Keq1cap(j,i))/(DEN(j,i))^2;
f2(j,i)=(yCO(j,i)*yH2O(j,i)/yH2(j,i)-yCO2(j,i)/Keq2(j,i))/(DEN(j,i))^2;
f3(j,i)=(yCH4(j,i)*yH2O(j,i)^2/(yH2(j,i)^3.5)-
yH2(j,i)^0.5*yCO2(j,i)/Keq3cap(j,i))/(DEN(j,i))^2;
%---------- wall heat transfer coeficients(U) ------
lamda_w(j,i)=0.0146+1.27*10^(-5)*(Y6(j,i)-273);
Re_p(j,i)=vg(j,i)*ro_gm(j,i)*dp/miu_g(j,i);
Pr_p(j,i)=miu_g(j,i)*Cp_g(j,i)/(M_g(j,i)*lamda_g(j,i));
Re_c(j,i)=ro_c(j,i)*vc*dc/miu_c(j,i);
Pr_c(j,i)=Cp_c(j,i)*miu_c(j,i)/lamda_c(j,i);
if(Re_c(j,i)>4000)
   Nu_c(j,i)=0.027*Re_c(j,i)^0.8*Pr_c(j,i)^0.3;%turbulent
   elseif(Re_c(j,i)>2300&&Re_c(j,i)<4000)
   Nu_c(j,i)=0.012*(((Re_c(j,i)^0.87)-
280)*(Pr_c(j,i)^0.4)*(1+(dc/L)^0.66));%intermediate regime
```

```
else

Nu_c(j,i)=3.66+0.065*Re_c(j,i)*Pr_c(j,i)*(dc/L)/(1+0.04*(Re_c(j,i)*Pr_c(j,i)*
dc/L)^(2/3));
end
Nu_p(j,i)=24+0.34*Re_p(j,i)^0.77;
hwr(j,i)=lamda_g(j,i)*Nu_p(j,i)/dp;
hwc(j,i)=lamda_c(j,i)*Nu_c(j,i)/dc;
Ucw(j,i)=1/(1/hwr(j,i)+1/hwc(j,i)+dw/lamda_w(j,i));
% dil=0.05;kil=1.7e-3;hnc=14e-3;
% Urw(j,i)=1/(1/hwr(j,i)+dil/kil+1/hnc+dw/lamda_w(j,i));
%----------axial heat transfer coefficient-----
%kae=lamda_s+0.5*Cp_g*vg*ro_g*dp;
kae_pb(j,i)=lamda_g(j,i)*(8+0.05*Re_p(j,i)^1.09);
kae(j,i)=alpha*kae_pb(j,i)+(1-alpha)*lamda_w(j,i);
%----------effectiveness factor(eta)--------
Dm(j,i)=1e-07*Y6(j,i)^1.8766/Pt(j,i);
ksr1(j,i)=k1(j,i)*ro_s*(1-epsi)/(sqrt(Ptf)*ro_g(j,i)*epsi);
phi1(j,i)=sqrt(ksr1(j,i)*dp^2/(4*Dm(j,i)));
if phi1(j,i)<0.001
    phi1(j,i)=0.001;
end
eta1(j,i)=(3/phi1(j,i))*(1/tanh(phi1(j,i))-1/phi1(j,i));
ksr2(j,i)=k2(j,i)*ro_s*(1-epsi)*Ptf/(ro_g(j,i)*epsi);
phi2(j,i)=sqrt(ksr2(j,i)*dp^2/(4*Dm(j,i)));
if phi2(j,i)<0.001
    phi2(j,i)=0.001;
end
eta2(j,i)=(3/phi2(j,i))*(1/tanh(phi2(j,i))-1/phi2(j,i));
ksr3(j,i)=k3(j,i)*ro_s*(1-epsi)/(sqrt(Ptf)*ro_g(j,i)*epsi);
phi3(j,i)=sqrt(ksr3(j,i)*dp^2/(4*Dm(j,i)));
if phi3(j,i)<0.001
    phi3(j,i)=0.001;
end
eta3(j,i)=(3/phi3(j,i))*(1/tanh(phi3(j,i))-1/phi3(j,i));
%---- axial mass transfer coefficient -----
tau=1/(epsi^0.5);
Dae(j,i)=epsi*(Dm(j,i)/tau+0.5*dp*vg(j,i));
%----------dimensionless term-------
% sigma=(epsi*ro_g*Cp_g+(1-epsi)*ro_s*Cp_s)/(epsi*ro_g*Cp_g);
%beta=(-deltaH1)*Ctf/(ro_g(j,i)*Cp_g(j,i)*Tad);
%beta=(-deltaH1)/(Cp_g(j,i)*Tad);
%------------- Damkohler Number -------------------
Wc(j,i)=ro_s*(1-epsi);Ftf(j,i)=(Ctf*vg(j,i)/L)*epsi;
Da(j,i)=Wc(j,i)*k1ad/(Ftf(j,i)*(Pt(j,i))^0.5);
%------------------- other parameters ----------------------
Pem(j,i)=epsi*vg(j,i)*L/Dae(j,i);
Per(j,i)=L*vg(j,i)*epsi*ro_g(j,i)*Cp_g(j,i)/kae(j,i);
Pec(j,i)=L*vc*ro_c(j,i)*Cp_c(j,i)/lamda_c(j,i);
Str1(j,i)=Ucw(j,i)*avhe*L/(epsi*ro_g(j,i)*Cp_g(j,i)*vg(j,i));Str2(j,i)=Urw*av
hl*L/(epsi*ro_g(j,i)*Cp_g(j,i)*vg(j,i));Stc(j,i)=Ucw(j,i)*ache*L/(ro_c(j,i)*C
p_c(j,i)*vc);%--St
SCH4l(j,i)=(yCH4(j,i)-uf5)/(yCH4(j,i)+yCO(j,i)-uf5); % for SR
SCO=yCO/(yCO+yCO2)
CH4yieldl(j,i)=(yCH4(j,i)-uf5)/(yCH4(j,i)+yCO(j,i)+yCO2(j,i)-uf5); %for SR
H2yield=(4*yCO2+3*yCO)/(4*(yCH4+yCO2+yCO))
```

```
XCO2l(j,i)=(yCH4(j,i)+yCO(j,i)-uf5)/(yCO2(j,i)+yCO(j,i)+yCH4(j,i)-uf5); %for
SR XCH4l=(yCO2+yCO)/(yCO2+yCO+yCH4)

%-----mole fraction after water removal---------
utr(j,i)=ut(j,i)-Y4(j,i);
yrCO2(j,i)=Y1(j,i)/utr(j,i);yrH2(j,i)=Y2(j,i)/utr(j,i);yrCO(j,i)=Y3(j,i)/utr(
j,i);yrCH4(j,i)=Y5(j,i)/utr(j,i);
carbon(j,i) = Y8(j,i);
activity(j,i) = Y9(j,i);



%********************************* ACTUAL REACTION RATES******************
Rdct1(j,i)=real(-Da(j,i)*activity(j,i)*eta1(j,i)*k1cap(j,i)*f1(j,i));%  CO
Methanation
Rdct2(j,i)=real(-Da(j,i)*activity(j,i)*eta2(j,i)*k2cap(j,i)*f2(j,i)); % RWGS
Rdct3(j,i)=real(-Da(j,i)*activity(j,i)*eta3(j,i)*k3cap(j,i)*f3(j,i));%
Sabatier Reaction(CO2 methanation)

    end
end
Y6(end)
%-----SS outlet data------
SCH4=yCH4(end)/(yCH4(end)+yCO(end))
CH4yield=yCH4(end)/(yCH4(end)+yCO(end)+yCO2(end))
%---conversion----
%X5=(yCO2(j,i)+yCO(j,i))/(yCO2(j,i)+yCO(j,i)+yCH4(j,i))%CH4
CO2CONVERSION=(yCH4(end)+yCO(end))/(yCO2(end)+yCO(end)+yCH4(end))
yH2(end)
UTend=Y1(end)+Y2(end)+Y3(end)+Y4(end)+Y5(end)
Ytend=yCO2(end)+yCO(end)+yCH4(end)+yH2O(end)+yH2(end)
%------plot-------
UT=Y1_s+Y2_s+Y3_s+Y4_s+Y5_s;% for plot
Yt=yCO2(end,:)+yCO(end,:)+yCH4(end,:)+yH2O(end,:)+yH2(end,:);% should be 1
G
vc
ratio
%----steady state data-----
%----for loop-----
%NNf(1,k)=NN*uf1*deltaH3*VT*(Ptf/(R*Tf))*SVf/(dT*Cpcf);%kg/s
Tr_out(1,k)=T_rs(end);
Tc_out(1,k)=T_cs(end);
SCH4k(1,k)=(yCH4(end)-uf5)/(yCH4(end)+yCO(end)-uf5);
CH4yieldk(1,k)=(yCH4(end)-uf5)/(yCH4(end)+yCO(end)+yCO2(end)-uf5);
XCO2k(1,k)=(yCH4(end)+yCO(end)-uf5)/(yCO2(end)+yCO(end)+yCH4(end)-uf5);
Ptk(1,k)=(Ptf-Pt(end))/Ptf;
if XCO2l(end,:)<0.01
    SCH4l(end,:)=0;
end
if XCO2k(1,k)<0.01
    SCH4k(1,k)=0;
end
end
%save('GfigUSS.txt','NNf','SCH4k','CH4yieldk','XCO2k','Trmax','Tcmax','Tr_out
','Tc_out','Ptk','-ascii')
%type('GfigUSS.txt')
```

```
%----figures----------------
figure(1)
plot(t(2:end),yrCO2(2:end,end),'m-.','LineWidth',3)
hold on;plot(t(2:end),yrH2(2:end,end),'g-','LineWidth',3);
hold on;plot(t(2:end),yrCH4(2:end,end),'b-','LineWidth',3);
hold on;plot(t(2:end),yrCO(2:end,end),'r-','LineWidth',3);
axis([0 tmax_h 0 1.2]);
xlabel('t [h]');
ylabel('mole fraction','FontSize',18);
set(gcf,'color','w');
set(gca,'FontSize',16);
legend('CO_2','H_2','CH_4','CO')

%----3D plots----
figure(2)
mesh(x,t,yH2);
title('H2 mole fraction');
xlabel('z/L');
ylabel('t [h]');
zlabel('y_{H_2}')
set(gcf,'color','w')
set(gca,'FontSize',16);
axis([0 1 0 tmax_h 0 uf2+0.4])
colormap jet

figure(3)
mesh(x,t,yCO);
title('CO mole fraction');
xlabel('z/L');
ylabel('t [h]');
zlabel('y_{CO}')
set(gcf,'color','w')
set(gca,'FontSize',16);
axis([0 1 0 tmax_h 0 0.2])
colormap jet

figure(4)
mesh(x,t,yH2O);
title('H2O mole fraction');
xlabel('z/L');
ylabel('t [h]');
zlabel('y_{H_2O}')
set(gcf,'color','w')
set(gca,'FontSize',16);
axis([0 1 0 tmax_h 0 2*uf1+0.4])
colormap jet

figure(5)
mesh(x,t,yCH4);
title('CH_4 mole fraction');
xlabel('z/L');
ylabel('t [h]');
zlabel('y_{CH_4}')
set(gcf,'color','w')
set(gca,'FontSize',16);
```

```
axis([0 1 0 tmax_h 0 uf1+0.2])
colormap jet

figure(6)
mesh(x,t,Y6);
title('packed bed temperature');
xlabel('z/L');
ylabel('t [h]');
zlabel('T_{PB} [K]')
set(gcf,'color','w')
set(gca,'FontSize',16);
axis([0 1 0 tmax_h 500 1000])
colormap jet
h = colorbar; set(h,'FontSize',12,'Ticks',[550 600 650 700 750 800 850]);

figure(7)
mesh(x,t,Y7);
title('coolant temperature');
xlabel('z/L');
ylabel('t [h]');
zlabel('T_{MS} [K]')
set(gcf,'color','w')
set(gca,'FontSize',16);
axis([0 1 0 tmax_h 500 1000])
colormap jet
h = colorbar; set(h,'FontSize',12,'Ticks',[550 600 650 700 750 800 850]);

%------1D plots for different times------

figure(15)
plot(x,Pt*0.01','k-');
hold on; plot(x,vgcap','k-');
xlabel('z/L');
ylabel('P_t [bar], v_g/v_{gf}');
axis([0 1 0 Ptf*1.5e-2]);
set(gcf,'color','w')
set(gca,'FontSize',16);
title('gas velocity & total pressure')

%-----steady state reactor and coolant temperature profile(final time)----
figure(18)
plot(x,T_rs,'r-','LineWidth',3);
hold on;plot(x,T_cs,'b-.','LineWidth',3)
axis([0 1 300 1200]);
xlabel('z/L');
ylabel('T [K]');
set(gcf,'color','w');
set(gca,'FontSize',16);
legend('T_{PB}','T_{MS}')
% print(figure(18),'-dpng')
% title('Steady state temperature')

figure(23)
plot(x,UT,'r-','LineWidth',2);
hold on;plot(x,Yt,'c-','LineWidth',2);
axis([0 1 0 4]);
```

```
xlabel('z/L');
ylabel('y_t, u_t');
set(gcf,'color','w');
set(gca,'FontSize',16);
legend('u_t','y_t')
title('total mole fraction')

figure(24)
plot(x,SCH4l(end,:),'g-','LineWidth',3);
hold on;plot(x,CH4yieldl(end,:),'k-.','LineWidth',3);
hold on;plot(x,XCO2l(end,:),'b--','LineWidth',3);
hold on;plot(x,(Ptf-Pt(end,:))/Ptf,'r:','LineWidth',3);
axis([0 1 0 1.2]);
xlabel('z/L');
ylabel('X, Y, S, \DeltaP_N','FontSize',18);
set(gcf,'color','w');
set(gca,'FontSize',16);
legend('S_{CH_4}','Y_{CH_4}','X_{CO_2}','\DeltaP_N')
title('reactor performance')
% print(figure(24),'-dpng')

figure(25)
plot(x,yCO2(end,:),'r-','LineWidth',3);
hold on;plot(x,yH2(end,:),'c--','LineWidth',3);
hold on;plot(x,yCO(end,:),'g-.','LineWidth',3);
hold on;plot(x,yH2O(end,:),'k--.','LineWidth',3);
hold on;plot(x,yCH4(end,:),'b:','LineWidth',3);
axis([0 1 0 1]);
xlabel('z/L');
ylabel('y_i');
set(gcf,'color','w');
set(gca,'FontSize',16);
legend('CO_2','H_2','CO','H_2O','CH_4')
% print(figure(25),'-dpng')
title('mole fraction profiles')

figure(26)
plot(x,yrCO2(end,:),'r-','LineWidth',3);
hold on;plot(x,yrH2(end,:),'c--','LineWidth',3);
hold on;plot(x,yrCO(end,:),'g-.','LineWidth',3);
hold on;plot(x,yrCH4(end,:),'b:','LineWidth',3);
axis([0 1 0 1]);
xlabel('z/L');
ylabel('y_i');
set(gcf,'color','w');
set(gca,'FontSize',16);
legend('CO_2','H_2','CO','CH_4')
title('mole fractions on dry basis')
% print(figure(26),'-dpng')

%------deactivation----
figure(30)
plot(t(2:end),SCH4l(2:end,end),'g-','LineWidth',3);
hold on;plot(t(2:end),CH4yieldl(2:end,end),'k-.','LineWidth',3);
hold on;plot(t(2:end),XCO2l(2:end,end),'b--','LineWidth',3);
axis([0 tmax_h 0 1.2]);
```

```
xlabel('t [h]');
ylabel('X_{CO_2}, S_{CH_4}, Y_{CH_4}','FontSize',18);
set(gcf,'color','w');
set(gca,'FontSize',16);
legend('S_{CH_4}','Y_{CH_4}','X_{CO_2}')
title('reactor performance')

figure(31)
plot(t,T_rd,'r-','LineWidth',3);
hold on;plot(t,Trdmax,'b--','LineWidth',3);
axis([0 tmax_h 300 1200]);
xlabel('t [h]');
ylabel('T [K]');
set(gcf,'color','w');
set(gca,'FontSize',16);
legend('T_{PB,out}','T_{PB,max}')
title('packed bed temperature')

figure(32)
plot(t,T_cd,'r-','LineWidth',3);
hold on;plot(t,Tcdmax,'b--','LineWidth',3);
axis([0 tmax_h 300 1200]);
xlabel('t [h]');
ylabel('T [K]');
set(gcf,'color','w');
set(gca,'FontSize',16);
legend('T_{MS,out}','T_{MS,max}')
title('coolant temperature')

figure(33)
mesh(x,t,Y6)
xlabel('z/L');
ylabel('t[h]');
zlabel('T_{PB}');
% axis([0 1 0 tmax_h 0 1]);
set(gcf,'color','w')
set(gca,'FontSize',16);
colormap jet
colorbar

%********** DEACTIVATION PLOTS ****************
figure(34)
mesh(x,t,eta1)
xlabel('z/L');
ylabel('t [h]');
zlabel('eta1');
axis([0 1 0 tmax_h 0 1]);
set(gcf,'color','w')
set(gca,'FontSize',16);
title('eta1')
colormap jet

figure(35)
mesh(x,t,eta2)
xlabel('z/L');
ylabel('t [h]');
```

```
zlabel('eta2');
axis([0 1 0 tmax_h 0 1]);
set(gcf,'color','w')
set(gca,'FontSize',16);
title('eta2')
colormap jet

figure(36)
mesh(x,t,eta3)
xlabel('z/L');
ylabel('t [h]');
zlabel('eta3');
axis([0 1 0 tmax_h 0 1]);
set(gcf,'color','w')
set(gca,'FontSize',16);
title('eta3')
colormap jet

figure(37)
mesh(x,t,Rdct1)
xlabel('z/L');
ylabel('t [h]');
zlabel('actual rate');
% axis([0 1 0 tmax_h 0 1]);
set(gcf,'color','w')
set(gca,'FontSize',16);
title('CO methanation')
colormap jet

figure(38)
mesh(x,t,Rdct2)
xlabel('z/L');
ylabel('t [h]');
zlabel('actual rate');
% axis([0 1 0 tmax_h 0 1]);
set(gcf,'color','w')
set(gca,'FontSize',16);
title('RWGS')
colormap jet

figure(39)
mesh(x,t,Rdct3)
xlabel('z/L');
ylabel('t [h]');
zlabel('actual rate');
% axis([0 1 0 tmax_h 0 1]);
set(gcf,'color','w')
set(gca,'FontSize',16);
title('Sabaier reaction')
colormap jet

figure(40)
plot(t(2:end),carbon(2:end,end),'b-','LineWidth',3)
xlabel('t [h]');
ylabel('carbon, g/g_{cat}');
```

```
figure(41)
plot(t(2:end),activity(2:end,end),'r-','LineWidth',3)
axis([0 tmax_h 0 1.2]);
xlabel('t [h]');
ylabel('activity, r/r_{max}');

figure(42)
plot(x,carbon(end,:),'b--','LineWidth',3);
xlabel('z/L');
ylabel('carbon g/g_{cat}');

figure(43)
plot(x,activity(end,:),'r--','LineWidth',3);
axis([0 1 0 1]);
xlabel('z/L');
ylabel('activity, r/r_{max}');

figure(44)
mesh(x,t,activity)
xlabel('z/L');
ylabel('t [h]');
zlabel('activity');
axis([0 1 0 tmax_h 0 1]);
set(gcf,'color','w')
set(gca,'FontSize',16);
title('activity')
colormap jet

figure(45)
mesh(x,t,carbon)
xlabel('z/L');
ylabel('t [h]');
zlabel('carbon g/g_{cat}');
set(gcf,'color','w')
set(gca,'FontSize',16);
title('carbon')
colormap jet

figure(46)
mesh(x,t,yH2M);
xlabel('z/L');
ylabel('t [h]');
zlabel('y_{H_2}')
set(gcf,'color','w')
set(gca,'FontSize',16);
axis([0 1 0 tmax_h 0 uf8+0.2])
colormap jet

figure(47)
title('H2 membrane mole fraction');
plot(x,yH2M(end,:),'r-','LineWidth',3);
hold on;
plot(x,yIM(end,:),'b-','LineWidth',3);
set(gcf,'color','w');
set(gca,'FontSize',16);
axis([0 1 0 1]);
```

```
xlabel('z/L');
ylabel('y_{i}');
legend('y_{H2,mem}','y_{inert,mem}')


%-------------------------------------------------------------------
function
[c,f,s]=eqns(x,tao,y,DyDx,N,Tad,deltaHcap1,deltaHcap2,deltaHcap3,Tf,Ptf,PtfM,
R,L,n,dp,epsi,dw,dc,ache,avhe,avhl,vc,uf1,uf2,uf3,uf4,uf5,uf6,uf7,uf8,uf9,uf1
0,uf11,Tcf,Te,Ea1,Ea2,Ea3,EaP,EaH,deltaHeq1,deltaHeq2,deltaHeq3,thetaf,thetae
,thetacf,vgf,vgfM,Ctf,CtfM,M_CH4,M_H2,M_H2O,M_CO2,M_CO,A1,A2,A3,Ap,D0,B1,B2,B
3,ACO,ACH4,AH2O,AH2,deltaHCO,deltaHCH4,deltaHH2O,deltaHH2,deltaH1,ro_s,G,t_ma
x,Urw,alpha,VT,A,A_pb,SVf,Sm,nm,VTM)

% ------------------------ STEPWISE CHANGES IN PARAMETERS -----------------
% if tao>t_max*0.2
%     Ctf=Ptf/(R*400);
% %     vgf=L*(500/3600)/epsi;
% vc=(5*uf1*165*VT*(Ptf/(R*400))*SVf/(300*1.425))/(1850*A);
% end

% ----------------- CALCULATIONS ------------------------------------------
% ----- Molar Fractions (y=Pi/Pt=ui/ut) -------
ut=real(y(1)+y(2)+y(3)+y(4)+y(5));                          %dimensionless
utm = real(y(10)+uf9+uf10+uf11);                            %dimensionless
yCO2=real(y(1)/ut); yH2=real(y(2)/ut);                      %dimensionless
yCO=real(y(3)/ut); yH2O=real(y(4)/ut); yCH4=real(y(5)/ut);  %dimensionless
yH2M = real(y(10)/utm);

carbon = real(y(8)); %dimensionless
activity = real(y(9)); %dimensionless
% ------------- Gas Velocity -----------------------------
vg=vgf*ut; %vgcap=vg/vgf; %m/s
vgM = vgfM*utm; %m/s
%--------- Dimensional Temperatures -------
T=real(y(6))*Tad;  %K
Tc=real(y(7))*Tad; %K

%-------------------- THERMOPHYSICAL PROPERTIES --------------------------
M_g=yH2*M_H2+yH2O*M_H2O+yCH4*M_CH4+yCO2*M_CO2+yCO*M_CO; %kg/mol
M_gf=uf2*M_H2+uf4*M_H2O+uf5*M_CH4+uf1*M_CO2+uf3*M_CO; %kg/mol
ro_gmf=M_gf*Ctf; %kg/m3
Cp_H2=3e-9*T^2-2e-6*T+0.0297; lamda_H2=5e-7*T+4e-5; miu_H2=2e-8*T+5e-6;
%kJ/(mol K), kW/(m K), Pa*s
Cp_H2O=1e-8*T^2-5e-6*T+0.0356; lamda_H2O=1e-7*T-2e-5; miu_H2O=4e-8*T-3e-6;
%kJ/(mol K), kW/(m K), Pa*s
Cp_CH4=0.03*log(T)-0.1394; lamda_CH4=2e-7*T-3e-5; miu_CH4=3e-8*T+4e-6;
%kJ/(mol K), kW/(m K), Pa*s
Cp_CO2=-2e-8*T^2+5e-5*T+0.0256; lamda_CO2=8e-8*T-4e-6; miu_CO2=4e-8*T+6e-6;
%kJ/(mol K), kW/(m K), Pa*s
Cp_CO=4e-6*T+0.0276; lamda_CO=6e-8*T+8e-6; miu_CO=4e-8*T+7e-6;
%kJ/(mol K), kW/(m K), Pa*s
Cp_g=yH2*Cp_H2+yH2O*Cp_H2O+yCH4*Cp_CH4+yCO2*Cp_CO2+yCO*Cp_CO;
%kJ/(mol K)
lamda_g=yH2*lamda_H2+yH2O*lamda_H2O+yCH4*lamda_CH4+yCO2*lamda_CO2+yCO*lamda_C
O; %(kW/(m K)
```

```
miu_g=yH2*miu_H2+yH2O*miu_H2O+yCH4*miu_CH4+yCO2*miu_CO2+yCO*miu_CO;
%Pa*s
lamda_s=5.5e-3+(34.5e-3)*exp(-0.0033*(T-273));
%kW/(m K)
Cp_s=1.0446+(1.742e-4)*T-(2.796e+4)*T^-2;
%kJ/(kg K)

%ro_c=350.95/Tc; Cp_c=10^3*(2e-10*Tc^2-1e-8*Tc+0.001); %lamda_c=6e-8*Tc+9e-6;
miu_c=4e-11*Tc+8e-9;              % AIR
%ro_c=244.05/Tc; Cp_c=10^3*(6e-12*Tc^3+1e-8*Tc^2-8e-6*Tc+0.0037);
%lamda_c=8e-8*Tc-7e-6; miu_c=4e-11*Tc-1e-9;  % STEAM
%ro_c=-0.5572*Tc+2219.1; Cp_c=2e-4*Tc+1.2738; lamda_c=2e-7*Tc+4e-4;
miu_c=0.0744*exp(-0.005*Tc);                % MS-1(503-858)
ro_c=-0.6882*Tc+2287.8; Cp_c=6e-5*Tc+1.5557;       % kg/m3, kJ/(kg K); MS-2
(403-773)
lamda_c=2e-7*Tc+5e-4; miu_c=0.4134*exp(-0.008*Tc); % kW/(m K), Pa*s; MS-2
(403-773)

%-------------------------- PRESSURE DROP ---------------------------------
vgsuper=vg*epsi; %m/s
MASS=ro_gmf*vgsuper; %kg/(m^2 s)
J=(vgsuper)*miu_g*(1-epsi)/(1e3*Ptf*epsi^3*dp); %dimensionless
S=150*(1-epsi)*L/dp; %dimensionless
Re=L*MASS/miu_g; %dimensionless
Ptcap=1+J*(S+1.75*Re)*(1-x); %dimensionless     CORRECTED!!!!!!
Pt=Ptcap*Ptf; %kPa
ro_g=Pt/(R*T); %mol/m3
% ro_g=ut*Ctf;
ro_gm=M_g*ro_g; %kg/m3

%---------- REACTION KINETICS ----------------------------------------------
yita1ad=Ea1/(R*Tad); %dimensionless
yitapad = EaP/(R*Tad); %membrane dimensionless
yita1=Ea1/(R*T); yita2=Ea2/(R*T); yita3=Ea3/(R*T); %dimensionless
yitap = EaP/(R*T);
yitaeq1=deltaHeq1/T;yitaeq2=deltaHeq2/T;yitaeq3=deltaHeq3/T; %dimensionless
k1ad=A1*exp(-yita1ad); %(mol kPa^0.5)/(kg s)
kpad = Ap*exp(-yitapad); %membrane mol/m2 s kPa0.5
k1=A1*exp(-yita1);     %(mol kPa^0.5)/(kg s)
k2=A2*exp(-yita2);     %(mol/(kPa kg s)
k3=A3*exp(-yita3);     %(mol kPa^0.5)/(kg s)
kp = Ap*exp(-yitap);   %membrane mol/m2 s kPa0.5
k1cap=k1/k1ad;   k2cap=k2*Pt^1.5/k1ad;   k3cap=k3/k1ad; %dimensionless
kpcap = kp/kpad; %membrane dimensionless

Keq1=B1*exp(-yitaeq1); %kPa^2
Keq2=B2*exp(-yitaeq2); %dimensionless
Keq3=B3*exp(-yitaeq3); %kPa^2
Keq1cap=Keq1/(Pt^2); Keq3cap=Keq3/(Pt^2); %dimensionless

%-------- DEACTIVATION KINETICS-------------------------------------------
p_adj=5;
kd = exp(20.492 - 104200/(T*8.314)); % specific rate of carbon deposition,
(bar*hr)^-1
Kp = p_adj*5.088e5*exp(-91200/(T*8.314)); % Equilibrium constant for methane
cracking, bar
```

```
KH = exp(163200/(8.314*T) - 22.426); % Eqilibrium constant for hydrogen
adsorption , bar^-0.5
ka = exp(135600/(8.314*T) - 32.077); % Deactivation rate constant, g^3*hr/g^3
Kphat = Kp/(Pt/100); %dimensionless
KHhat = KH*((Pt/100)^0.5); %dimensionless

%------------ Adsorption Constants ----------------------------------
KCO=ACO*exp(-deltaHCO/(R*T));KCH4=ACH4*exp(-deltaHCH4/(R*T)); %1/kPa
KH2=AH2*exp(-deltaHH2/(R*T)); %1/kPa
KH2O=AH2O*exp(-deltaHH2O/(R*T)); %dimensionless
KCOcap=KCO*Pt;KCH4cap=KCH4*Pt;KH2cap=KH2*Pt; %dimensionless

fctr=0;
if yH2<0
    yH2=0;
end

if yH2==0
    yH2=0.01;
end
%------------- Reaction Rates ----------------------------------------
DEN=real(1+KCOcap*yCO+KH2cap*yH2+KCH4cap*yCH4+KH2O*yH2O/(yH2+fctr));
%dimensionless
f1=real((yCH4*yH2O/((yH2+fctr)^2.5)-yH2^0.5*yCO/Keq1cap)/(DEN)^2);
%dimensionless
f2=real((yCO*yH2O/(yH2+fctr)-yCO2/Keq2)/(DEN)^2); %dimensionless
f3=real((yCH4*yH2O^2/((yH2+fctr)^3.5)-yH2^0.5*yCO2/Keq3cap)/(DEN)^2);
%dimensionless
rmax = real((yCH4-yH2^2/Kphat)/((1+KHhat*sqrt(yH2+fctr))^2));


%---------------------- TRANSPORT COEFFICIENTS ----------------------------
% ---------- Dimensionless Numbers -----------------
Re_p=vg*ro_gm*dp/miu_g;              %dimensionless
Pr_p=miu_g*Cp_g/(M_g*lamda_g);       %dimensionless
Re_c=ro_c*vc*dc/miu_c;               %dimensionless
Pr_c=Cp_c*miu_c/lamda_c;             %dimensionless
Nu_p=0.34*Re_p^0.77+24;              %dimensionless

% --------- Nusselt Numbers for Cooling, dimensionless -------------
if(Re_c>4000)
   Nu_c=0.027*Re_c^0.8*Pr_c^0.3;                                  %turbulent
elseif(Re_c>2300&&Re_c<4000)
   Nu_c=0.012*(((Re_c^0.87)-280)*(Pr_c^0.4)*(1+(dc/L)^0.66)); %intermediate
else
   Nu_c=3.66+0.065*Re_c*Pr_c*(dc/L)/(1+0.04*(Re_c*Pr_c*dc/L)^(2/3)); %laminar
end

% ---------- Wall Heat Transfer Coefficients ----------------------
% ------- Heat Exchange ---------------------
lamda_w=0.0146+1.27*10^(-5)*(T-273); %kW/(m K)
hwr=lamda_g*Nu_p/dp; %kW/(m^2 K)
hwc=lamda_c*Nu_c/dc; %kW/(m^2 K)
Ucw=1/(1/hwr+1/hwc+dw/lamda_w); %kW/(m^2 K)
% ------- Heat Losses -----------------------
```

```
% dil=0.05; kil=1.7e-3; hnc=14e-3;
% Urw=1/(1/hwr+dil/kil+1/hnc+dw/lamda_w);

%---------- Axial Mass & Heat Transfer Coefficints ------------------------
% ----- Binary Diffusion Coefficient (CO2-H2) ---------
Dm=1e-07*T^1.8766/Pt; %m^2/s
tau=1/(epsi^0.5); %dimensionless
if( Re_p<1)
    Dae=epsi*Dm/tau; %m^2/s
else
    Dae=epsi*(Dm/tau+0.5*dp*vg); %m^2/s
end
%kae=lamda_s+0.5*Cp_g*vg*ro_g*dp;
kae_pb=lamda_g*(8+0.05*Re_p^1.09);  %kW/(m K)
kae=alpha*kae_pb+(1-alpha)*lamda_w; %kW/(m K)

%-------------------- EFFECTIVENESS FACTORS -------------------------------
% ----- Binary Diffusion Coefficient (CO2-H2) ---------
Dm=1e-07*T^1.8766/Pt; %m^2/s
% ----- Thiele Modulii & Effectiveness Factors --------
ksr1=k1*ro_s*(1-epsi)/(sqrt(Ptf)*ro_g*epsi); %1/s
phi1=sqrt(ksr1*dp^2/(4*Dm)); %dimensionless
if phi1<0.001
    phi1=0.001;
end
eta1=real((3/phi1)*(1/tanh(phi1)-1/phi1)); %dimensionless

ksr2=k2*ro_s*(1-epsi)*Ptf/(ro_g*epsi); %1/s
phi2=sqrt(ksr2*dp^2/(4*Dm));%dimensionless
if phi2<0.001
    phi2=0.001;
end
eta2=real((3/phi2)*(1/tanh(phi2)-1/phi2));%dimensionless

ksr3=k3*ro_s*(1-epsi)/(sqrt(Ptf)*ro_g*epsi); %1/s
phi3=sqrt(ksr3*dp^2/(4*Dm));%dimensionless
if phi3<0.001
    phi3=0.001;
end
eta3=real((3/phi3)*(1/tanh(phi3)-1/phi3));%dimensionless

%---------- DIMENSIONLESS TERMS IN EQUATIONS ------------------------------
sigma=(epsi*ro_g*Cp_g+(1-epsi)*ro_s*Cp_s)/(epsi*ro_g*Cp_g); %dimensionless
beta=(-deltaH1)/(Cp_g*Tad*ut);                              %dimensionless
% beta=(-deltaH1)*Ctf/(ro_g*Cp_g*Tad); <- PROBABLY WRONG

% ----- Damkohler Number ---PROBLEM with using vgf-!!!!!--
p_ceff=ro_s*(1-epsi);           % kg/m3
                            Ftf_V=(Ctf*vg/L)*epsi;          % mol/(m3 s)
if tao>0.01*t_max
Ftf_V=(Ctf*vgf/L)*epsi;
end

Da=p_ceff*k1ad/(Ftf_V*(Pt)^0.5);  % dimensionless
```

```
%----Deactivation Damkohler Number-------------------
restime = (L/(vgf))/3600; %hr
DaC = restime*(Pt/100)*kd; %dimensionless
DaA = restime*((Pt/100)^2)*(kd^2)*ka; %dimensionless

% ----- Peclet Numbers --------------------------------
Pem=epsi*vgf*L/Dae;                %dimensionless
Per=L*vgf*epsi*ro_g*Cp_g/kae;      %dimensionless
Pec=L*vgf*ro_c*Cp_c/lamda_c;       %dimensionless

%---- Deactivation Peclet Numbers--------------------
Pe_C = 1000000; % dimensionless, used for numerical purposes
Pe_A = 1000000; % dimensionless, used for numerical purposes

%---- Membrane Peclet Numbers--------------------
restimePb = L/vgf; %s
DaeH = D0*exp(-EaH/(R*T)); %m2/s
PecMPb= restimePb*Sm*kpad/(epsi*Ctf*VT); %Membrane Peclet number, packed bed
side
PecM = restimePb*Sm*kpad/(CtfM*VTM); %Peclet number, membrane side
PemM = vgf*L/DaeH;
Dinert = (6e-6)*(T^2)+0.0001*T+0.1997; %cm2/s
Dinert = Dinert/(100*100); %m2/s
PemI = vgf*L/Dinert;

% ----- Stanton Numbers --------------------------------
Str1=Ucw*avhe*L/(epsi*ro_g*Cp_g*vgf); %dimensionless
Str2=Urw*avhl*L/(epsi*ro_g*Cp_g*vgf); %dimensionless
Stc=Ucw*ache*L/(ro_c*Cp_c*vgf);       %dimensionless

act=y(9);
if act<0
    act=0;
end
if act>1
    act=1;
end

% ------------- SIMILATION PROGRESS ----------------------------------------
time=tao/t_max;    % dimensionless
t_d=tao*L/vgf/60;  % min
time_h=t_d/60     % hours

% ----------------- EQUATIONS AND INITIAL & BOUNDARY CONDITIONS -----------

%---------- Equations ---------------
ut_der=real(DyDx(1)+DyDx(2)+DyDx(3)+DyDx(4)+DyDx(5));
per_rc=real(nm*PecMPb*kpcap*((sqrt(yH2M)*sqrt(PtfM))-(sqrt(yH2)*sqrt(Pt))));
per_mc=real(PecM*kpcap*((sqrt(yH2)*sqrt(Pt))-(sqrt(yH2M)*sqrt(PtfM))));
RH=real(Da*act*beta*(k1cap*f1*deltaHcap1*eta1+k2cap*f2*deltaHcap2*eta2+k3cap*
f3*deltaHcap3*eta3));

cfctr=1;
if tao<0.01*t_max
cfctr=0;
```

```
end

c=[ 1%CO2
    1%H2
    1%CO
    1%H2O
    1%CH4
    1
    1
    1
    1
    1
    1];

f=[ 1/Pem
    1/Pem
    1/Pem
    1/Pem
    1/Pem
    1/(Per*sigma)
    1/Pec
    1/Pe_C
    1/Pe_A
    1/PemM
    1/PemI].*DyDx;

s=[ -real(DyDx(1))+real(Da*act*(k2cap*f2*eta2+k3cap*f3*eta3)-y(1)*ut_der)
    -
real(DyDx(2))+real(Da*act*(3*k1cap*f1*eta1+k2cap*f2*eta2+4*k3cap*f3*eta3)-
y(2)*ut_der+per_rc)
    -real(DyDx(3))+real(Da*act*(k1cap*f1*eta1-k2cap*f2*eta2)-y(3)*ut_der)
    -real(DyDx(4))+real(Da*act*(-k1cap*f1*eta1-k2cap*f2*eta2-
2*k3cap*f3*eta3)-y(4)*ut_der)
    -real(DyDx(5))+real(Da*act*(-k1cap*f1*eta1-k3cap*f3*eta3)-y(5)*ut_der)
    (-real(DyDx(6))+RH-real(n*Str1*(y(6)-y(7)))-real(Str2*(y(6)-
thetae)))/sigma
    -real(DyDx(7)*vc/vgf)-real(Stc*(y(7)-y(6)))
     real(DaC*rmax*act)
    -real(DaA*rmax^2*y(8)*act)
    -real(DyDx(10)*utm*(vgfM/vgf))+real(per_mc-
y(10)*(vgfM/vgf)*(DyDx(10)+cfctr*DyDx(11)))
    -real(DyDx(11)*utm*(vgfM/vgf)-y(11)*(vgfM/vgf)*(DyDx(10)+DyDx(11)))];

%---------------------- Initial Conditions ----------------
function
y0=eqn_ic(x,N,Tad,deltaHcap1,deltaHcap2,deltaHcap3,Tf,Ptf,PtfM,R,L,n,dp,epsi,
dw,dc,ache,avhe,avhl,vc,uf1,uf2,uf3,uf4,uf5,uf6,uf7,uf8,uf9,uf10,uf11,Tcf,Te,
Ea1,Ea2,Ea3,EaP,EaH,deltaHeq1,deltaHeq2,deltaHeq3,thetaf,thetae,thetacf,vgf,v
gfM,Ctf,CtfM,M_CH4,M_H2,M_H2O,M_CO2,M_CO,A1,A2,A3,Ap,D0,B1,B2,B3,ACO,ACH4,AH2
O,AH2,deltaHCO,deltaHCH4,deltaHH2O,deltaHH2,deltaH1,ro_s,G,t_max,Urw,alpha,VT
,A,A_pb,SVf,Sm,nm,VTM)
y0=[uf1
    uf2
    uf3
    uf4
    uf5
```

```
    650/Tad
    650/Tad
    uf6
    uf7
    uf8
    uf11];

%---------------------- Boundary Conditions ---------------
function
[pl,ql,pr,qr]=eqn_bc(xl,yl,xr,yr,tao,N,Tad,deltaHcap1,deltaHcap2,deltaHcap3,T
f,Ptf,PtfM,R,L,n,dp,epsi,dw,dc,ache,avhe,avhl,vc,uf1,uf2,uf3,uf4,uf5,uf6,uf7,
uf8,uf9,uf10,uf11,Tcf,Te,Ea1,Ea2,Ea3,EaP,EaH,deltaHeq1,deltaHeq2,deltaHeq3,th
etaf,thetae,thetacf,vgf,vgfM,Ctf,CtfM,M_CH4,M_H2,M_H2O,M_CO2,M_CO,A1,A2,A3,Ap
,D0,B1,B2,B3,ACO,ACH4,AH2O,AH2,deltaHCO,deltaHCH4,deltaHH2O,deltaHH2,deltaH1,
ro_s,G,t_max,Urw,alpha,VT,A,A_pb,SVf,Sm,nm,VTM)

% ------------------------ STEPWISE CHANGES IN BCs ------------------------
% if tao>t_max*0.2
%      thetaf=400/Tad;
% end
% -------------------------------------------------------------------------

pl=[real(uf1-yl(1))
    real(uf2-yl(2))
    real(uf3-yl(3))
    real(uf4-yl(4))
    real(uf5-yl(5))
    real(thetaf-yl(6))
    real(thetacf-yl(7))
    0
    0
    real(uf8-yl(10))
    uf11-yl(11)];

ql=[1
    1
    1
    1
    1
    1
    1
    1
    1
    1];

pr=[0
    0
    0
    0
    0
    0
    0
    0
    0
    0
```

```
    0];

qr=[1
    1
    1
    1
    1
    1
    1
    1
    1
    1
    1];
```

I. Actively cooled Sabatier reactor code (non-membrane)

```
function SR
close all

% --------- REACTOR GEOMETRY ----------------------------------------------
L=0.4; dp=0.003; dr=0.1; dc=0.02; dw=0.002; dm = 0.01; %m
epsi=0.5; n=5; %dimensionless
%------------------------------------ $$$ NUMBER OF MEMBRANES $$$ --------
                                                    nm =0*4; %dimensionless
%-------------------------------------------------------------------------
ro_s=1.274e+3; %kg/m3
ache=4/dc; avhe=4*(dc+dw)/(dr^2-n*(dc+dw)^2-nm*dm^2); %1/m
avhl=4*dr/(dr^2-n*(dc+dw)^2-nm*dm^2); %1/m
A=n*pi*(dc/2)^2; A_pb=pi*(dr^2-n*(dc+dw)^2-nm*dm^2)/4; %m^2
A_total=pi*((dr+dw)^2-n*dc^2-nm*dm^2)/4; %m^2
Sm = pi*dm*L; %m^2 membrane surface area
VT=L*pi*(dr/2)^2-n*L*pi*((dc+dw)/2)^2-nm*L*pi*(dm/2)^2; %m^3
VTM = L*pi*(dm/2)^2; %single membrane volume
alpha=A_pb/A_total; %dimensionless
%------------- Membrane Permeability -----------------------------------
Ap = 5.6; % Hydrogen permeability pre-exponential factor mol/m2 s bar0.5
Ap = Ap*sqrt(0.01); %mol/m2 s kPa0.5
D0 = 0.294*10^-6; %hydrogen diffusion pre-exponential factor m2/s
% ------ Heat Losses to Environment ------------------------------------
                                                    Urw=10e-3; %kW/(m2 K)

%------------------- KINETICS (Xu & Froment; NEW PARAMETERS) --------------
R=8.314e-3;    %kJ/(mol K)
% ---- Parameters for Equilibrium Constants ----------
deltaHeq1=26830; deltaHeq2=-4400; deltaHeq3=22430; %K
B1=1.198e17; %kPa^2          (MSR)
B2=1.767e-2; %dimensionless (WGS)
B3=2.117e15; %kPa^2       (MSR + WGS)
% ---- Parameters for Reaction Rate Constants---------
Ea1=122.4; Ea2=93.1; Ea3=104.8; %kJ/mol
EaP = 11; %hydrogem permeability activation energy kJ/mol
EaH = 22; %Hydrogen diffusion activation energy kJ/mol
kref1=6.55e-3;       %(kmol bar^0.5)/(kg h)
```

```
kref2=91.2e-3;    %kmol/(kPa kg h)
kref3=23.38e-15;        %(kmol bar^0.5)/(kg h)
kref1 = kref1/(sqrt(0.01));  %(kmol kPa^0.5)/(kg h)
kref3 = kref3/(sqrt(0.01));  %(kmol kPa^0.5)/(kg h)
kref1 = kref1*1000/3600;     %(mol kPa^0.5)/(kg s)
kref2 = kref2*1000/3600;     %mol/(kPa kg s)
kref3 = kref3*1000/3600;     %(mol kPa^0.5)/(kg s)
% conversion to pre-exponent factors according to A*exp(-Ea/RT)
A1 = kref1*exp(Ea1/(R*598.15)) %(mol kPa^0.5)/(kg s)
A2 = kref2*exp(Ea2/(R*598.15)) %mol/(kPa kg s)
A3 = kref3*exp(Ea3/(R*598.15)) %(mol kPa^0.5)/(kg s)
% ---- Parameters for Adsorption Constants -----------
deltaHCO=-97.3;  %kJ/mol
deltaHCH4=-57.7; %kJ/mol
deltaHH2O=104.4;  %kJ/mol
deltaHH2=-103.4;   %kJ/mol
KCOref=104.79e-3; %1/kPa
KH2Oref=1.52e-3; %dimensionless
KH2ref=401.9e-6; %1/kPa
KCH4ref=2.52e-3; %1/kPa
ACO = KCOref*exp(deltaHCO/(R*648))
ACH4 = KCH4ref*exp(deltaHCH4/(R*823))
AH2 = KH2ref*exp(deltaHH2/(R*648))
AH2O = KH2Oref*exp(deltaHH2O/(R*823))

%------------------------------ DEACTIVATION KINETICS --------------------
deltaH1=206; %kJ/mol
deltaH2=-41; %kJ/mol
deltaH3=165; %kJ/mol
deltaHcap1=(-deltaH1)/(-deltaH1); %dimensionless
deltaHcap2=(-deltaH2)/(-deltaH1); %dimensionless
deltaHcap3=(-deltaH3)/(-deltaH1); %dimensionless

%------------------ MOLECULAR WEIGHTS (CO@, H2, CO, H2O, CH4) -------------
M_CO2=44e-3; M_H2=2e-3; M_CO=28e-3; M_H2O=18e-3; M_CH4=16e-3; %kg/mol

% ************************** REACTOR OPERATING CONDITIONS ***************

%---- Packed bed feed (CO2,H2,CO,H2O,CH4), dimensionless -----
%---- Deactivation feed parameters---(carbon deposition, catalyst activity)
                                        uf6 = 0; uf7 = 1;

                  uf1=0.2;uf2=0.8;uf3=0;uf4=0;uf5=0; % ***NON-MEMBRANE***
%                     uf1=0.9;uf2=0.1;uf3=0;uf4=0;uf5=0; % $$$ MEMBRANE $$$

%---- Membrane feed -----------------------------------------------------
           uf8=0.6; uf9=0; uf10=0; uf11=1-uf8;    %pure H2
%          uf8=0.56; uf9=0.247; uf10=0.133; uf11=0.06; %gasified biomass
% ----------- OUTLET Pressure, Space Velocity, & Temperatures -------------

                                                        Ptf=300+700; %kPa
% AIR COOLANT pressure:
    Pc = 10; %bar
                            SVf=0.2*(1000)/3600; %1/s ***NON-MEMBRANE***
%                         SVf=1.5*(0.2/0.9)*1000/3600; %1/s $$$ MEMBRANE $$$
```

```
%
   % !!!!!!!!-----molten salt range: 523-838K (Dynalene MS-1) ------- !!!!!
Te=298;                                                    Tf=650; Tcf=550; %K
% ---------- Membrane Pressure, Space Velocity ------
                                                              PtfM = 2000; %kPa
                                                         SVfM =5*10*SVf ; %1/s

% ---------------- LOOP FOR SCANS OVER PARAMETER RANGES -------------------
count = 1;
for k=1:count

% ----------- Reference Coolant Mass Flow Rate ----
dT=300; %K
% Cpcf=1.425; %kJ/(kg K); MS
Cpcf=1.1142-0.0005*Tcf+(9e-7)*(Tcf^2)-(4e-10)*(Tcf^3); %kJ/(kg K); AIR
G0=uf1*deltaH3*VT*(Ptf/(R*Tf))*SVf/(dT*Cpcf) %kg/s
                                                                 G=1*G0; %kg/s
ro_mean=1850;     %kg/m3; MS

Rg_c = 8.314*10^-5; %m3 bar/K mol
Mc = 28.96; %g/mol
ro_cf=Pc/(Rg_c*Tcf)*Mc/1000;  %kg/m3; AIR
Qair=G/ro_cf;  %m3/s

Ctf=Ptf/(R*Tf);   %mol/m3
vgf=L*SVf/epsi;   %m/s

vc=G/(ro_mean*A); %m/s MS
vc=G/(ro_cf*A); %m/s   AIR

ratio=vc/vgf;     %dimensionless

vgfM = L*SVfM; %m/s
CtfM = PtfM/(R*Tf); %mol/m3

% ----- Adiabatic Temperature ----------------------
Cpgf=uf1*(-2e-8*Tf^2+5e-5*Tf+0.0256)+uf2*(3e-9*Tf^2-2e-6*Tf+0.0297)+uf3*(4e-
6*Tf+0.0276)+uf4*(1e-8*Tf^2-5e-6*Tf+0.0356)+uf5*(0.03*log(Tf)-0.1394);
%kJ/(mol K)
Tad=Tf+deltaH1*0.2/Cpgf %K
% ---- Dimensionless Feed and Environment Temperatures ---------
thetaf=Tf/Tad; thetae=Te/Tad; thetacf=Tcf/Tad; %dimensionless

% ---------------- SIMULATIONS PARAMETERS --------------------------------
m=0;      % cartezian geometry
tcnt=50;  % number of time output point
N=100; x=linspace(0,1,N);   %number of space points
% N1=80; N2=20; x=[linspace(0,0.2,N1) linspace(0.21,1,N2)]; N=N1+N2;

% ------------- Maximum Time of Simulation ---------------------------------
                                                    tmax_h=1; %h
t_max=tmax_h*(vgf/L)*3600    %dimensionless
tao=linspace(0,t_max,tcnt);   %dimensionless time
t=tao*L/(3600*vgf);           %dimensional time, h
```

```
%-------------------- PDE SOLVER ----------------------------------------
options=odeset('RelTol',1e-3,'AbsTol',1e-6,'Normcontrol','on');
sol=pdepe(m,@eqns,@eqn_ic,@eqn_bc,x,tao,options,N,Tad,deltaHcap1,deltaHcap2,d
eltaHcap3,Pc,ro_cf,Tf,Ptf,PtfM,R,L,n,dp,epsi,dw,dc,ache,avhe,avhl,vc,uf1,uf2,
uf3,uf4,uf5,uf6,uf7,uf8,uf9,uf10,uf11,Tcf,Te,Ea1,Ea2,Ea3,EaP,EaH,deltaHeq1,de
ltaHeq2,deltaHeq3,thetaf,thetae,thetacf,vgf,vgfM,Ctf,CtfM,M_CH4,M_H2,M_H2O,M_
CO2,M_CO,A1,A2,A3,Ap,D0,B1,B2,B3,ACO,ACH4,AH2O,AH2,deltaHCO,deltaHCH4,deltaHH
2O,deltaHH2,deltaH1,ro_s,G,t_max,Urw,alpha,VT,A,A_pb,SVf,Sm,nm,VTM);

%---------------------- SOLVER OUTPUT ------------------------------------
%----- dimensionless concentrations & temperatures -----
Y1=real(sol(:,:,1));%CO2
Y2=real(sol(:,:,2));%H2
Y3=real(sol(:,:,3));%CO
Y4=real(sol(:,:,4));%H2O
Y5=real(sol(:,:,5));%CH4
Y6=real(Tad*sol(:,:,6));%reactor temp
Y7=real(Tad*sol(:,:,7));%coolant temp
Y8=real(sol(:,:,8));% carbon
Y9=real(sol(:,:,9));% activity
Y10 = real(sol(:,:,10));% H2 membrane

%---- steady state moole fractions & temperatures -----
Y1_s=real(sol(tcnt,:,1));
Y2_s=real(sol(tcnt,:,2));
Y3_s=real(sol(tcnt,:,3));
Y4_s=real(sol(tcnt,:,4));
Y5_s=real(sol(tcnt,:,5));
T_rs=real(Tad*sol(tcnt,:,6));
T_cs=real(Tad*sol(tcnt,:,7));
Y8_s=real(sol(tcnt,:,8));% carbon
Y9_s=real(sol(tcnt,:,9));% activity
Y10_s=real(sol(tcnt,:,10)); % H2 Membrane
%---- deactivation temperature plot ------
T_rd=real(Tad*sol(:,end,6));
T_cd=real(Tad*sol(:,end,7));
Trdmax=max(Y6,[],2);
Tcdmax=max(Y7,[],2);
%---- maximum temperature -----
Trmax(1,k)=max(T_rs);
Tcmax(1,k)=max(T_cs);
for i=1:N
    for j=1:tcnt

if Y8(j,i)<0
    Y8(j,i)=0;
end
if Y9(j,i)>1
    Y9(j,i)=1;
end
if Y9(j,i)<0
    Y9(j,i)=0;
end

% ---------- Gas velocities & Mole fractions -----------------------------
%-----ut-------
```

```
ut(j,i)=Y1(j,i)+Y2(j,i)+Y3(j,i)+Y4(j,i)+Y5(j,i);
utm(j,i) = Y10(j,i)+uf9+uf10+uf11;
% -----y=Pi/Pt=ui/ut------
yCO2(j,i)=Y1(j,i)/ut(j,i);yH2(j,i)=Y2(j,i)/ut(j,i);
yCO(j,i)=Y3(j,i)/ut(j,i);yH2O(j,i)=Y4(j,i)/ut(j,i);
yCH4(j,i)=Y5(j,i)/ut(j,i);

% yH2M (j,i) = Y10(j,i);
yH2M (j,i) = Y10(j,i) /utm(j,i);

%----velocity of gas-----------
vg(j,i)=vgf*ut(j,i); vgcap(j,i)=vg(j,i)/vgf;

%---------thermophysical properties of gas, solid, and coolant---------
%----gas: mol/m^3, kJ/mol K, kW/mk, pa*s; solid : kg/m^3, kJ/kg K, kW/mk;
% coolant: kg/m^3, kJ/kg K, kW/mk, pa*s(kg/m s)
M_gf=uf2*M_H2+uf4*M_H2O+uf5*M_CH4+uf1*M_CO2+uf3*M_CO;
M_g(j,i)=yH2(j,i)*M_H2+yH2O(j,i)*M_H2O+yCH4(j,i)*M_CH4+yCO2(j,i)*M_CO2+yCO(j,
i)*M_CO;
ro_gmf=M_gf*Ctf;
Cp_H2(j,i)=3e-9*Y6(j,i)^2-2e-6*Y6(j,i)+0.0297; lamda_H2(j,i)=5e-7*Y6(j,i)+4e-
5; miu_H2(j,i)=2e-8*Y6(j,i)+5e-6;
Cp_H2O(j,i)=1e-8*Y6(j,i)^2-5e-6*Y6(j,i)+0.0356; lamda_H2O(j,i)=1e-7*Y6(j,i)-
2e-5; miu_H2O(j,i)=4e-8*Y6(j,i)-3e-6;
Cp_CH4(j,i)=0.03*log(Y6(j,i))-0.1394; lamda_CH4(j,i)=2e-7*Y6(j,i)-3e-5;
miu_CH4(j,i)=3e-8*Y6(j,i)+4e-6;
Cp_CO2(j,i)=-2e-8*Y6(j,i)^2+5e-5*Y6(j,i)+0.0256; lamda_CO2(j,i)=8e-8*Y6(j,i)-
4e-6; miu_CO2(j,i)=4e-8*Y6(j,i)+6e-6;
Cp_CO(j,i)=4e-6*Y6(j,i)+0.0276; lamda_CO(j,i)=6e-8*Y6(j,i)+8e-6;
miu_CO(j,i)=4e-8*Y6(j,i)+7e-6;
Cp_g(j,i)=yH2(j,i)*Cp_H2(j,i)+yH2O(j,i)*Cp_H2O(j,i)+yCH4(j,i)*Cp_CH4(j,i)+yCO
2(j,i)*Cp_CO2(j,i)+yCO(j,i)*Cp_CO(j,i);
lamda_g(j,i)=yH2(j,i)*lamda_H2(j,i)+yH2O(j,i)*lamda_H2O(j,i)+yCH4(j,i)*lamda_
CH4(j,i)+yCO2(j,i)*lamda_CO2(j,i)+yCO(j,i)*lamda_CO(j,i);
miu_g(j,i)=yH2(j,i)*miu_H2(j,i)+yH2O(j,i)*miu_H2O(j,i)+yCH4(j,i)*miu_CH4(j,i)
+yCO2(j,i)*miu_CO2(j,i)+yCO(j,i)*miu_CO(j,i);%gas
lamda_s(j,i)=5.5e-3+(34.5e-3)*exp(-0.0033*(Y6(j,i)-273));Cp_s=1.0446+(1.742e-
4)*Y6(j,i)-(2.796e+4)*Y6(j,i)^-2; %solid
%ro_c=350.95/Tc; Cp_c=10^3*(2e-10*Tc^2-1e-8*Tc+0.001); lamda_c=6e-8*Tc+9e-6;
miu_c=4e-11*Tc+8e-9;%air
%ro_c=244.05/Tc; Cp_c=10^3*(6e-12*Tc^3+1e-8*Tc^2-8e-6*Tc+0.0037); lamda_c=8e-
8*Tc-7e-6; miu_c=4e-11*Tc-1e-9;%steam
%ro_c(j,i)=-0.5572*Y7(j,i)+2219.1; Cp_c(j,i)=2e-
4*Y7(j,i)+1.2738;lamda_c(j,i)=2e-7*Y7(j,i)+4e-4; miu_c(j,i)=0.0744*exp(-
0.005*Y7(j,i));%molten salt MS-1

% MS COOLANT PROPERTIES
ro_c(j,i)=-0.6882*Y7(j,i)+2287.8;Cp_c(j,i)=6e-
5*Y7(j,i)+1.5557;lamda_c(j,i)=2e-7*Y7(j,i)+5e-4; miu_c(j,i)=0.4134*exp(-
0.008*Y7(j,i)); %MS-2 (403-773)

%AIR COOLANT PROPERITES
Rg_c = 8.314*10^-5; %m3 bar/K mol
Mc = 28.96; %g/mol
ro_c(j,i) = Pc/(Rg_c*Y7(j,i)); %mol/m3
ro_c(j,i) = ro_c(j,i)*Mc/1000; %kg/m3
```

```
%heat capacity kJ/kg K
Cp_c(j,i) = 1.1142-0.0005*Y7(j,i)+(9e-7)*(Y7(j,i)^2)-(4e-10)*(Y7(j,i)^3);
%viscosity Pa s
miu_c(j,i) = 1e-5+(3e-8)*Y7(j,i);
%Thermal Conductivity kW/m K
lamda_c(j,i) = (0.0074+(6e-5*Y7(j,i)))/1000;

%--------- pressure drop -------------
vgsuper(j,i)=vg(j,i)*epsi;MASS(j,i)=ro_gmf*vgsuper(j,i);
J(j,i)=vgsuper(j,i)*miu_g(j,i)*(1-epsi)/(1e3*Ptf*epsi^3*dp);
S=150*(1-epsi)*L/dp;Re(j,i)=L*MASS(j,i)/miu_g(j,i);
Ptcap(j,i)=1+J(j,i)*(S+1.75*Re(j,i))*(1-x(i));
Pt(j,i)=Ptcap(j,i)*Ptf;
ro_g(j,i)=Pt(j,i)/(R*Y6(j,i));
% ro_g(j,i)=ut(j,i)*Ctf;
ro_gm(j,i)=M_g(j,i)*ro_g(j,i);

%--------- kinetic parameters ---------
yita1ad=Ea1/(R*Tad);
yita1(j,i)=Ea1/(R*Y6(j,i)); yita2(j,i)=Ea2/(R*Y6(j,i));
yita3(j,i)=Ea3/(R*Y6(j,i));
yitaeq1(j,i)=deltaHeq1/Y6(j,i);yitaeq2(j,i)=deltaHeq2/Y6(j,i);yitaeq3(j,i)=de
ltaHeq3/Y6(j,i);
k1ad=A1*exp(-yita1ad);
k1(j,i)=A1*exp(-yita1(j,i));k2(j,i)=A2*exp(-yita2(j,i));k3(j,i)=A3*exp(-
yita3(j,i));
k1cap(j,i)=k1(j,i)/k1ad;k2cap(j,i)=k2(j,i)*Pt(j,i)^1.5/k1ad;k3cap(j,i)=k3(j,i
)/k1ad;
Keq1(j,i)=B1*exp(-yitaeq1(j,i));Keq2(j,i)=B2*exp(-
yitaeq2(j,i));Keq3(j,i)=B3*exp(-yitaeq3(j,i));
Keq1cap(j,i)=Keq1(j,i)/(Pt(j,i)^2);Keq3cap(j,i)=Keq3(j,i)/(Pt(j,i)^2);
%---- gas adsorption equilibrium constants -----
KCO(j,i)=ACO*exp(-deltaHCO/(R*Y6(j,i)));KCH4(j,i)=ACH4*exp(-
deltaHCH4/(R*Y6(j,i)));KH2O(j,i)=AH2O*exp(-
deltaHH2O/(R*Y6(j,i)));KH2(j,i)=AH2*exp(-deltaHH2/(R*Y6(j,i)));
KCOcap(j,i)=KCO(j,i)*Pt(j,i);KCH4cap(j,i)=KCH4(j,i)*Pt(j,i);KH2cap(j,i)=KH2(j
,i)*Pt(j,i);
% %------ reaction rate ------
DEN(j,i)=1+KCOcap(j,i)*yCO(j,i)+KH2cap(j,i)*yH2(j,i)+KCH4cap(j,i)*yCH4(j,i)+K
H2O(j,i)*yH2O(j,i)/yH2(j,i);
f1(j,i)=(yCH4(j,i)*yH2O(j,i)/(yH2(j,i)^2.5)-
yH2(j,i)^0.5*yCO(j,i)/Keq1cap(j,i))/(DEN(j,i))^2;
f2(j,i)=(yCO(j,i)*yH2O(j,i)/yH2(j,i)-yCO2(j,i)/Keq2(j,i))/(DEN(j,i))^2;
f3(j,i)=(yCH4(j,i)*yH2O(j,i)^2/(yH2(j,i)^3.5)-
yH2(j,i)^0.5*yCO2(j,i)/Keq3cap(j,i))/(DEN(j,i))^2;
%---------- wall heat transfer coeficients(U) ------
lamda_w(j,i)=0.0146+1.27*10^(-5)*(Y6(j,i)-273);
Re_p(j,i)=vg(j,i)*ro_gm(j,i)*dp/miu_g(j,i);
Pr_p(j,i)=miu_g(j,i)*Cp_g(j,i)/(M_g(j,i)*lamda_g(j,i));
Re_c(j,i)=ro_c(j,i)*vc*dc/miu_c(j,i);
Pr_c(j,i)=Cp_c(j,i)*miu_c(j,i)/lamda_c(j,i);
if(Re_c(j,i)>4000)
   Nu_c(j,i)=0.027*Re_c(j,i)^0.8*Pr_c(j,i)^0.3;%turbulent
   elseif(Re_c(j,i)>2300&&Re_c(j,i)<4000)
   Nu_c(j,i)=0.012*(((Re_c(j,i)^0.87)-
280)*(Pr_c(j,i)^0.4)*(1+(dc/L)^0.66));%intermediate regime
```

```
else

Nu_c(j,i)=3.66+0.065*Re_c(j,i)*Pr_c(j,i)*(dc/L)/(1+0.04*(Re_c(j,i)*Pr_c(j,i)*
dc/L)^(2/3));
end
Nu_p(j,i)=24+0.34*Re_p(j,i)^0.77;
hwr(j,i)=lamda_g(j,i)*Nu_p(j,i)/dp;
hwc(j,i)=lamda_c(j,i)*Nu_c(j,i)/dc;
Ucw(j,i)=1/(1/hwr(j,i)+1/hwc(j,i)+dw/lamda_w(j,i));
% dil=0.05;kil=1.7e-3;hnc=14e-3;
% Urw(j,i)=1/(1/hwr(j,i)+dil/kil+1/hnc+dw/lamda_w(j,i));
%----------axial heat transfer coefficient-----
%kae=lamda_s+0.5*Cp_g*vg*ro_g*dp;
kae_pb(j,i)=lamda_g(j,i)*(8+0.05*Re_p(j,i)^1.09);
kae(j,i)=alpha*kae_pb(j,i)+(1-alpha)*lamda_w(j,i);
%----------effectiveness factor(eta)--------
Dm(j,i)=1e-07*Y6(j,i)^1.8766/Pt(j,i);
ksr1(j,i)=k1(j,i)*ro_s*(1-epsi)/(sqrt(Ptf)*ro_g(j,i)*epsi);
phi1(j,i)=sqrt(ksr1(j,i)*dp^2/(4*Dm(j,i)));
if phi1(j,i)<0.001
    phi1(j,i)=0.001;
end
eta1(j,i)=(3/phi1(j,i))*(1/tanh(phi1(j,i))-1/phi1(j,i));
ksr2(j,i)=k2(j,i)*ro_s*(1-epsi)*Ptf/(ro_g(j,i)*epsi);
phi2(j,i)=sqrt(ksr2(j,i)*dp^2/(4*Dm(j,i)));
if phi2(j,i)<0.001
    phi2(j,i)=0.001;
end
eta2(j,i)=(3/phi2(j,i))*(1/tanh(phi2(j,i))-1/phi2(j,i));
ksr3(j,i)=k3(j,i)*ro_s*(1-epsi)/(sqrt(Ptf)*ro_g(j,i)*epsi);
phi3(j,i)=sqrt(ksr3(j,i)*dp^2/(4*Dm(j,i)));
if phi3(j,i)<0.001
    phi3(j,i)=0.001;
end
eta3(j,i)=(3/phi3(j,i))*(1/tanh(phi3(j,i))-1/phi3(j,i));
%---- axial mass transfer coefficient -----
tau=1/(epsi^0.5);
Dae(j,i)=epsi*(Dm(j,i)/tau+0.5*dp*vg(j,i));
%----------dimensionless term-------
% sigma=(epsi*ro_g*Cp_g+(1-epsi)*ro_s*Cp_s)/(epsi*ro_g*Cp_g);
%beta=(-deltaH1)*Ctf/(ro_g(j,i)*Cp_g(j,i)*Tad);
%beta=(-deltaH1)/(Cp_g(j,i)*Tad);
%------------- Damkohler Number -------------------
Wc(j,i)=ro_s*(1-epsi);Ftf(j,i)=(Ctf*vg(j,i)/L)*epsi;
Da(j,i)=Wc(j,i)*k1ad/(Ftf(j,i)*(Pt(j,i))^0.5);
%------------------- other parameters ----------------------
Pem(j,i)=epsi*vg(j,i)*L/Dae(j,i);
Per(j,i)=L*vg(j,i)*epsi*ro_g(j,i)*Cp_g(j,i)/kae(j,i);
Pec(j,i)=L*vc*ro_c(j,i)*Cp_c(j,i)/lamda_c(j,i);
Str1(j,i)=Ucw(j,i)*avhe*L/(epsi*ro_g(j,i)*Cp_g(j,i)*vg(j,i));Str2(j,i)=Urw*av
hl*L/(epsi*ro_g(j,i)*Cp_g(j,i)*vg(j,i));Stc(j,i)=Ucw(j,i)*ache*L/(ro_c(j,i)*C
p_c(j,i)*vc);%--St
SCH4l(j,i)=(yCH4(j,i)-uf5)/(yCH4(j,i)+yCO(j,i)-uf5); % for SR
SCO=yCO/(yCO+yCO2)
CH4yieldl(j,i)=(yCH4(j,i)-uf5)/(yCH4(j,i)+yCO(j,i)+yCO2(j,i)-uf5); %for SR
H2yield=(4*yCO2+3*yCO)/(4*(yCH4+yCO2+yCO))
```

```
XCO2l(j,i)=(yCH4(j,i)+yCO(j,i)-uf5)/(yCO2(j,i)+yCO(j,i)+yCH4(j,i)-uf5); %for
SR XCH4l=(yCO2+yCO)/(yCO2+yCO+yCH4)

%-----mole fraction after water removal---------
utr(j,i)=ut(j,i)-Y4(j,i);
yrCO2(j,i)=Y1(j,i)/utr(j,i);yrH2(j,i)=Y2(j,i)/utr(j,i);yrCO(j,i)=Y3(j,i)/utr(
j,i);yrCH4(j,i)=Y5(j,i)/utr(j,i);
carbon(j,i) = Y8(j,i);
activity(j,i) = Y9(j,i);



%********************************* ACTUAL REACTION RATES******************
Rdct1(j,i)=real(-Da(j,i)*activity(j,i)*eta1(j,i)*k1cap(j,i)*f1(j,i));%  CO
Methanation
Rdct2(j,i)=real(-Da(j,i)*activity(j,i)*eta2(j,i)*k2cap(j,i)*f2(j,i)); % RWGS
Rdct3(j,i)=real(-Da(j,i)*activity(j,i)*eta3(j,i)*k3cap(j,i)*f3(j,i));%
Sabatier Reaction(CO2 methanation)

    end
end
save('CA.mat','carbon','activity');
Y6(end)
%-----SS outlet data------
SCH4=yCH4(end)/(yCH4(end)+yCO(end));
CH4yield=yCH4(end)/(yCH4(end)+yCO(end)+yCO2(end));
%---conversion----
%X5=(yCO2(j,i)+yCO(j,i))/(yCO2(j,i)+yCO(j,i)+yCH4(j,i))%CH4
CO2CONVERSION=(yCH4(end)+yCO(end))/(yCO2(end)+yCO(end)+yCH4(end));
UTend=Y1(end)+Y2(end)+Y3(end)+Y4(end)+Y5(end)
Ytend=yCO2(end)+yCO(end)+yCH4(end)+yH2O(end)+yH2(end)
%------plot-------
UT=Y1_s+Y2_s+Y3_s+Y4_s+Y5_s;% for plot
Yt=yCO2(end,:)+yCO(end,:)+yCH4(end,:)+yH2O(end,:)+yH2(end,:);% should be 1
G
vc
ratio
%----steady state data-----
%----for loop-----
%NNf(1,k)=NN*uf1*deltaH3*VT*(Ptf/(R*Tf))*SVf/(dT*Cpcf);%kg/s
Tr_out(1,k)=T_rs(end);
Tc_out(1,k)=T_cs(end);
SCH4k(1,k)=(yCH4(end)-uf5)/(yCH4(end)+yCO(end)-uf5);
CH4yieldk(1,k)=(yCH4(end)-uf5)/(yCH4(end)+yCO(end)+yCO2(end)-uf5);
XCO2k(1,k)=(yCH4(end)+yCO(end)-uf5)/(yCO2(end)+yCO(end)+yCH4(end)-uf5);
Ptk(1,k)=(Ptf-Pt(end))/Ptf;
if XCO2l(end,:)<0.01
    SCH4l(end,:)=0;
end
if XCO2k(1,k)<0.01
    SCH4k(1,k)=0;
end
end
%save('GfigUSS.txt','NNf','SCH4k','CH4yieldk','XCO2k','Trmax','Tcmax','Tr_out
','Tc_out','Ptk','-ascii')
%type('GfigUSS.txt')
```

```
%----figures----------------
figure(1)
plot(t(2:end),yrCO2(2:end,end),'m-.','LineWidth',3)
hold on;plot(t(2:end),yrH2(2:end,end),'g-','LineWidth',3);
hold on;plot(t(2:end),yrCH4(2:end,end),'b-','LineWidth',3);
hold on;plot(t(2:end),yrCO(2:end,end),'r-','LineWidth',3);
axis([0 tmax_h 0 1.2]);
xlabel('t [h]');
ylabel('mole fraction','FontSize',18);
set(gcf,'color','w');
set(gca,'FontSize',16);
legend('CO_2','H_2','CH_4','CO')

%----3D plots----
figure(2)
mesh(x,t,yH2);
title('H2 mole fraction');
xlabel('z/L');
ylabel('t [h]');
zlabel('y_{H_2}')
set(gcf,'color','w')
set(gca,'FontSize',16);
axis([0 1 0 tmax_h 0 uf2+0.4])
colormap jet

figure(3)
mesh(x,t,yCO);
title('CO mole fraction');
xlabel('z/L');
ylabel('t [h]');
zlabel('y_{CO}')
set(gcf,'color','w')
set(gca,'FontSize',16);
axis([0 1 0 tmax_h 0 0.2])
colormap jet

figure(4)
mesh(x,t,yH2O);
title('H2O mole fraction');
xlabel('z/L');
ylabel('t [h]');
zlabel('y_{H_2O}')
set(gcf,'color','w')
set(gca,'FontSize',16);
axis([0 1 0 tmax_h 0 2*uf1+0.4])
colormap jet

figure(5)
mesh(x,t,yCH4);
title('CH_4 mole fraction');
xlabel('z/L');
ylabel('t [h]');
zlabel('y_{CH_4}')
set(gcf,'color','w')
set(gca,'FontSize',16);
```

```
axis([0 1 0 tmax_h 0 uf1+0.2])
colormap jet

figure(6)
mesh(x,t,Y6);
title('packed bed temperature');
xlabel('z/L');
ylabel('t [h]');
zlabel('T_{PB} [K]')
set(gcf,'color','w')
set(gca,'FontSize',16);
axis([0 1 0 tmax_h 500 1000])
colormap jet
h = colorbar; set(h,'FontSize',12,'Ticks',[550 600 650 700 750 800 850]);

figure(7)
mesh(x,t,Y7);
title('coolant temperature');
xlabel('z/L');
ylabel('t [h]');
zlabel('T_{MS} [K]')
set(gcf,'color','w')
set(gca,'FontSize',16);
axis([0 1 0 tmax_h 500 1000])
colormap jet
h = colorbar; set(h,'FontSize',12,'Ticks',[550 600 650 700 750 800 850]);

%------1D plots for different times------

figure(15)
plot(x,Pt*0.01','k-');
hold on; plot(x,vgcap','k-');
xlabel('z/L');
ylabel('P_t [bar], v_g/v_{gf}');
axis([0 1 0 Ptf*1.5e-2]);
set(gcf,'color','w')
set(gca,'FontSize',16);
title('gas velocity & total pressure')

%-----steady state reactor and coolant temperature profile(final time)----
figure(18)
plot(x,T_rs,'r-','LineWidth',3);
hold on;plot(x,T_cs,'b-.','LineWidth',3)
axis([0 1 200 1000]);
xlabel('z/L');
ylabel('T [K]');
set(gcf,'color','w');
set(gca,'FontSize',16);
legend('T_{PB}','T_{air}')
% print(figure(18),'-dpng')
% title('Steady state temperature')
pbaspect([2 1 1])

figure(23)
plot(x,UT,'r-','LineWidth',2);
hold on;plot(x,Yt,'c-','LineWidth',2);
```

```
axis([0 1 0 4]);
xlabel('z/L');
ylabel('y_t, u_t');
set(gcf,'color','w');
set(gca,'FontSize',16);
legend('u_t','y_t')
% title('total mole fraction')
pbaspect([2 1 1])

figure(24)
plot(x,SCH4l(end,:),'g-','LineWidth',3);
hold on;plot(x,CH4yieldl(end,:),'k-.','LineWidth',3);
hold on;plot(x,XCO2l(end,:),'b--','LineWidth',3);
% hold on;plot(x,(Ptf-Pt(end,:))/Ptf,'r:','LineWidth',3);
axis([0 1 0 1.2]);
xlabel('z/L');
ylabel('X, Y, S','FontSize',18);
set(gcf,'color','w');
set(gca,'FontSize',16);
legend('S_{CH_4}','Y_{CH_4}','X_{CO_2}')
% title('reactor performance')
% print(figure(24),'-dpng')
pbaspect([2 1 1])

figure(25)
plot(x,yCO2(end,:),'r-','LineWidth',3);
hold on;plot(x,yH2(end,:),'c--','LineWidth',3);
hold on;plot(x,yCO(end,:),'g-.','LineWidth',3);
hold on;plot(x,yH2O(end,:),'k--.','LineWidth',3);
hold on;plot(x,yCH4(end,:),'b:','LineWidth',3);
axis([0 1 0 1]);
xlabel('z/L');
ylabel('y_i');
set(gcf,'color','w');
set(gca,'FontSize',16);
legend('CO_2','H_2','CO','H_2O','CH_4')
% print(figure(25),'-dpng')
% title('mole fraction profiles')
pbaspect([2 1 1])

figure(26)
plot(x,yrCO2(end,:),'r-','LineWidth',3);
hold on;plot(x,yrH2(end,:),'c--','LineWidth',3);
hold on;plot(x,yrCO(end,:),'g-.','LineWidth',3);
hold on;plot(x,yrCH4(end,:),'b:','LineWidth',3);
axis([0 1 0 1]);
xlabel('z/L');
ylabel('y_i');
set(gcf,'color','w');
set(gca,'FontSize',16);
legend('CO_2','H_2','CO','CH_4')
title('mole fractions on dry basis')
% print(figure(26),'-dpng')

%------deactivation----
figure(30)
```

```
plot(t(2:end),SCH4l(2:end,end),'g-','LineWidth',3);
hold on;plot(t(2:end),CH4yieldl(2:end,end),'k-.','LineWidth',3);
hold on;plot(t(2:end),XCO2l(2:end,end),'b--','LineWidth',3);
axis([0 tmax_h 0 1.2]);
xlabel('t [h]');
ylabel('X_{CO_2}, S_{CH_4}, Y_{CH_4}','FontSize',18);
set(gcf,'color','w');
set(gca,'FontSize',16);
legend('S_{CH_4}','Y_{CH_4}','X_{CO_2}')
title('reactor performance')

figure(31)
plot(t,T_rd,'r-','LineWidth',3);
hold on;plot(t,Trdmax,'b--','LineWidth',3);
axis([0 tmax_h 300 1200]);
xlabel('t [h]');
ylabel('T [K]');
set(gcf,'color','w');
set(gca,'FontSize',16);
legend('T_{PB,out}','T_{PB,max}')
title('packed bed temperature')

figure(32)
plot(t,T_cd,'r-','LineWidth',3);
hold on;plot(t,Tcdmax,'b--','LineWidth',3);
axis([0 tmax_h 300 1200]);
xlabel('t [h]');
ylabel('T [K]');
set(gcf,'color','w');
set(gca,'FontSize',16);
legend('T_{MS,out}','T_{MS,max}')
title('coolant temperature')

%********** DEACTIVATION PLOTS *****************
figure(34)
mesh(x,t,eta1)
xlabel('z/L');
ylabel('t [h]');
zlabel('eta1');
axis([0 1 0 tmax_h 0 1]);
set(gcf,'color','w')
set(gca,'FontSize',16);
title('eta1')
colormap jet

figure(35)
mesh(x,t,eta2)
xlabel('z/L');
ylabel('t [h]');
zlabel('eta2');
axis([0 1 0 tmax_h 0 1]);
set(gcf,'color','w')
set(gca,'FontSize',16);
title('eta2')
colormap jet
```

```
figure(36)
mesh(x,t,eta3)
xlabel('z/L');
ylabel('t [h]');
zlabel('eta3');
axis([0 1 0 tmax_h 0 1]);
set(gcf,'color','w')
set(gca,'FontSize',16);
title('eta3')
colormap jet

figure(37)
mesh(x,t,Rdct1)
xlabel('z/L');
ylabel('t [h]');
zlabel('actual rate');
% axis([0 1 0 tmax_h 0 1]);
set(gcf,'color','w')
set(gca,'FontSize',16);
title('CO methanation')
colormap jet

figure(38)
mesh(x,t,Rdct2)
xlabel('z/L');
ylabel('t [h]');
zlabel('actual rate');
% axis([0 1 0 tmax_h 0 1]);
set(gcf,'color','w')
set(gca,'FontSize',16);
title('RWGS')
colormap jet

figure(39)
mesh(x,t,Rdct3)
xlabel('z/L');
ylabel('t [h]');
zlabel('actual rate');
% axis([0 1 0 tmax_h 0 1]);
set(gcf,'color','w')
set(gca,'FontSize',16);
title('Sabaier reaction')
colormap jet

figure(40)
plot(t(2:end),carbon(2:end,end),'b-','LineWidth',3)
xlabel('t [h]');
ylabel('carbon, g/g_{cat}');

figure(41)
plot(t(2:end),activity(2:end,end),'r-','LineWidth',3)
axis([0 tmax_h 0 1.2]);
xlabel('t [h]');
ylabel('activity, r/r_{max}');

figure(42)
```

```
plot(x,carbon(end,:),'b--','LineWidth',3);
xlabel('z/L');
ylabel('carbon g/g_{cat}');

figure(43)
plot(x,activity(end,:),'r--','LineWidth',3);
axis([0 1 0 1]);
xlabel('z/L');
ylabel('activity, r/r_{max}');

figure(44)
mesh(x,t,activity)
xlabel('z/L');
ylabel('t [h]');
zlabel('activity');
axis([0 1 0 tmax_h 0 1]);
set(gcf,'color','w')
set(gca,'FontSize',16);
title('activity')
colormap jet

figure(45)
mesh(x,t,carbon)
xlabel('z/L');
ylabel('t [h]');
zlabel('carbon g/g_{cat}');
set(gcf,'color','w')
set(gca,'FontSize',16);
title('carbon')
colormap jet

figure(46)
mesh(x,t,yH2M);
xlabel('z/L');
ylabel('t [h]');
zlabel('y_{H_2}')
set(gcf,'color','w')
set(gca,'FontSize',16);
axis([0 1 0 tmax_h 0 uf8+0.2])
colormap jet

figure(47)
title('H2 membrane mole fraction');
plot(x,yH2M(end,:),'r-','LineWidth',3);
set(gcf,'color','w');
set(gca,'FontSize',16);
axis([0 1 0 1]);
xlabel('z/L');
ylabel('y_{H_2}');


%-----------------------------------------------------------------
function
[c,f,s]=eqns(x,tao,y,DyDx,N,Tad,deltaHcap1,deltaHcap2,deltaHcap3,Pc,ro_cf,Tf,
Ptf,PtfM,R,L,n,dp,epsi,dw,dc,ache,avhe,avhl,vc,uf1,uf2,uf3,uf4,uf5,uf6,uf7,uf
```

```
8,uf9,uf10,uf11,Tcf,Te,Ea1,Ea2,Ea3,EaP,EaH,deltaHeq1,deltaHeq2,deltaHeq3,thet
af,thetae,thetacf,vgf,vgfM,Ctf,CtfM,M_CH4,M_H2,M_H2O,M_CO2,M_CO,A1,A2,A3,Ap,D
0,B1,B2,B3,ACO,ACH4,AH2O,AH2,deltaHCO,deltaHCH4,deltaHH2O,deltaHH2,deltaH1,ro
_s,G,t_max,Urw,alpha,VT,A,A_pb,SVf,Sm,nm,VTM)

% ------------------------ STEPWISE CHANGES IN PARAMETERS -----------------
% if tao>t_max*0.2
%     Ctf=Ptf/(R*400);
% %     vgf=L*(500/3600)/epsi;
% vc=(5*uf1*165*VT*(Ptf/(R*400))*SVf/(300*1.425))/(1850*A);
% end

% ----------------- CALCULATIONS ----------------------------------------
% ----- Molar Fractions (y=Pi/Pt=ui/ut) -------
ut=real(y(1)+y(2)+y(3)+y(4)+y(5));                          %dimensionless
utm = real(y(10)+uf9+uf10+uf11);                            %dimensionless
yCO2=real(y(1)/ut); yH2=real(y(2)/ut);                      %dimensionless
yCO=real(y(3)/ut); yH2O=real(y(4)/ut); yCH4=real(y(5)/ut);  %dimensionless
yH2M = real(y(10)/utm);

carbon = real(y(8)); %dimensionless
activity = real(y(9)); %dimensionless
% ------------- Gas Velocity ----------------------------
vg=vgf*ut; %vgcap=vg/vgf; %m/s
vgM = vgfM*utm; %m/s
%--------- Dimensional Temperatures -------
T=real(y(6))*Tad;  %K
Tc=real(y(7))*Tad; %K

%-------------------- THERMOPHYSICAL PROPERTIES --------------------------
M_g=yH2*M_H2+yH2O*M_H2O+yCH4*M_CH4+yCO2*M_CO2+yCO*M_CO; %kg/mol
M_gf=uf2*M_H2+uf4*M_H2O+uf5*M_CH4+uf1*M_CO2+uf3*M_CO; %kg/mol
ro_gmf=M_gf*Ctf; %kg/m3
Cp_H2=3e-9*T^2-2e-6*T+0.0297; lamda_H2=5e-7*T+4e-5; miu_H2=2e-8*T+5e-6;
%kJ/(mol K), kW/(m K), Pa*s
Cp_H2O=1e-8*T^2-5e-6*T+0.0356; lamda_H2O=1e-7*T-2e-5; miu_H2O=4e-8*T-3e-6;
%kJ/(mol K), kW/(m K), Pa*s
Cp_CH4=0.03*log(T)-0.1394; lamda_CH4=2e-7*T-3e-5; miu_CH4=3e-8*T+4e-6;
%kJ/(mol K), kW/(m K), Pa*s
Cp_CO2=-2e-8*T^2+5e-5*T+0.0256; lamda_CO2=8e-8*T-4e-6; miu_CO2=4e-8*T+6e-6;
%kJ/(mol K), kW/(m K), Pa*s
Cp_CO=4e-6*T+0.0276; lamda_CO=6e-8*T+8e-6; miu_CO=4e-8*T+7e-6;
%kJ/(mol K), kW/(m K), Pa*s
Cp_g=yH2*Cp_H2+yH2O*Cp_H2O+yCH4*Cp_CH4+yCO2*Cp_CO2+yCO*Cp_CO;
%kJ/(mol K)
lamda_g=yH2*lamda_H2+yH2O*lamda_H2O+yCH4*lamda_CH4+yCO2*lamda_CO2+yCO*lamda_C
O; %(kW/(m K)
miu_g=yH2*miu_H2+yH2O*miu_H2O+yCH4*miu_CH4+yCO2*miu_CO2+yCO*miu_CO;
%Pa*s
lamda_s=5.5e-3+(34.5e-3)*exp(-0.0033*(T-273));
%kW/(m K)
Cp_s=1.0446+(1.742e-4)*T-(2.796e+4)*T^-2;
%kJ/(kg K)

%ro_c=350.95/Tc; Cp_c=10^3*(2e-10*Tc^2-1e-8*Tc+0.001); %lamda_c=6e-8*Tc+9e-6;
miu_c=4e-11*Tc+8e-9;             % AIR
```

```
%ro_c=244.05/Tc; Cp_c=10^3*(6e-12*Tc^3+1e-8*Tc^2-8e-6*Tc+0.0037);
%lamda_c=8e-8*Tc-7e-6; miu_c=4e-11*Tc-1e-9;  % STEAM
%ro_c=-0.5572*Tc+2219.1; Cp_c=2e-4*Tc+1.2738; lamda_c=2e-7*Tc+4e-4;
miu_c=0.0744*exp(-0.005*Tc);                % MS-1(503-858)

% MS COOLANT PROPERTIES
ro_c=-0.6882*Tc+2287.8; Cp_c=6e-5*Tc+1.5557;       % kg/m3, kJ/(kg K); MS-2
(403-773)
lamda_c=2e-7*Tc+5e-4; miu_c=0.4134*exp(-0.008*Tc); % kW/(m K), Pa*s; MS-2
(403-773)

%AIR COOLANT PROPERITES
Rg_c = 8.314*10^-5; %m3 bar/K mol
Mc = 28.96; %g/mol
%density kg/m3
ro_c = Pc/(Rg_c*Tc); %mol/m3
ro_c = ro_c*Mc/1000; %kg/m3
%heat capacity kJ/kg K
Cp_c = 1.1142-0.0005*Tc+(9e-7)*(Tc^2)-(4e-10)*(Tc^3);
%viscosity Pa s
miu_c = 1e-5+(3e-8)*Tc;
%Thermal Conductivity kW/m K
lamda_c = (0.0074+(6e-5*Tc))/1000;

%------------------------- PRESSURE DROP --------------------------------
vgsuper=vg*epsi; %m/s
MASS=ro_gmf*vgsuper; %kg/(m^2 s)
J=(vgsuper)*miu_g*(1-epsi)/(1e3*Ptf*epsi^3*dp); %dimensionless
S=150*(1-epsi)*L/dp; %dimensionless
Re=L*MASS/miu_g; %dimensionless
Ptcap=1+J*(S+1.75*Re)*(1-x); %dimensionless     CORRECTED!!!!!!
Pt=Ptcap*Ptf; %kPa
ro_g=Pt/(R*T); %mol/m3
% ro_g=ut*Ctf;
ro_gm=M_g*ro_g; %kg/m3

%---------- REACTION KINETICS ----------------------------------------------
yita1ad=Ea1/(R*Tad); %dimensionless
yitapad = EaP/(R*Tad); %membrane dimensionless
yita1=Ea1/(R*T); yita2=Ea2/(R*T); yita3=Ea3/(R*T); %dimensionless
yitap = EaP/(R*T);
yitaeq1=deltaHeq1/T;yitaeq2=deltaHeq2/T;yitaeq3=deltaHeq3/T; %dimensionless
k1ad=A1*exp(-yita1ad); %(mol kPa^0.5)/(kg s)
kpad = Ap*exp(-yitapad); %membrane mol/m2 s kPa0.5
k1=A1*exp(-yita1);     %(mol kPa^0.5)/(kg s)
k2=A2*exp(-yita2);     %(mol/(kPa kg s)
k3=A3*exp(-yita3);     %(mol kPa^0.5)/(kg s)
kp = Ap*exp(-yitap);   %membrane mol/m2 s kPa0.5
k1cap=k1/k1ad;   k2cap=k2*Pt^1.5/k1ad;   k3cap=k3/k1ad; %dimensionless
kpcap = kp/kpad; %membrane dimensionless

Keq1=B1*exp(-yitaeq1); %kPa^2
Keq2=B2*exp(-yitaeq2); %dimensionless
Keq3=B3*exp(-yitaeq3); %kPa^2
Keq1cap=Keq1/(Pt^2); Keq3cap=Keq3/(Pt^2); %dimensionless
```

```
%-------- %********** DEACTIVATION KINETICS *********-----------------------
--------
ka_adj=1; kd_adj=1; p_adj=0*5+3;

ka = ka_adj*exp(135600/(8.314*T) - 32.077); % Deactivation rate constant,
g^3*hr/g^3
kd = kd_adj*exp(20.492 - 104200/(T*8.314)); % specific rate of carbon
deposition, (bar*hr)^-1
Kp = p_adj*5.088e5*exp(-91200/(T*8.314)); % Equilibrium constant for methane
cracking, bar

Kphat = Kp/(Pt/100); %dimensionless
KH = exp(163200/(8.314*T) - 22.426); % Eqilibrium constant for hydrogen
adsorption , bar^-0.5
KHhat = KH*((Pt/100)^0.5); %dimensionless

%------------ Adsorption Constants ----------------------------------
KCO=ACO*exp(-deltaHCO/(R*T));KCH4=ACH4*exp(-deltaHCH4/(R*T)); %1/kPa
KH2=AH2*exp(-deltaHH2/(R*T)); %1/kPa
KH2O=AH2O*exp(-deltaHH2O/(R*T)); %dimensionless
KCOcap=KCO*Pt;KCH4cap=KCH4*Pt;KH2cap=KH2*Pt; %dimensionless

fctr=0;
if yH2<0
    yH2=0;
end

if yH2==0
    yH2=0.01;
end
%------------- Reaction Rates ----------------------------------------
rmax = real((yCH4-yH2^2/Kphat)/((1+KHhat*sqrt(yH2+fctr))^2));

DEN=real(1+KCOcap*yCO+KH2cap*yH2+KCH4cap*yCH4+KH2O*yH2O/(yH2+fctr));
%dimensionless
f1=real((yCH4*yH2O/((yH2+fctr)^2.5)-yH2^0.5*yCO/Keq1cap)/(DEN)^2);
%dimensionless
f2=real((yCO*yH2O/(yH2+fctr)-yCO2/Keq2)/(DEN)^2); %dimensionless
f3=real((yCH4*yH2O^2/((yH2+fctr)^3.5)-yH2^0.5*yCO2/Keq3cap)/(DEN)^2);
%dimensionless

%---------------------- TRANSPORT COEFFICIENTS ---------------------------
% ---------- Dimensionless Numbers -----------------
Re_p=vg*ro_gm*dp/miu_g;              %dimensionless
Pr_p=miu_g*Cp_g/(M_g*lamda_g);       %dimensionless
Re_c=ro_c*vc*dc/miu_c;               %dimensionless
Pr_c=Cp_c*miu_c/lamda_c;             %dimensionless
Nu_p=0.34*Re_p^0.77+24;              %dimensionless

% --------- Nusselt Numbers for Cooling, dimensionless -------------
if(Re_c>4000)
   Nu_c=0.027*Re_c^0.8*Pr_c^0.3;                                  %turbulent
elseif(Re_c>2300&&Re_c<4000)
   Nu_c=0.012*(((Re_c^0.87)-280)*(Pr_c^0.4)*(1+(dc/L)^0.66)); %intermediate
else
```

```
   Nu_c=3.66+0.065*Re_c*Pr_c*(dc/L)/(1+0.04*(Re_c*Pr_c*dc/L)^(2/3)); %laminar
end

% ---------- Wall Heat Transfer Coefficients ------------------------
% ------- Heat Exchange ----------------------
lamda_w=0.0146+1.27*10^(-5)*(T-273); %kW/(m K)
hwr=lamda_g*Nu_p/dp; %kW/(m^2 K)
hwc=lamda_c*Nu_c/dc; %kW/(m^2 K)
Ucw=1/(1/hwr+1/hwc+dw/lamda_w); %kW/(m^2 K)
% ------- Heat Losses ----------------------
% dil=0.05; kil=1.7e-3; hnc=14e-3;
% Urw=1/(1/hwr+dil/kil+1/hnc+dw/lamda_w);

%---------- Axial Mass & Heat Transfer Coefficints ------------------------
% ----- Binary Diffusion Coefficient (CO2-H2) ---------
Dm=1e-07*T^1.8766/Pt; %m^2/s
tau=1/(epsi^0.5); %dimensionless
if( Re_p<1)
    Dae=epsi*Dm/tau; %m^2/s
else
    Dae=epsi*(Dm/tau+0.5*dp*vg); %m^2/s
end
%kae=lamda_s+0.5*Cp_g*vg*ro_g*dp;
kae_pb=lamda_g*(8+0.05*Re_p^1.09);  %kW/(m K)
kae=alpha*kae_pb+(1-alpha)*lamda_w; %kW/(m K)

%-------------------- EFFECTIVENESS FACTORS -----------------------------
% ----- Binary Diffusion Coefficient (CO2-H2) ---------
Dm=1e-07*T^1.8766/Pt; %m^2/s
% ----- Thiele Modulii & Effectiveness Factors --------
ksr1=k1*ro_s*(1-epsi)/(sqrt(Ptf)*ro_g*epsi); %1/s
phi1=sqrt(ksr1*dp^2/(4*Dm)); %dimensionless
if phi1<0.001
    phi1=0.001;
end
eta1=real((3/phi1)*(1/tanh(phi1)-1/phi1)); %dimensionless

ksr2=k2*ro_s*(1-epsi)*Ptf/(ro_g*epsi); %1/s
phi2=sqrt(ksr2*dp^2/(4*Dm));%dimensionless
if phi2<0.001
    phi2=0.001;
end
eta2=real((3/phi2)*(1/tanh(phi2)-1/phi2));%dimensionless

ksr3=k3*ro_s*(1-epsi)/(sqrt(Ptf)*ro_g*epsi); %1/s
phi3=sqrt(ksr3*dp^2/(4*Dm));%dimensionless
if phi3<0.001
    phi3=0.001;
end
eta3=real((3/phi3)*(1/tanh(phi3)-1/phi3));%dimensionless

%---------- DIMENSIONLESS TERMS IN EQUATIONS -----------------------------
sigma=(epsi*ro_g*Cp_g+(1-epsi)*ro_s*Cp_s)/(epsi*ro_g*Cp_g); %dimensionless
beta=(-deltaH1)/(Cp_g*Tad*ut);                              %dimensionless
% beta=(-deltaH1)*Ctf/(ro_g*Cp_g*Tad); <- PROBABLY WRONG
```

```
% ----- Damkohler Number ---PROBLEM with using vgf-!!!!!--
p_ceff=ro_s*(1-epsi);           % kg/m3
                            Ftf_V=(Ctf*vg/L)*epsi;         % mol/(m3 s)
if tao>0.01*t_max
Ftf_V=(Ctf*vgf/L)*epsi;
end

Da=p_ceff*k1ad/(Ftf_V*(Pt)^0.5);  % dimensionless

%----Deactivation Damkohler Number-------------------
restime = (L/(vgf))/3600; %hr
DaC = restime*(Pt/100)*kd; %dimensionless
DaA = restime*((Pt/100)^2)*(kd^2)*ka; %dimensionless

% ----- Peclet Numbers --------------------------------
Pem=epsi*vgf*L/Dae;               %dimensionless
Per=L*vgf*epsi*ro_g*Cp_g/kae;     %dimensionless
Pec=L*vgf*ro_c*Cp_c/lamda_c;      %dimensionless

%---- Deactivation Peclet Numbers--------------------
Pe_C = 1000000; % dimensionless, used for numerical purposes
Pe_A = 1000000; % dimensionless, used for numerical purposes

%---- Membrane Peclet Numbers-------------------
restimePb = L/vgf; %s
DaeH = D0*exp(-EaH/(R*T)); %m2/s
PecMPb= restimePb*Sm*kpad/(epsi*Ctf*VT); %Membrane Peclet number, packed bed
side
PecM = restimePb*Sm*kpad/(CtfM*VTM); %Peclet number, membrane side
PemM = vgf*L/DaeH;
Dinert = (6e-6)*(T^2)+0.0001*T+0.1997; %cm2/s
Dinert = Dinert/(100*100); %m2/s
PemI = vgf*L/Dinert;

% ----- Stanton Numbers -------------------------------
Str1=Ucw*avhe*L/(epsi*ro_g*Cp_g*vgf); %dimensionless
Str2=Urw*avhl*L/(epsi*ro_g*Cp_g*vgf); %dimensionless
Stc=Ucw*ache*L/(ro_c*Cp_c*vgf);       %dimensionless

act=y(9);
if act<0
    act=0;
end
if act>1
    act=1;
end

act(isnan(act)) = 1;

act=1;

% ------------- SIMILATION PROGRESS ----------------------------------------
time=tao/t_max;    % dimensionless
t_d=tao*L/vgf/60;  % min
```

```
time_h=t_d/60     % hours

% ----------------- EQUATIONS AND INITIAL & BOUNDARY CONDITIONS -----------

%---------- Equations ---------------
ut_der=real(DyDx(1)+DyDx(2)+DyDx(3)+DyDx(4)+DyDx(5));
per_rc=real(nm*PecMPb*kpcap*((sqrt(yH2M)*sqrt(PtfM))-(sqrt(yH2)*sqrt(Pt))));
per_mc=real(PecM*kpcap*((sqrt(yH2)*sqrt(Pt))-(sqrt(yH2M)*sqrt(PtfM))));
RH=real(Da*act*beta*(k1cap*f1*deltaHcap1*eta1+k2cap*f2*deltaHcap2*eta2+k3cap*
f3*deltaHcap3*eta3));

cfctr=1;
if tao<0.01*t_max
cfctr=0;
end

c=[ 1%CO2
    1%H2
    1%CO
    1%H2O
    1%CH4
    1
    1
    1
    1
    1
    1];

f=[ 1/Pem
    1/Pem
    1/Pem
    1/Pem
    1/Pem
    1/(Per*sigma)
    1/Pec
    1/Pe_C
    1/Pe_A
    1/PemM
    1/PemI].*DyDx;

% f(find(isnan(f)))=0.01;
f=real(f);

s=[ -real(DyDx(1))+real(Da*act*(k2cap*f2*eta2+k3cap*f3*eta3)-y(1)*ut_der)
    -
real(DyDx(2))+real(Da*act*(3*k1cap*f1*eta1+k2cap*f2*eta2+4*k3cap*f3*eta3)-
y(2)*ut_der+per_rc)
    -real(DyDx(3))+real(Da*act*(k1cap*f1*eta1-k2cap*f2*eta2)-y(3)*ut_der)
    -real(DyDx(4))+real(Da*act*(-k1cap*f1*eta1-k2cap*f2*eta2-
2*k3cap*f3*eta3)-y(4)*ut_der)
    -real(DyDx(5))+real(Da*act*(-k1cap*f1*eta1-k3cap*f3*eta3)-y(5)*ut_der)
    (-real(DyDx(6))+RH-real(n*Str1*(y(6)-y(7)))-real(Str2*(y(6)-
thetae)))/sigma
    -real(DyDx(7)*vc/vgf)-real(Stc*(y(7)-y(6)))
     real(DaC*rmax*act)
```

```
    -real(DaA*rmax^2*y(8)*act)
    -real(DyDx(10)*utm*(vgfM/vgf))+real(per_mc-
y(10)*(vgfM/vgf)*(DyDx(10)+cfctr*DyDx(11)))
    -real(DyDx(11)*utm*(vgfM/vgf)-y(11)*(vgfM/vgf)*(DyDx(10)+DyDx(11)))];

% s(find(isnan(s)))=0.01;
s=real(s);

%---------------------- Initial Conditions ----------------
function
y0=eqn_ic(x,N,Tad,deltaHcap1,deltaHcap2,deltaHcap3,Pc,ro_cf,Tf,Ptf,PtfM,R,L,n
,dp,epsi,dw,dc,ache,avhe,avhl,vc,uf1,uf2,uf3,uf4,uf5,uf6,uf7,uf8,uf9,uf10,uf1
1,Tcf,Te,Ea1,Ea2,Ea3,EaP,EaH,deltaHeq1,deltaHeq2,deltaHeq3,thetaf,thetae,thet
acf,vgf,vgfM,Ctf,CtfM,M_CH4,M_H2,M_H2O,M_CO2,M_CO,A1,A2,A3,Ap,D0,B1,B2,B3,ACO
,ACH4,AH2O,AH2,deltaHCO,deltaHCH4,deltaHH2O,deltaHH2,deltaH1,ro_s,G,t_max,Urw
,alpha,VT,A,A_pb,SVf,Sm,nm,VTM)
y0=[uf1
    uf2
    uf3
    uf4
    uf5
    650/Tad
    650/Tad
    uf6
    uf7
    uf8
    uf11];

%---------------------- Boundary Conditions ---------------
function
[pl,ql,pr,qr]=eqn_bc(xl,yl,xr,yr,tao,N,Tad,deltaHcap1,deltaHcap2,deltaHcap3,P
c,ro_cf,Tf,Ptf,PtfM,R,L,n,dp,epsi,dw,dc,ache,avhe,avhl,vc,uf1,uf2,uf3,uf4,uf5
,uf6,uf7,uf8,uf9,uf10,uf11,Tcf,Te,Ea1,Ea2,Ea3,EaP,EaH,deltaHeq1,deltaHeq2,del
taHeq3,thetaf,thetae,thetacf,vgf,vgfM,Ctf,CtfM,M_CH4,M_H2,M_H2O,M_CO2,M_CO,A1
,A2,A3,Ap,D0,B1,B2,B3,ACO,ACH4,AH2O,AH2,deltaHCO,deltaHCH4,deltaHH2O,deltaHH2
,deltaH1,ro_s,G,t_max,Urw,alpha,VT,A,A_pb,SVf,Sm,nm,VTM)

% ------------------------ STEPWISE CHANGES IN BCs ------------------------
% if tao>t_max*0.2
%      thetaf=400/Tad;
% end
% -------------------------------------------------------------------------

pl=[real(uf1-yl(1))
    real(uf2-yl(2))
    real(uf3-yl(3))
    real(uf4-yl(4))
    real(uf5-yl(5))
    real(thetaf-yl(6))
    real(thetacf-yl(7))
    0
    0
    real(uf8-yl(10))
    uf11-yl(11)];

% pl(find(isnan(pl)))=0.01;
```

```
pl=real(pl);

ql=[1
    1
    1
    1
    1
    1
    1
    1
    1
    1
    1];

pr=[0
    0
    0
    0
    0
    0
    0
    0
    0
    0
    0];

qr=[1
    1
    1
    1
    1
    1
    1
    1
    1
    1
    1];
```

J. Parameter Estimation Code

```
function SSE_lsqnonlin

close all
clear
clc
R=8.314e-3; %gas constant kJ/(mol K)
deltaHCO=-70.65;  %kJ/mol
deltaHCH4=-38.82; %kJ/mol
deltaHH2O=88.68;  %kJ/mol
deltaHH2=-82.9;   %kJ/mol
ACO=8.23e-7;   %1/kPa
ACH4=6.65e-6;  %1/kPa
AH2O=1.77e5;   %dimensionless
AH2=6.12e-11;  %1/kPa
```

```
kref1 = 0.5*4.55e-6;
kref2 = 0.026833;
kref3 = 2*2.47e-6;
Ea1 = 100; %kJ/mol
Ea2 = 75; %kJ/mol
Ea3 = 100; %kJ/mol


KCOref=0.409 %1/kPa
KCH4ref=0.0018 %1/kPa
KH2ref=2.95e-4 %1/kPa
KH2Oref=0.4152 %dimensionless

deltaHCO=-70.65;  %kJ/mol
deltaHCH4=-38.82; %kJ/mol
deltaHH2O=88.68;  %kJ/mol
deltaHH2=-82.9;   %kJ/mol

% KCOref=ACO*exp(-deltaHCO/(R*648))
% KCH4ref=ACH4*exp(-deltaHCH4/(R*823)) %1/kPa
% KH2ref=AH2*exp(-deltaHH2/(R*648)) %1/kPa
% KH2Oref=AH2O*exp(-deltaHH2O/(R*823)) %dimensionless

parms0 = [kref1 kref2 kref3 Ea1 Ea2 Ea3 KCOref KH2Oref KH2ref KCH4ref
deltaHCO deltaHCH4 deltaHH2O deltaHH2];% initial guesses for activation
energy and pre-exponential factor
ub = [kref1*10000 kref2*10000 kref3*10000 150 100 150 KCOref*1.5 KH2Oref*1.5
KH2ref*1.5 KCH4ref*1.5 deltaHCO*0.5 deltaHCH4*0.5 deltaHH2O*1.5 deltaHH2*0.5
]; %lower bounds for the solver
lb = [0 0 0 50 50 50 0 0 0 0 deltaHCO*1.5 deltaHCH4*1.5 deltaHH2O*0.5
deltaHH2*1.5]; %upper bounds for the solver
options = optimoptions(@lsqnonlin,'Display','iter','MaxIter',10000,'TolX',1e-
8,'TolFun',1e-8,'MaxFunctionEvaluations',10000);

%options = optimset('Display','iter','MaxIter',1000); %Tolerances, took this
from Kim's students
[parmshat,resnorm,residual,exitflag,output]=
lsqnonlin('SSE_CSTR_ALL_v2',parms0,lb,ub,options);

format shortEng
parmshat=parmshat'
format short
output;
SSE = resnorm
residual



end


 function resids = SSE_CSTR_ALL(parms)
global kref1 kref2 kref3 Ea1 Ea2 Ea3 KCOref KH2Oref KH2ref KCH4ref deltaHCO
deltaHCH4 deltaHH2O deltaHH2
```

```
kref1 = parms(1);
kref2 = parms(2);
kref3 = parms(3);

Ea1 = parms(4);
Ea2 = parms(5);
Ea3 = parms(6);

KCOref = parms(7);
KH2Oref = parms(8);
KH2ref = parms(9);
KCH4ref = parms(10);

deltaHCO = parms(11);
deltaHCH4 = parms(12);
deltaHH2O = parms(13);
deltaHH2 = parms(14);


%constants
R = 8.314e-3; %kJ/mol
Wc = 0.000256; %kg

%----Ea & equilibrium enthopy---


deltaHeq1=26830; deltaHeq2=-4400; deltaHeq3=22430; %K

B1=1.198e17; B3=2.117e15; %kPa^2
B2=1.767e-2; %dimensionless


kref1 = kref1/sqrt(0.01); %(kmol kPa^0.5)/(kg h)
kref1 =kref1*1000/3600;     %(mol kPa^0.5)/(kg s)

kref2 = kref2*1000/3600;     %mol/(kPa kg s)

kref3 = kref3 / sqrt(0.01);
kref3 = kref3*1000/3600;



% ---- Parameters for Adsorption Constants -----------

ACO=8.23e-7;   %1/kPa
ACH4=6.65e-6;  %1/kPa
AH2O=1.77e5;   %dimensionless
AH2=6.12e-11;  %1/kPa


%Experimental Results
```

```
flow = [(53.68/(60*1000*1000)) (161.05/(60*1000*1000)) (268.4/(60*1000*1000))
(536.83/(60*1000*1000))];
temp = [300+273.15 325+273.15 350+273.15 375+273.15 400+273.15 425+273.15
450+273.15];

%mole fractions

TCO2exp1 = [21.9 21.1 18.6 14.5 10.8 8.7 8.0];
TCH4exp1 = [0.29 3.65 12.0 26.4 39.2 45.5 46.6];
TCOexp1 = [0.18 0.39 0.69 0.79 0.49 0.39 0.49];

TCO2exp2 = [20.1 17.8 14.6 10.7 6.9 5.8 6.7];
TCH4exp2 = [1.4 5.5 14.3 27.4 42.0 47.7 48.4];
TCOexp2 = [0.08 0.19 0.39 0.49 0.29 0.18 0.18];

TCO2exp3 = [20.3 18.8 15.4 10.5 7.2 6.6 6.6];
TCH4exp3 = [1.04 5.6 15.0 29.3 41.3 47.7 49.8];
TCOexp3 = [0.08 0.18 0.39 0.39 0.29 0.19 0.29];

%---------GHSV Ramp--------------
%Wc  = 0.2565 g, T = 350C, Pure Feed
QCO2exp1 = [15.0 19.0 19.4 21.2];
QCH4exp1 = [31.6 10.5 5.70 1.62];
QCOexp1 = [0.165 0.165 0.063 0.063];

QCO2exp2= [15.4 19.3 19.5 21.2];
QCH4exp2 = [30.9 10.2 5.4 1.6];
QCOexp2 = [0.165 0.165 0.165 0.165];

QCO2exp3 = [16.9 20.6 20.6 21.9];
QCH4exp3 = [25.2 7.1 3.4 0.48];
QCOexp3 = [0.063 0.063 0.165 0.063];

TCO2exp = [];
TCH4exp = [];
TCOexp = [];

QCO2exp = [];
QCH4exp = [];
QCOexp = [];

CO2exp = [];
COexp = [];
CH4exp = [];

TCO2exp = [TCO2exp TCO2exp1];
TCO2exp = [TCO2exp TCO2exp2];
TCO2exp = [TCO2exp TCO2exp3];

TCOexp = [TCOexp TCOexp1];
TCOexp = [TCOexp TCOexp2];
TCOexp = [TCOexp TCOexp3];

TCH4exp = [TCH4exp TCH4exp1];
```

```
TCH4exp = [TCH4exp TCH4exp2];
TCH4exp = [TCH4exp TCH4exp3];

QCO2exp = [QCO2exp QCO2exp1];
QCO2exp = [QCO2exp QCO2exp2];
QCO2exp = [QCO2exp QCO2exp3];


QCOexp = [QCOexp QCOexp1];
QCOexp = [QCOexp QCOexp2];
QCOexp = [QCOexp QCOexp3];


QCH4exp = [QCH4exp QCH4exp1];
QCH4exp = [QCH4exp QCH4exp2];
QCH4exp = [QCH4exp QCH4exp3];



CO2exp = [CO2exp TCO2exp];
CO2exp = [CO2exp QCO2exp];
CO2exp = CO2exp';

COexp = [COexp TCOexp];
COexp = [COexp QCOexp];
COexp = COexp';

CH4exp = [CH4exp TCH4exp];
CH4exp = [CH4exp QCH4exp];
CH4exp = CH4exp';



% CO2exp = [21.9 21.1 18.6 14.5 10.8 8.7 9.6 17.9 20.4 24.1 24.5]';
% CH4exp = [0.29 3.65 12.0 26.4 39.2 45.5 40.4 20.6 12.3 1.15 0.72]';
% COexp = [0.18 0.39 0.69 0.79 0.49 0.39 0.29 1.00 1.9 1.6 1.6]';
% CO2exp = [8.88 8.88 10.1 11.3 12.0 11.7 10.4 11.0 13.2 13.4 13.0]';
% CH4exp = [50.9 50.5 44.4 36.3 27.8 20.1 35.9 39.4 29.3 23.1 19.4]';
% COexp = [0.084 0.18 0.59 1.61 3.34 5.99 0.90 1.1 3.1 5.4 6.9]';


P = 45/0.145038; %kPa


%dimensionless concentrations
ufCO2 = 0.2; %CO2
ufH2 = 0.8; %H2
ufCO = 0;
ufH2O = 0;
ufCH4 = 0;

%initial conditions
y0 = [ufCO2 ufH2 ufCO ufH2O ufCH4];
```

```
%dimensionless time
tspan = [0 10];


tempcount = 1;
flowcount = 1;
yCO2PRED = zeros(length(CO2exp),1);
yCH4PRED = zeros(length(CO2exp),1);
yCOPRED = yCH4PRED;
Ttest = [];
Qtest = [];
for k=1:1:length(CO2exp)

if k <=length(TCO2exp)

    T = temp(tempcount);
    Q = 125/(60*1000*1000); %m^3/s
    Ttest = [Ttest T];
    tempcount  = tempcount+1;
    if tempcount > length(TCO2exp1)
        tempcount = 1;
    end


else
    T = 350 + 273.15;
    Wc = 0.000644;
    Q = flow(flowcount);
    Qtest = [Qtest Q];
    flowcount = flowcount+1;
    if flowcount > length(QCO2exp1)
        flowcount = 1;
    end

end

Ctf = P/(R*T);

[t,y] = ode15s(@(t,y)
CSTRREG(t,y,ufCO2,ufH2,ufCO,ufH2O,ufCH4,B1,B2,B3,deltaHeq1,deltaHeq2,deltaHeq
3,T,P,R,Ctf,Q,Wc,ACO,ACH4,AH2O,AH2),tspan,y0);

CO2pre = y(:,1);
H2pre = y(:,2);
COpre = y(:,3);
H2Opre = y(:,4);
CH4pre = y(:,5);

utpre = CO2pre+H2pre+COpre+H2Opre+CH4pre;
utdpre = utpre-H2Opre;

yCO2pre = CO2pre./utpre;
yH2pre = H2pre./utpre;
```

```
yCOpre = COpre./utpre;
yH2Opre = H2Opre./utpre;
yCH4pre = CH4pre./utpre;

ydCO2pre = CO2pre./utdpre;
ydH2pre = H2pre./utdpre;
ydCOpre = COpre./utdpre;
ydCH4pre = CH4pre./utdpre;

m = length(ydCO2pre);

yCO2PRED(k,1) = ydCO2pre(m)*100;
yCH4PRED(k,1) = ydCH4pre(m)*100;
yCOPRED(k,1) = ydCOpre(m)*100;

end

varCO2 = 2.4;
varCH4 = 10.4;
varCO = 0.03;

varCO2 = 1;
varCH4 = 1;
varCO = 1;

% save('exp.mat','CO2exp','COexp','CH4exp')
% save('sim.mat','yCO2PRED','yCOPRED','yCH4PRED')
% save('cond.mat','Qtest','Ttest')

%resids = [(CO2exp-yCO2PRED)'*(CO2exp-yCO2PRED)/varCO2 (COexp-
yCOPRED)'*(COexp-yCOPRED)/varCO]
resids = [(CO2exp-yCO2PRED)/sqrt(varCO2) ; (COexp-yCOPRED)/sqrt(varCO) ;
(CH4exp-yCH4PRED)/sqrt(varCH4) ]; % %
%reguar residuals



SSE_scaled = sum(resids.^2);

end

function dydt =
CSTRREG(t,y,ufCO2,ufH2,ufCO,ufH2O,ufCH4,B1,B2,B3,deltaHeq1,deltaHeq2,deltaHeq
3,T,P,R,Ctf,Q,Wc,ACO,ACH4,AH2O,AH2)
global kref1 kref2 kref3 Ea1 Ea2 Ea3 KCOref KH2Oref KH2ref KCH4ref deltaHCO
deltaHCH4 deltaHH2O deltaHH2


%-----------inlet & outlet molar density-----------
Ct = P/(R*T);
gamma = Ctf/Ct; % 1 assuming that pressure in the reactor doesn't change
because it is dil
uCO2 = (y(1));
uH2 = (y(2));
```

```
uCO = (y(3));
uH2O = (y(4));
uCH4 = (y(5));



%---------Kinetics-------------
k1 = kref1*exp((Ea1/R)*((1/598.15)-(1/T)));%(mol kpa^0.5)/(kg s)
k2 = kref2*exp((Ea2/R)*((1/598.15)-(1/T)));%(mol kpa^0.5)/(kg s)
k3 = kref3*exp((Ea3/R)*((1/598.15)-(1/T)));%(mol kpa^0.5)/(kg s)
kappa1 = k1/k3; %dimensionless
kappa2 = ((P)^1.5)*k2/k3;  %dimensionless
Keq1 = B1*exp(-deltaHeq1/(T)); %kPa^2
Keq2 = B2*exp(-deltaHeq2/(T)); %dimensionless
Keq3 = B3*exp(-deltaHeq3/(T)); %kPa^2
Keq1hat = Keq1/(P^2); %dimensionless
Keq2hat = Keq2; %dimensionless
Keq3hat = Keq3/(P^2); %dimensionless


%------------ Adsorption Constants ----------------------------------
KCO = KCOref*exp((deltaHCO/R)*((1/648)-(1/T)));
KH2 = KH2ref*exp((deltaHH2/R)*((1/648)-(1/T)));
KCH4 = KCH4ref*exp((deltaHCH4/R)*((1/823)-(1/T)));
KH2O = KH2Oref*exp((deltaHH2O/R)*((1/823)-(1/T)));


KCOcap=KCO*P;KCH4cap=KCH4*P;KH2cap=KH2*P; %dimensionless

DEN = 1+KCOcap*gamma*uCO+KH2cap*gamma*uH2+KCH4cap*gamma*uCH4+KH2O*uH2O/uH2;
%DEN = 1;

%dimensionless reaction rates
f1 = real(((1/(gamma^0.5))*(uCH4*uH2O/(uH2^2.5) -
(gamma^1.5)*(uH2^0.5)*uCO/Keq1hat))/(DEN^2));
f2 = real((gamma*(uCO*uH2O/uH2 - uCO2/Keq2hat))/(DEN^2));
f3 = real(((1/sqrt(gamma))*(uCH4*(uH2O^2)/(uH2^3.5) -
(gamma^1.5)*(uH2^0.5)*uCO2/Keq3hat))/(DEN^2));


Ftf =(Q*44.643); % mol/s
Da = Wc*k3/(Ftf*sqrt(P)); %dimensionless

dydt = zeros(5,1);


dydt(1) = ufCO2 -y(1)+ real(Da*(kappa2*f2 + f3));
dydt(2) = ufH2 -y(2) + real(Da*(3*kappa1*f1+kappa2*f2+4*f3));
dydt(3) = ufCO -y(3)+ real(Da*(kappa1*f1 - kappa2*f2));
dydt(4) = ufH2O -y(4) + real(Da*(-kappa1*f1 - kappa2*f2 - 2*f3));
dydt(5) = ufCH4 -y(5) + real(Da*(-kappa1*f1-f3));
```

```
end
```